

AXIAL VANE-TYPE SWIRLER PERFORMANCE
CHARACTERISTICS

By

GLENN FERRIS SANDER

Bachelor of Science in Mechanical Engineering

Oklahoma State University

Stillwater, Oklahoma

1982

Submitted to the Faculty of the Graduate College
of the Oklahoma State University
in partial fulfillment of the requirements
for the Degree of
MASTER OF SCIENCE
July, 1983



AXIAL VANE-TYPE SWIRLER PERFORMANCE
CHARACTERISTICS

Thesis Approved:

David G. Riley

Thesis Adviser

A. J. Ghajar

P. M. Morel

Norman D. Durbin

Dean of the Graduate College

ACKNOWLEDGMENTS

The author would like to express his sincere gratitude to his major adviser, Dr. David G. Lilley, for his guidance and encouragement. Appreciation is also extended to the other members of the committee, Dr. Afshin J. Ghajar and Dr. Peter M. Moretti.

Thanks are due to Ms. Rhonda Thomson and Ms. Neisa Lock for typing the draft copy of the thesis, and to Ms. Rhonda Smith for typing the final copy.

The author also wishes to gratefully acknowledge financial support for the project from NASA Lewis Research Center and Air Force Wright Aeronautical Laboratories under NASA Grant No. NAG 3-74.

This study is dedicated to the author's parents, Dr. and Mrs. David A. Sander, for their loving concern and encouragement.

TABLE OF CONTENTS

Chapter	Page
I. INTRODUCTION	1
1.1 Combustor Flowfield Investigations	1
1.2 Previous Studies	2
1.3 Scope and Objectives	3
1.4 Outline of Thesis.	4
II. IDEALIZED PROFILE DERIVATIONS.	5
2.1 Idealized Profiles	5
2.2 Definition of Swirl Parameters	6
2.3 Swirl Numbers for Idealized Profiles	7
III. EXPERIMENTAL EQUIPMENT AND PROCEDURE	12
3.1 Flowfield Facility	12
3.2 Swirler.	13
3.3 Five-Hole Pitot Probe and Instrumentation.	14
3.4 Calibration, Measurement, and Reduction Procedures	15
IV. RESULTS OF MEASUREMENTS.	17
4.1 Velocity Profiles From Radial Traverses.	18
4.2 Velocity Profiles From Azimuthal Traverses	20
4.3 Calibration Sensitivity Verification	24
4.4 Swirl Strength Comparison.	25
V. CLOSURE.	28
5.1 Summary and Conclusions.	28
5.2 Recommendations for Further Work	29
REFERENCES.	30
APPENDIXES.	32
APPENDIX A - TABLES.	32
APPENDIX B - FIGURES	57

Chapter	Page
APPENDIX C - DESCRIPTION OF REVISIONS TO COMPUTER PROGRAM FOR FIVE-HOLE PITOT DATA REDUCTION.	80
APPENDIX D - LISTING OF FIVE-HOLE PITOT DATA REDUCTION PROGRAM WITH SAMPLE INPUT DATA.	89

LIST OF TABLES

Table	Page
I. Ratios of Maximum Swirl and Axial Velocities F-J of Idealized Profile Cases I - V, for Common Values of Swirl Numbers S and S'	33
II. Summary of Operating Conditions	38
III. Normalized Velocity Components, Yaw Angle, Pitch Angle, and Static Pressure Difference ($p-p_\infty$) From Radial Traverse, $\phi = 0$ deg. (No Swirler)	39
IV. Normalized Velocity Components, Yaw Angle, Pitch Angle, and Static Pressure Difference ($p-p_\infty$) From Radial Traverse, $\phi = 0$ deg. (Swirler Installed)	40
V. Normalized Velocity Components, Yaw Angle, Pitch Angle, and Static Pressure Difference ($p-p_\infty$) From Radial Traverse, $\phi = 38$ deg.	41
VI. Normalized Velocity Components, Yaw Angle, Pitch Angle, and Static Pressure Difference ($p-p_\infty$) From Radial Traverse, $\phi = 45$ deg.	42
VII. Normalized Velocity Components, Yaw Angle, Pitch Angle, and Static Pressure Difference ($p-p_\infty$) From Radial Traverse, $\phi = 60$ deg.	43
VIII. Normalized Velocity Components, Yaw Angle, Pitch Angle, and Static Pressure Difference ($p-p_\infty$) From Radial Traverse, $\phi = 70$ deg.	44
IX. Normalized Velocity Components, Yaw Angle, Pitch Angle, and Static Pressure Difference ($p-p_\infty$) From Azimuthal Traverse, $\phi = 0$ deg. at $r/D = 0.179$ (Swirler Installed)	45
X. Normalized Velocity Components, Yaw Angle, Pitch Angle, and Static Pressure Difference ($p-p_\infty$) From Azimuthal Traverse, $\phi = 38$ deg. at $r/D = 0.179$	46

Table	Page
XI. Normalized Velocity Components, Yaw Angle, Pitch Angle, and Static Pressure Difference ($p-p_\infty$) From Azimuthal Traverse, $\phi = 45$ deg. at $r/D = 0.179$	47
XII. Normalized Velocity Components, Yaw Angle, Pitch Angle, and Static Pressure Difference ($p-p_\infty$) From Azimuthal Traverse, $\phi = 60$ deg. at $r/D = 0.179$	48
XIII. Normalized Velocity Components, Yaw Angle, Pitch Angle, and Static Pressure Difference ($p-p_\infty$) From Azimuthal Traverse, $\phi = 70$ deg. at $r/D = 0.179$	49
XIV. Normalized Velocity Components, Yaw Angle, Pitch Angle, and Static Pressure Difference ($p-p_\infty$) From Azimuthal Traverse, $\phi = 70$ deg. at $r/D = 0.204$	50
XV. Normalized Velocity Components, Yaw Angle, Pitch Angle, and Static Pressure Difference ($p-p_\infty$) From Azimuthal Traverse, $\phi = 70$ deg. at $r/D = 0.179$ measured $0.109 D$ Downstream of Swirler Exit	51
XVI. Normalized Velocity Components, Yaw Angle, Pitch Angle, and Static Pressure Difference ($p-p_\infty$) From Azimuthal Traverse, $\phi = 70$ deg. at $r/D = 0.204$ measured $0.109 D$ Downstream of Swirler Exit	52
XVII. Calibration Sensitivity Comparison, Actual vs. 10% Higher Pitch Coefficient Only	53
XVIII. Calibration Sensitivity Comparison, Actual vs. 10% Higher Velocity Coefficient Only	54
XIX. Calibration Sensitivity Comparison, Actual vs. 10% Higher, Both Pitch and Velocity Coefficients	55
XX. Swirl Numbers S and S' From Radial Traverses	56
XXI. Theoretical Swirl Numbers by Two Methods	56

LIST OF FIGURES

Figure	Page
1. Idealized Axial and Tangential Velocity Profile Cases. . .	58
2. Variation of Velocity Ratios F Through J (Cases I Through V, respectively) with S and S'	60
3. Photograph of Swirler - Upstream End	61
4. Photograph of Swirler - Downstream End	62
5. Diagram of Swirler - Section and Downstream View	63
6. Swirl Vanes.	64
7. Five-Hole Pitot Probe With Angles and Velocities Measured	65
8. Measurement Locations - Radial and Azimuthal Traverses . .	66
9. Normalized Velocity Profiles From Radial Traverse, $\phi = 0$ deg. (No Swirler).	67
10. Normalized Velocity Profiles From Radial Traverse, $\phi = 0$ deg. (Swirler Installed)	68
11. Normalized Velocity Profiles From Radial Traverse, $\phi = 38$ deg	69
12. Normalized Velocity Profiles From Radial Traverse, $\phi = 45$ deg	70
13. Normalized Velocity Profiles From Radial Traverse, $\phi = 60$ deg	71
14. Normalized Velocity Profiles From Radial Traverse, $\phi = 70$ deg	72
15. Normalized Velocity Profiles From Azimuthal Traverse, $\phi = 0$ deg. at $r/D = 0.179$ (Swirler Installed).	73
16. Normalized Velocity Profiles From Azimuthal Traverse, $\phi = 38$ deg. at $r/D = 0.179$	74

Figure	Page
17. Normalized Velocity Profiles From Azimuthal Traverse, $\phi = 45$ deg. at $r/D = 0.179$	75
18. Normalized Velocity Profiles From Azimuthal Traverse, $\phi = 60$ deg. at $r/D = 0.179$	76
19. Normalized Velocity Profiles From Azimuthal Traverse, $\phi = 70$ deg. at $r/D = 0.179$	77
20. Normalized Velocity Profiles From Azimuthal Traverse, $\phi = 70$ deg. at $r/D = 0.204$	78
21. Normalized Velocity Profiles From Azimuthal Traverse, $\phi = 70$ deg. at $r/D = 0.179$ measured $0.109 D$ Down- stream of Swirler Exit.	79
22. Normalized Velocity Profiles From Azimuthal Traverse, $\phi = 70$ deg. at $r/D = 0.204$ measured $0.109 D$ Down- stream of Swirler Exit.	80

NOMENCLATURE

English Symbols

c	blade chord width
d	swirler exit diameter
D	test section diameter
F	velocity ratio w_o/u_o for case I
G	axial flux of momentum; velocity ratio w_{mo}/u_o for case II
H,I,J	w_{mo}/u_{mo} for cases III - V
p	time-mean pressure, $N/m^2 = Pa$
s	blade spacing or pitch
S	swirl number = $G_\theta/(G_x d/2)$
u,v,w	axial, radial and tangential components of velocity
x,r, θ	axial, radial, azimuthal cylindrical polar coordinates
z	hub-to-swirler diameter ratio d_h/d

Greek Symbols

β	yaw angle of probe = $\tan^{-1} (w/u)$
δ	pitch angle of probe = $\tan^{-1} [v/(u^2 + w^2)^{1/2}]$
θ	azimuth angle
ρ	density
σ	pitch - to - chord ratio
ϕ	swirl vane angle = $\tan^{-1} (w_{in}/u_{in})$, assuming perfect vanes

Subscripts

atm	ambient atmospheric conditions
C,N,S,E,W	center, north, south, east, west pitot pressure ports
h	hub
in	inlet conditions, upstream of swirler
m	maximum profile value
o	value at swirler outlet
x	axial direction
θ	tangential direction
∞	reference value at edge of swirler exit

Superscripts

'	alternate form, neglecting pressure variation; fluctuating quantity
—	time-mean quantity

CHAPTER I

INTRODUCTION

1.1 Combustor Flowfield Investigations

The problem of optimizing gas turbine combustion chamber design is complex, because of the many conflicting design requirements. The need for a more complete understanding of the fluid dynamics of the flow in such combustion chambers has been recognized by designers in recent years, and research is continuing on several fronts to alleviate the problem.

As part of an on-going project at Oklahoma State University, studies are in progress concerned with experimental and theoretical research in 2-D axisymmetric geometries under low speed, nonreacting, turbulent, swirling flow conditions. The flow enters the test section and proceeds into a larger chamber (expansion ratio $D/d = 2$) via a sudden or gradual expansion (side-wall angle $\alpha = 90$ and 45 degrees). Inlet swirl vanes are adjustable to a variety of vane angles with $\phi = 0, 38, 45, 60$ and 70 degrees being emphasized. The general aim of the entire study is to characterize the time-mean and turbulence flowfield, recommend appropriate turbulence model advances, and implement and exhibit results of flowfield predictions. The present contribution concentrates on the time-mean flow characteristics being generated by the upstream annular swirler, using a five-hole pitot probe technique.

1.2 Previous Studies

Research is progressing in several areas related to the flow facility investigation just described. Computer simulation techniques are being used to study the effect of geometry and other parameter changes on the flowfield. An advanced computer code (1) has been developed to predict confined swirling flows corresponding to those studied experimentally. Tentative predictions (2) have now been supplemented by predictions made from realistic inlet conditions (3) for a complete range of swirl strengths with downstream nozzle effects (4). Accuracy of predictions from a computer model is strongly dependent on the inlet boundary conditions used, which are primarily determined by the swirler and its performance at different vane angle settings. In the earlier predictions, the velocity boundary conditions at the inlet to the model combustor were approximated by idealized flat profiles for axial and swirl velocity, with radial velocity assumed to be zero. However, recent measurements taken closer to the swirler exit show that the profiles produced are quite nonuniform, with nonzero radial velocity and nonaxisymmetry.

The flowfield in the test section is being characterized experimentally in a variety of ways. Flow visualization has been achieved via still (5) and movie (6) photography of neutrally buoyant helium-filled soap bubbles and smoke produced by an injector and a smoke wire. Time-mean velocities have been measured with a five-hole pitot probe at low (5) and high (7) swirl strengths. To help in turbulence modeling, complete turbulence measurements have been made on weakly (8) and strongly (9) swirling flows, using a six-orientation single-wire hot-wire technique. An alternative three-wire technique has also been shown to be

useful in the complex flow situations (10).

References to previous work done elsewhere are found in Chapter II, relating to theoretical analysis of swirler performance.

1.3 Scope and Objectives

A key element in swirling flow studies is the swirl generator used. Since it lies at the inlet to the combustor model, the swirler can have a strong influence on the measurements or predictions made downstream. Better definition of the swirler's performance characteristics is needed.

In the present study, the main objective has been to make time-mean velocity measurements as close as possible to the swirler exit, so as to define more accurately the performance characteristics of the swirler. A range of swirl-blade angles ϕ from 0 to 70 deg. is considered. Specific objectives include:

1. Investigate the flow turning effectiveness of flat blades in annular axial vane swirlers at various blade angles, ϕ .
2. Investigate the degree of nonaxisymmetry introduced by vane-type swirlers.
3. Establish correlations between the blade angle ϕ and the velocity profiles and degree of swirl actually produced.
4. Evaluate the applicability of idealized velocity profiles used recently in flowfield prediction codes, and specify more realistic idealized profiles for future use.
5. Provide swirler exit data usable as inlet conditions in prediction codes being used to establish, evaluate, and improve turbulence models.

1.4 Outline of the Thesis

In the previous sections, the scope and objectives of this study were presented, with the significance of the study in relation to past and present work on combustor flowfield investigations being highlighted.

Chapter II describes mathematical derivations from idealized swirler exit velocity profiles, relating the swirl number to the ratio of maximum swirl and axial velocities for several cases.

Chapter III covers the experimental equipment and procedures used for measurement of the swirler exit flowfield. It includes descriptions of the flowfield facility, the swirler, and the five-hole pitot probe and its associated instrumentation. Calibration, measurement, and data reduction procedures are also briefly described.

The first two sections of Chapter IV discuss experimental results from radial and azimuthal traverses, respectively, noting the presence of nonaxisymmetry, recirculation, and strong velocity gradients at the swirler exit plane. A third section describes the results of a check on sensitivity of the measurements to calibration errors. The last section of Chapter IV compares the swirl numbers calculated from measured profiles and from the idealizations of Chapter II to judge the usefulness of the idealized profiles.

Chapter V presents conclusions drawn from the above results and makes recommendations for further research on this topic.

Appendixes A and B include tables and figures, respectively. A description of revisions to the computer program for reduction of five-hole pitot probe data is in Appendix C, and a listing of the program with sample input is in Appendix D.

CHAPTER II

IDEALIZED PROFILE DERIVATIONS

2.1 Idealized Velocity Profiles

All theoretical analyses of swirler performance and most numerical simulations of combustor flowfields have used simple idealized swirler exit velocity profiles. Common assumptions made include flat axial and swirl velocity profiles downstream of the swirler for swirlers with vanes of constant angle (2, 5, 11, 12), and flat axial profile with linear swirl profile (solid-body rotation) for swirlers with helicoidal vanes and for tangential-entry swirl generators (13, 14). These, however, have been shown to be quite unrealistic (3, 12, 15) and to lead to considerable errors in computer simulations (4). Although the best approach for numerical simulations is to use experimentally measured profiles if they are available, idealized profiles are very useful in theoretical work. If more realistic profile assumptions can be developed which are still mathematically tractable, more useful analytical results may be derived. Better idealized profiles would also be useful as inlet boundary conditions for computer modeling when measured data is not available.

Measurements have shown (3) that linear and parabolic profiles of axial velocity are more appropriate for moderate and high swirl cases, and that the swirl velocity also approaches a parabolic profile at high swirl strengths, with most of the flow leaving near the outer boundary of the swirler. Several combinations of linear and parabolic idealized

profiles are shown in Figure 1, along with the flat and linear profile assumptions used in previous studies. Parameters associated with these profiles are investigated in Section 2.3.

2.2 Definition of Swirl Parameters

The swirl number is a nondimensional parameter used to characterize the degree of swirl generated by a swirler. It is defined as follows

$$(13): \quad S = \frac{G_{\theta}}{G_x(d/2)} \quad (1)$$

where the axial flux of angular momentum G_{θ} is given by

$$G_{\theta} = \int_0^{2\pi} d\theta \int_0^{d/2} [\rho u w + \overline{\rho u' w'}] r^2 dr \quad (2)$$

and the axial flux of axial momentum G_x is given by

$$G_x = \int_0^{2\pi} d\theta \int_0^{d/2} [\rho u^2 + \overline{\rho u'^2} + (p - p_{\infty})] r dr \quad (3)$$

and $d/2$ is the swirler exit radius (4). These equations are obtained from appropriate manipulation of the axial and azimuthal momentum equations, respectively. In free jet flows these two expressions are invariant with respect to downstream location. In the axial momentum expression, the pressure term $(p - p_{\infty})$ is given from radial integration of the radial momentum equation (16) by

$$(p - p_{\infty}) = \int_{d/2}^r [\rho w^2 \frac{1}{r}] dr - \overline{\rho v'^2} \quad (4)$$

If the pressure term is omitted from the axial momentum, the dynamic axial momentum flux G_x' is obtained:

$$G_x' = \int_0^{2\pi} d\theta \int_0^{d/2} [\rho u^2 + \overline{\rho u'^2}] r dr \quad (5)$$

This leads to an alternate definition of swirl number (17):

$$S' = \frac{G_{\theta}}{G'_x(d/2)} \quad (6)$$

If turbulent stress terms are neglected, it is apparent that a knowledge of the distribution of the time-mean u and w velocity components across the swirler is sufficient to calculate either swirl number. The idealized exit velocity profiles provide just such knowledge, and expressions relating swirl number to the ratio of maximum exit swirl and axial velocities can now be derived for each of the profile types. As the procedure is similar for each of the five cases, a detailed derivation will be shown for the first case only, with only final results given for the other four.

2.3 Swirl Numbers for Idealized Profiles

By assuming axisymmetric flow and neglecting turbulent stresses as stated previously, the definitions in Equations (2) through (4) reduce to

$$G_{\theta} = 2\pi \int_0^{d/2} [\rho u w] r^2 dr \quad (7)$$

$$G_x = 2\pi \int_0^{d/2} [\rho u^2 + (p - p_{\infty})] r dr \quad (8)$$

and

$$(p - p_{\infty}) = \int_{d/2}^r [\rho w^2 \frac{1}{r}] dr \quad (9)$$

When the expressions for axial and swirl velocity for case I (see Figure 1) are substituted into Equation (7), one obtains

$$G_{\theta} = \frac{2}{3}\pi\rho u_0 w_0 (d/2)^3 \quad (10)$$

Substitution of $w(r) = w_0$ into Equation (9) and integrating produces

$$(p - p_{\infty}) = \rho w_0^2 [\ln(r) - \ln(d/2)] \quad (11)$$

After substituting Equation (11) into Equation (8) and integrating, the expression becomes

$$G_x = \pi\rho u_0^2 (d/2)^2 \left[1 - \frac{1}{2} \left(\frac{w_0}{u_0}\right)^2\right] \quad (12)$$

Finally, putting Equations (10) and (12) into Equation (1) and defining the velocity ratio $F = w_0/u_0$, the swirl number S can be expressed thus:

$$S = \frac{2F/3}{1 - F^2/2} \quad (13)$$

The alternate swirl number S' follows from finding the dynamic axial flux of axial momentum:

$$G'_x = \pi\rho u_0^2 (d/2)^2 \quad (14)$$

Using this in Equation (6) leads to the simple expression,

$$S' = 2F/3 \quad (15)$$

By the same procedure, expressions for S and S' for the other four cases are found to be as follows:

For case II with $u(r) = u_0$, $w(r) = w_{m0} \left(\frac{r}{d/2}\right)$, and defining G as w_{m0}/u_0 :

$$S = \frac{G/2}{1 - G^2/4} \quad (16)$$

and

$$S' = G/2 \quad (17)$$

For case III with $u(r) = u_{mo} \left(\frac{r}{d/2}\right)$, $w(r) = w_{mo} \left(\frac{r}{d/2}\right)$, and defining H as w_{mo}/u_{mo} :

$$S = \frac{4H/5}{1 - H^2/2} \quad (18)$$

and

$$S' = 4H/5 \quad (19)$$

For case IV with $u(r) = u_{mo} \left(\frac{r}{d/2}\right)$, $w(r) = w_{mo} \left(\frac{r}{d/2}\right)^2$, and defining I as w_{mo}/u_{mo} :

$$S = \frac{I}{1 - 3I^2/4} \quad (20)$$

and

$$S' = I \quad (21)$$

Finally, for case V with $u(r) = u_{mo} \left(\frac{r}{d/2}\right)^2$, $w(r) = w_{mo} \left(\frac{r}{d/2}\right)^2$, and defining J as w_{mo}/u_{mo} :

$$S = \frac{4J/7}{1 - 2J^2/3} \quad (22)$$

and

$$S' = 4J/7 \quad (23)$$

Each of these expressions for S and S' may be inverted to yield the velocity ratio as a function of swirl number. A summary of the

inverse relations follows:

Case I -

$$F = \frac{-4/(3S) + [4/(3S)]^2 + 8}{2}$$

$$F = 3S'/2$$

Case II -

$$G = \frac{-2/(S) + [2/(S)]^2 + 16}{2}$$

$$G = 2S'$$

Case III -

$$H = \frac{-8/(5S) + [8/(5S)]^2 + 8}{2}$$

$$H = 5S'/4$$

Case IV -

$$I = \frac{-4/(3S) + [4/(3S)]^2 + 16/3}{2}$$

$$I = S'$$

Case V -

$$J = \frac{-6/(7S) + [6/(7S)]^2 + 6}{2}$$

$$J = 7S'/4$$

Numerical values from each of these expressions are given in Table I, and the same relationships are shown graphically in Fig. 2 for a range of commonly-encountered swirl numbers.

It is evident from the equations alone that the S' expressions are all simple linear relations. The parameters F through J will increase without bound as the swirl number is increased in each case. In contrast, the parameter variation with S shows asymptotic behavior; the exit velocity ratios all approach definite values as swirl number increases. The asymptotic values are also given in Table I.

Although the curves are generally similar in shape, some observations can be made. The curves for cases II and IV are the upper and lower extremes for both the S and S' relations, with the curves for cases I, III, and V falling in between. This may be anticipated since the w profile is of higher order than the u profile for case II (that is, linear versus constant) and the opposite is true for case IV (linear versus parabolic). In the other three cases the u and w profiles are of the same order.

In appraising the usefulness of the idealized profiles, comparison may be made with the measured profiles given later in Chapter IV. As the swirl strength increases from 0 to 70 deg., corresponding profiles of cases I to V appear roughly appropriate. The moderate swirl case ($\phi = 45$ deg.) gives the best match with its corresponding idealization (case III, linear axial and swirl profiles), by visual inspection alone. However, the presence of the hub and central recirculation zone prevent adequate representation by the idealized profiles, as demonstrated by the experimental results discussed in Chapter IV.

CHAPTER III

EXPERIMENTAL EQUIPMENT AND PROCEDURE

3.1 Combustor Flowfield Facility

The installation on which all tests were performed is a low-speed wind tunnel designed and built at Oklahoma State University. It produces uniform flow of relatively low turbulence intensity, with continuously adjustable flow rate. The facility consists of a filtered intake, an axial blower, a stilling chamber, a turbulence management section, and a contoured outlet nozzle. A schematic of the facility is shown in Fig. 2.

The intake consists of a rounded entrance containing fixed inlet guide vanes, surrounded by a coarse-mesh screen box covered with foam rubber panels to filter the incoming ambient air. The blower is a six-bladed propeller-type fan, driven by a 5 h.p. U.S. Varidrive motor which can be continuously varied from 1600 to 3100 rpm.

Air from the blower is expanded into the stilling chamber and passes through several fine mesh screens to help remove the turbulence generated by the blower. The turbulence level is further reduced by passage through the turbulence management section. This section, a round duct of 76 cm diameter, contains a perforated aluminum plate (2 mm diameter holes) followed by a fine mesh screen, a section of packed straws 12.7 cm long, and five more fine mesh screens. Most of the turbulence reduction occurs in this section, and any traces of fan-induced swirl are

effectively removed by the straws.

To reduce the duct diameter down to the 15 cm outlet diameter, a specially contoured nozzle is used. This was designed after the method of Morel (18) to minimize boundary layer growth and produce a uniform top-hat profile, with no separation or instabilities upstream. The nozzle is of molded fiberglass with a steel flange at the outlet for the attachment of various test articles. A 1 cm diameter hole a short distance upstream of the outlet allows for insertion of a standard pitot-static probe to measure the dynamic pressure upstream of the swirler. This measurement, with a small correction for difference in flow area, is used to calculate the swirler inlet reference velocity, u_{in} .

3.2 Swirler

The swirler used in this study is annular with hub and housing diameters of 3.75 and 15.0 cm respectively, giving a hub-to-swirler diameter ratio z of 0.25. The hub has a streamlined parabolic nose facing upstream and a blunt base (corner radius approximately 2 mm) facing downstream. It is supported by four thin rectangular-section struts or spider arms from the housing wall. The base of the hub protrudes approximately 3 mm downstream of the swirler exit plane. Photographs and schematics of the swirler are shown in Figures 3 through 5.

The ten vanes or blades are attached to shafts which pass through the housing wall and allow individual adjustment of each blade's angle. The standard vanes are wedge-shaped for nearly-constant pitch-to-chord ratio σ of approximately 0.68, which according to two-dimensional cascade data should give good flow-turning effectiveness. Sets of vanes with chord widths of 0.5 and 0.75 of the standard width may be

installed to study the effect of increased pitch-to-chord ratio on turning effectiveness, nonaxisymmetry, and radial secondary flow patterns. Vane planforms are shown in Figure 6.

3.3 Five-Hole Pitot Probe and Instrumentation

Velocity profile measurements were made using a five-hole pitot probe (Model DC-125-12-CD by United Sensor Division of United Electrical Controls Co.), one of the few instruments capable of measuring the magnitude and direction of the local time-mean velocity vector simultaneously. Detailed explanations of five-hole pitot operating techniques and basic principles may be found in Reference 5. A schematic of the probe tip geometry showing the velocities and angles measured is given in Figure 7.

The probe is mounted in a traversing mechanism (Model C1000-12 from United Sensor) which in turn is mounted on a 30-cm diameter plexiglass tube which fits closely over the swirler exit flange. This tube comprises the test section for combustor flowfield modeling in related studies (1-10) and creates confined-jet conditions downstream of the swirler. The presence of the test section tube has negligible effect on the flow patterns observed at the swirler exit plane.

The traversing mechanism allows the probe to be translated vertically (on a radial line outward from the test section axis) and rotated 360 degrees about the probe's yaw axis. In addition to the motion permitted by the traverse mechanism, the test section tube on which the traverse mechanism is mounted may be rotated about its axis with respect to the swirler, thereby allowing azimuthal traverses to be performed.

Tubing from the probe's five pressure taps is routed through selec-

tor valves so that pressure differences between any two of the probe's five holes may be measured by a differential pressure transducer (Type 590 Barocel Pressure Sensor by Datametrix Inc., ± 10 torr range). The resulting pressure difference values are then read directly from a digital voltmeter with selectable averaging time-constant (Model 1076 True RMS Voltmeter by TSI, Inc.).

3.4 Calibration, Measurement, and Reduction Procedure

Calibration of the five-hole probe is done using a small free jet which has a contoured nozzle similar to that of the flowfield facility. The probe tip is placed in the uniform parallel flow of the jet potential core and adjusted to zero yaw angle. The probe is then rotated about its pitch axis and values of $(p_N - p_S)$, $(p_C - p_W)$, and $(p_C - p_{atm})$ pressure differences are measured at different values of pitch angle δ .

Velocity measurements with the five-hole probe are made after the probe has been carefully aligned with the facility and the pressure transducer properly zeroed. At each measurement location, the probe is aligned with the local flow direction in the horizontal plane by nulling the pressure difference $(p_E - p_W)$. The value of yaw angle β is then read from the rotary vernier on the traverse mechanism. Finally, values of the pressure differences $(p_N - p_S)$, $(p_C - p_W)$, and $(p_C - p_{atm})$ are measured.

The raw pressure data are reduced by a computer program to yield nondimensionalized values of the u , v , and w velocity components, as well as the static pressure at each location. The reduction program also performs numerical integration on the radial traverses to obtain

values of the axial and angular momentum fluxes, and from these calculates the swirl numbers S and S' . Some details of the reduction procedure are given in Appendix C, the description of changes made to the reduction code, while more general descriptions of the original code are found in references (19) and (20). A listing of the code with sample input and output is given in Appendix D.

CHAPTER IV

EXPERIMENTAL RESULTS

Velocity profiles from both radial and azimuthal traverses for each of the flowfields investigated are now presented and discussed.

Table II gives a summary of the operating conditions used during the studies. With nonswirling conditions, the low fan speed delivers relatively high axial velocity and corresponding Reynolds number. At progressively higher swirl strength conditions, progressively higher fan speeds are used, but even so exit velocities and Reynolds numbers reduce because of increasing flow restriction of the swirler. However, based on a limited study elsewhere (4), it is expected that all flowfields are in the Reynolds number independent regime.

The radial traverses consist of ten points from the centerline to the swirler exit radius, spaced 7.6 mm apart. Of these ten, only seven stations were actually measured since the hub blocked the inner three positions. The azimuthal traverses contain nine points spaced 6 degrees apart at a constant radial distance from the centerline. Azimuth angles θ were taken from -24 to +24 degrees, with the $\theta = 0$ position in line with the shaft of one of the swirl vanes. A diagram showing the traverse patterns on the face of the swirler is given in Figure 8.

Unless otherwise stated all traverses are taken immediately after the swirler exit downstream face with no expansion blocks present. Nominally, this location is $x/D = -0.109$, where the position $x/D = 0.0$

is the expansion station, separated from the swirler in practice (5-10) with one of the expansion blocks. Only for the data presented in Tables XV and XVI and Figures 21 and 22 is the expansion block affixed to the downstream face of the swirler and measurements then taken at $x/D = 0.0$.

4.1 Velocity Profiles From Radial Traverses

Axial, radial and swirl velocity component data are tabulated in Tables III through VIII for radial traverses from the swirler centerline to the swirler exit radius. Data are presented for five values of swirl blade angle: zero (no swirler), zero (with swirler), 38, 45, 60, and 70 deg. Corresponding velocity profile plots are shown in Figure 9 to 14, with the profiles extending from the centerline to twice the exit radius ($r/D = 0.5$ where D is the test section diameter used in associated studies). All velocities shown are normalized with respect to the swirler inlet uniform axial velocity, deduced independently from the pitot-static measurement upstream of the swirler. The outer ten data points are zero in each profile because the presence of the solid boundary of the swirler flange precluded measurements at these locations.

The nonswirling case shown in Fig. 9 has a nearly-flat axial velocity profile, as expected for the plain nozzle opening without the swirler installed. There is no measurable swirl velocity, and the radial velocity is zero except for points very near the edge of the exit, where the flow begins to anticipate the abrupt expansion to twice the exit diameter. The second nonswirling case, see Figure 10, has the swirler installed with the blades set to $\phi = 0$ deg. The traverse was made midway between two blades and away from any of the hub supporting struts. Here again the axial profile is quite flat, with just a slight

increase toward the hub. However, the velocity has increased by nearly 25 percent, because of the decrease in flow area with swirler hub and vanes in place. In addition, the hub induces a negative radial velocity across the entire annulus, overriding the tendency to anticipate the expansion corner. The swirl velocity is, as expected, negligible.

The 38-degree blade-angle case in Figure 11 shows remnants of the flat inlet profile over a small portion of the radius near the outside edge in both the axial and swirl profiles. The presence of the hub now constrains the three innermost points to zero, and the region between the hub and the flat portion in the axial and swirl profiles is approximately linear. The maximum axial velocity is 1.5 times the inlet axial velocity because the flow area is decreased by the hub and also because centrifugal effects have shifted the profile outward. The radial velocity has an irregular profile with a maximum value of one-half the inlet axial velocity.

In the $\phi = 45$ degree case of Figure 12 the flat segments are no longer present and both axial and swirl profiles vary from zero at the hub to a maximum at or near the rim of the swirler in an almost linear fashion. The similar shape and magnitude of the profiles indicates that the turning angle is fairly uniform and only slightly less than 45 degrees. The radial velocity is again irregular, but shows a step at $r/D = 0.1$ similar to that in the axial and swirl profiles; this is probably due to the central recirculation zone downstream beginning to slow down the flow upstream of it.

Profiles ensuing from the case of $\phi = 60$ degrees, see Figure 13, all have a sharply peaked shape, with most of the flow leaving near the outer boundary. The radial component is considerably stronger, with a

peak value nearly twice that of the reference velocity upstream of the swirler. The step in the 45 degree axial profile has now developed into reverse flow, indicating that the central recirculation zone now extends upstream past the exit plane. The reverse flow is accompanied by reduced swirl velocity and very low values of radial velocity. The positive axial velocity adjacent to the hub may be the result of a slight clearance between the blades and the hub, allowing air with greater axial momentum to pass through.

Exit velocity profiles obtained for the strongest swirl case considered ($\phi = 70$ deg.) are shown in Figure 14. Almost all of the flow leaves the swirler at the outside edge. The maximum axial and swirl velocities are approximately 3 and 2.5 times the upstream reference values, respectively, and the velocity gradients across the profiles are quite large. The reverse flow in the center of the axial profile is stronger than in the 60-degree case and is now accompanied by negative or inward radial velocity. This suggests the possibility of a vortex ring structure occurring at the exit of the swirler under high-swirl conditions. The swirl velocity profile remains positive but shows a step corresponding to the outer boundary of the recirculation zone.

4.2 Velocity Profiles from Azimuthal Traverses

An indication of the azimuthal or θ -variation of axial, radial, and swirl velocities is now given for the same vane angle settings used in the radial traverses. The measurements were taken at a constant radial position of $r/D = 0.179$, which in most cases illustrates adequately the azimuthal flow variation. However, measurements at $r/D = 0.204$ were necessary in the $\phi = 70$ degree case to get data more repre-

sentative of the main region of the flow. In addition, azimuthal transverse measurements were taken $0.109 D$ downstream (at $x/D = 0.0$, expansion corner with the 90-degree block installed) for $\phi = 70$ degrees to investigate further the upstream extent of the central recirculation zone. Radial profiles at this location for all degrees of swirl are already available (3).

Measurements in each case span an angle of 48 degrees, somewhat more than the 36 degrees between successive blades. Data are tabulated in numerical form in Tables IX through XVI, and corresponding velocity profiles are given in Figures 15 through 22.

The variations in all normalized velocity components u , v , and w occur in approximately 36-degree cycles, coinciding with the blade spacing. The profiles all show significant variation with azimuthal position, except for those in or near recirculation zones where the w velocity component is dominant. These variations can be attributed to several causes, among them being blade stall from using flat blades at high angles of attack and wakes from blunt trailing edges.

Figure 15 shows the azimuthal profile with the swirler installed, but with the vanes set to zero angle. The $\theta = 0$ degree position is directly downstream of one of the swirl vanes, approximately 3 mm from the trailing edge at the $r/d = 0.179$ position. The velocity defect in the wake of the blade is clearly seen in the axial velocity profile, although the precise accuracy of these measurements is uncertain because of the velocity gradients across the width of the probe. The decreased u -velocity at the left side of the profile is caused by the presence of an upstream strut supporting the hub, located at $\theta = +24$ degrees. The radial velocity is uniformly negative indicating inflow over most of

the range, which agrees well with the results of the radial traverse shown earlier in Figure 10. The radial velocity is positive only in the blade wake region. The swirl velocity, as expected, is effectively zero.

Figure 16 presents the results of an azimuthal traverse for the $\phi = 38$ degrees low-swirl case. The measurement position at $r/D = 0.179$ is in the middle of the flat portion of the radial profile, as may be deduced from observation of Figure 3. The 36-degree cyclic variation from one blade to the next is apparent in each of the profiles. The u and w profiles have a flat portion, apparently between blade wakes, with an average yaw angle of about 39 degrees. This confirms the assumption that the blade pitch/chord ratio of 0.68 is sufficient to adequately turn the flow. In fact, over the rest of the profile, the turning angle is even higher than the blade angle ϕ . The radial velocity shows no flat region and varies the most of the three components. It is also quite large even at this low degree of swirl.

In the case of $\phi = 45$ degrees, Figure 17 illustrates that the 36-degree cycle is not as clear, but nevertheless significant variation exists in all profiles. The radial component is nearly as large as the axial and swirl components in some places, and again exhibits the greatest variation with azimuthal position.

For the 60-degree swirl case of Figure 18 variations with azimuthal position are again evident in all profiles. The variation is less than in the cases seen heretofore, possibly because the main flow has shifted further outward under centrifugal effects and the measurement position is in a region of reduced velocity.

This effect is even more notable in the $\phi = 70$ degrees profiles portrayed in Figure 19. The measurement position is now no longer in

the main exiting flow, but on the edge of the central recirculation zone. The axial velocity here is effectively zero, although considerable swirl and radial velocities are present. The radial velocity, it should be noted, is negative or inward towards the centerline. Azimuthal variations are fairly small here, which is to be expected since the flow is mainly in the azimuthal direction. To get a more representative sample of the exiting flow from the swirler with blades at 70 degrees a traverse was made at the next outward radial station at $r/D = 0.204$. When the velocity profiles shown in Figure 20 are compared with those in the previous figure, the effects of extreme velocity gradients in the radial direction may be perceived. The accuracy of the radial velocity and pitch angle measurements may be suspect in the presence of high radial velocity gradients, but the major features of the flow can still be assessed. In a radial distance of only 7.6 mm, the axial velocity jumps from zero to over 12 m/s. In addition, the swirl velocity increases over 50 percent and the radial velocity changes sign. The 36-degree cyclic variation with blade spacing is again present in all profiles.

To investigate further the complexities of the flow with swirl vane angle $\phi = 70$ degrees, azimuthal traverses were also made 3.25 cm downstream of the location of measurements just discussed. Both radial locations, $r/D = 0.179$ and 0.204 , were investigated at $x/D = 0.0$. This is the axial location of the expansion station in practice, (1,3,5, 7-9) and the 90 degree expansion block was affixed to the downstream face of the swirler for these measurements. The profiles appear in Figures 21 and 22; they may be compared with corresponding profiles from further upstream in Figures 19 and 20, respectively. It appears

from both sets of profiles that the recirculation zone has narrowed somewhat with the additional length before the expansion corner. At the inner radial position ($r/D = 0.179$) of Figure 21, the axial velocity is no longer zero. It is now positive, indicating that the main exit flow has moved slightly further inward. The azimuthal variation is still quite small, however, suggesting that the damping influence of the recirculation zone is still in effect. At the outer radial position ($r/D = 0.204$) of Figure 22 the axial and radial velocities are larger than at the upstream position, also implying that the outer high-velocity zone has moved further inward. The azimuthal variation is again similar to that of the exit-plane position at the same radius.

4.3 Calibration Sensitivity Verification

Since minor variations occur from one probe calibration to the next, it was decided to check the sensitivity of the data reduction procedure to these variations. The case of swirl vane angle $\phi = 70$ degrees was used, at $x/D = -0.109$ and $r/D = 0.179$. The most recent calibration provided the baseline values of the pitch and velocity coefficients, (5,7) which were then varied by increasing the magnitude of each value by ten percent. Three cases were tried: increased pitch coefficient with baseline velocity coefficient, increased velocity coefficient with baseline pitch coefficient, and increased values of both coefficients. The percent difference in the output values of the velocity components is shown in Tables XVII through XIX for each of these three cases respectively.

Referring to Table XVII, changing the pitch coefficient value is seen to affect the radial component the most, as expected. The change

in output stays below ten percent for all but three of the output values. For the case of increased velocity coefficient only, Table XVIII shows a quite uniform increase of less than five percent over all the values. This indicates a relatively predictable, low sensitivity response to changes in the calibration velocity coefficient.

The final case, shown in Table XIX, indicates that increases in both coefficients tend to cancel each other for the radial velocity measurement, which was the most sensitive to pitch coefficient variation. The axial and swirl components increase somewhat, but all variations remain well below ten percent. This relative insensitivity to calibration errors is satisfying but it should be noted if the coefficient changes are of opposite sign in the combined case, errors of greater than ten percent in the radial velocity measurements would probably ensue.

4.4 Swirl Strength Comparison

For comparison with the results of the idealized profile derivations, swirl numbers S and S' were calculated from experimental data using Equations (1) and (6) with the turbulent stress terms omitted. Measured velocities and pressures from the radial traverses described in Section 4.1 were used, with appropriate numerical integration performed by the computer data reduction program described in Appendixes C and D. Since actual wall static pressure measurements were unavailable, the reference pressure P_{∞} was taken as the static pressure measurement at $r/D = 0.230$, the point nearest the outer edge of the swirler. The results are given in Table XX, showing the asymptotic behavior of the flat swirl vanes in producing strong swirl. Also shown

in Table XX is the ratio w_{mo}/u_{mo} for each vane angle, taken from the measured radial traverse data. These ratios were used to compare the actual profiles with the idealized ones.

Two comparisons were made to investigate the usefulness of the idealized profiles. In the first, swirl numbers from the measured profiles were compared with those predicted by the Case I idealization. This was done by making the standard assumption that an "ideal" flat-blade swirler (with an infinite number of infinitely thin blades) operating on a plug flow would produce flat exit profiles as shown in Figure 1, part (a). The flow turning angle would be everywhere equal to the vane angle ϕ , and the ratio $w_o/u_o = F$ would be equal to $\tan \phi$. Corresponding S and S' values for each vane angle are then found using Equations (13) and (15) or Figure 2 with $F = \tan \phi$. The results for the four swirl vane angles used are shown in the left half of Table XXI. It is immediately apparent that the negative S values for $\phi = 60$ and 70 degrees are based on values of F greater than the asymptotic value, and are physically unrealistic. The S values for $\phi = 38$ and 45 degrees are considerably higher than the measured values, while the S' values start close to the measured ones but diverge rapidly at high vane angles. This confirms the unsuitability of the Case I idealization for modeling flat-bladed swirler performance.

The other comparison was done using the "most appropriate" idealized case, as judged by visual comparison of the profile shapes. The measured value of the ratio of maximum profile velocities from Table XX was used instead the $\tan \phi$ assumption, which has no theoretical basis for Cases II-V. Most appropriate cases were determined to be Case I for $\phi = 38$, Case III for $\phi = 45$, and Case V for $\phi = 60$ and 70 degrees. S

and S' values were then determined using Equations (13) and (15), (18) and (19), and (22) and (23). Results are shown in the right-hand side of Table XXI. Again we see considerable discrepancies between the actual and idealized values for both S and S' . Although use of Cases III and V gives a much better match for the higher swirl vane angles, the newer idealized profiles are still inappropriate for modeling actual swirler output. The disparities may be attributed to the presence of the central hub, the upstream extent of the central recirculation zone, and flat swirl-vane ineffectiveness at high angles of attack, with associated wakes and nonaxisymmetries.

CHAPTER V

CLOSURE

5.1 Summary and Conclusions

This study has investigated the performance characteristics of an axial vane-type swirler, used in combustor flowfield measurements and turbulence modeling research. A theoretical analysis of swirl numbers associated with several idealized exit velocity profiles is included, and values of the ratio of maximum swirl velocity to maximum axial velocity at different swirl numbers are tabulated for each case. Measurements of actual swirler exit velocity profiles were made for swirl vane angles $\phi = 0, 38, 45, 60,$ and 70 degrees using a five-hole pitot probe technique. The values of normalized velocity components are tabulated and plotted as part of the data base for the evaluation of flowfield prediction codes and turbulence models.

Assumptions of flat axial and swirl profiles with radial velocity equal to zero were found to be progressively less realistic as the swirler blade angle increases. At low swirl strengths ($\phi = 38$), portions of the u and w profiles remain flat while the v -component is already significant. At moderate swirl $\phi = 45$ degrees, approximately linear profiles of u and w with radius are found, with strong v velocity. At stronger swirl $\phi = 60$ degrees, even more spiked profiles are seen with most of the flow leaving the swirler near its outer edge, and some reverse flow near the hub. At strong swirl $\phi = 70$ degrees,

the profiles are extremely spiked with flow reversal. The central recirculation zone extends upstream of the exit plane, almost to the swirler blades in high-swirl cases. Because of this recirculation and the presence of the hub, none of the idealizations considered could model actual swirl cases adequately.

The flow-turning effectiveness of the flat blades was generally adequate for all vane angles tested. However, the large variations of flow angles and velocities with radius made meaningful comparisons with two-dimensional cascade data impossible. Nonaxisymmetry was found in all swirl cases investigated.

5.2 Recommendations for Further Work

Other aspects of swirler performance not covered by this project include pressure drop across the swirler and the efficiency of swirl generation. It is recommended that these be investigated for the present swirler to allow comparison with values quoted by other swirl researchers.

Development of idealized profiles accounting for annular flow and recirculation is another area in which further work is recommended. This should include relating the ratios at maximum profile velocities to effective vane angles to allow prediction of swirler output for a given vane angle setting.

Finally, it is suggested that an uncertainty analysis be done on the five-hole pitot technique to estimate the effects of turbulence intensity and velocity gradients on the accuracy of measurement results.

REFERENCES

- (1) Lilley, D. G., and Rhode, D. L., A Computer Code for swirling Turbulent Axisymmetric Recirculation Flows in Practical Isothermal Combustor Geometries, NASA CR-3442, Feb. 1982.
- (2) Rhode, D. L., Lilley, D. G., and McLaughlin, D. K., On the Prediction of Swirling Flowfields Found in Axisymmetric Combustor Geometries. ASME Journal of Fluids Engng., Vol. 104, 1982, pp. 378-384.
- (3) Sander, G. F., Annular Vane Swirler Performance. Proceedings, Thirteenth Southwestern Graduate Research Conference in Applied Mechanics, Norman, Oklahoma, April 16-17, 1982, pp. 274-278.
- (4) Abujelala, M. T., and Lilley, D. G., Confined Swirling Flow Predictions, Paper AIAA-83-0316, Reno, Nevada, Jan. 10-13, 1983.
- (5) Rhode, D. L., Lilley, D. G., and McLaughlin, D. K., Mean Flowfields in Axisymmetric Combustor Geometries with Swirl, Paper AIAA 82-0177, Orlando, Florida, Jan. 11-14, 1982. AIAA Journal, 1983 (in press).
- (6) Lilley, D. G., Turbulent Combustor Flowfield Investigation. Paper in Combustion Fundamentals Research Conference, held at NASA Lewis Research Center, Cleveland, Ohio, Oct. 21-22, 1982, pp. 152-168.
- (7) Yoon, H. K., and Lilley, D. G., Five-Hole Pitot Probe Time-Mean Velocity Measurements in Confined Swirling Flows. Paper AIAA-83-0315, Reno, Nevada, January 10-13, 1983.
- (8) Janjua, S. I., McLaughlin, D. K., Jackson, T. W., and Lilley, D. G., Turbulence Measurements in a Confined Jet Using a Six Orientation Hot-Wire Probe Technique, Paper AIAA 82-1262, Cleveland, Ohio, June 21-23, 1982.
- (9) Jackson, T. W., and Lilley, D. G., Swirl Flow Turbulence Measurements Using a Single-Wire Technique. Paper AIAA-83-1202, Seattle, Wash., June 27-29, 1983.
- (10) Janjua, S. I., and McLaughlin, D. K., Turbulence Measurements in a Swirling Confined Jet Flowfield Using a Triple Hot-Wire Probe. Report DT-8178-02, Dynamics Technology, Inc., Torrance, CA, Nov. 1982.

- (11) Kerr, N. M., and Fraser, D., Swirl. Part I: Effect on Axisymmetrical Turbulent Jets. *Journal of the Inst. of Fuel*, Vol. 38, Dec. 1965, pp. 519-526.
- (12) Mathur, M. L., and MacCallum, N. R. L., Swirling Air Jets Issuing from Vane Swirlers. Part I: Free Jets; Part II: Enclosed Jets. *Journal of the Inst. of Fuel*, Vol. 40, May 1967, pp. 214-245.
- (13) Chigier, N. A. and Chervinsky, A., Experimental Investigation of Swirling Vortex Motion in Jets. *Journal of Applied Mechanics*, Vol. 34, June 1967, pp. 443-451.
- (14) Beer, J. M., and Chigier, N. A., *Combustion Aerodynamics*. Applied Science Publishers, London, 1972.
- (15) Beltagui, S. A., and MacCallum, N. R. L., Aerodynamics of Vane-Swirled Flames in Furnaces. *Journal of the Inst. of Fuel*, Vol. 49, Dec. 1976, pp. 183-193.
- (16) Gupta, A. K., and Lilley, D. G., *Flowfield Modeling and Diagnostics*. Abacus Press, Tunbridge Wells, England, 1983 (in press).
- (17) Beltagui, S. A., and MacCallum, N. R. L., The Modelling of Vane-Swirled Flames in Furnaces. *Journal of the Inst. of Fuel*, Vol. 40, Dec. 1976, pp. 193-200.
- (18) Morel, T., *Comprehensive Design of Axisymmetric Wind Tunnel Contractions*. Paper ASME 75-FE-17, Minneapolis, Minnesota, May 5-7, 1975.
- (19) Rhode, D. L., "Predictions and Measurements of Isothermal Flowfields in Axisymmetric Combustor Geometries," Ph.D. Thesis, Dept. of Mechanical and Aerospace Engineering, Oklahoma State University, Dec. 1981.
- (20) Yoon, H. K., "Five-Hole Pitot Probe Time-Mean Velocity Measurements in Confined Swirling Flows," M.S. Thesis, Dept. of Mechanical and Aerospace Engineering, Oklahoma State University, July 1982.
- (21) Bryer, D. W., and Pankhurst, R. C., *Pressure-Probe Methods for Determining Wind Speed and Flow Direction*. Her Majesty's Stationery Office, London, 1971.
- (22) Lilley, D. G., and Rhode, D. L., "A Computer Code for Swirling Turbulent Axisymmetric Recirculating Flows in Practical Isothermal Combustor Geometries," Report NASA CR-3442, NASA Lewis Research Center, Cleveland, Ohio, Feb. 1982.

APPENDIX A

TABLES

TABLE I
 RATIOS OF MAXIMUM SWIRL AND AXIAL VELOCITIES F-J
 OF IDEALIZED PROFILE CASES I - V, FOR COMMON
 VALUES OF SWIRL NUMBERS S AND S'

S	F	S'	F
0.10	0.148	0.10	0.150
0.25	0.352	0.25	0.375
0.50	0.610	0.50	0.750
0.75	0.782	0.75	1.125
1.00	0.897	1.00	1.500
1.50	1.038	1.50	2.250
2.00	1.120	2.00	3.000
∞	1.414	∞	∞

(a) Case I - Flat axial and swirl profiles,
 $F = w_0/u_0$

TABLE I (Continued)

S	G	S'	G
0.10	0.198	0.10	0.200
0.25	0.472	0.25	0.500
0.50	0.828	0.50	1.000
0.75	1.070	0.75	1.500
1.00	2.236	1.00	2.000
1.50	1.442	1.50	3.000
2.00	1.562	2.00	4.000
∞	2.000	∞	∞

(b) Case II - Flat axial and linear swirl profiles,
 $G = w_o/u_{mo}$

TABLE I (Continued)

S	H	S'	H
0.10	0.124	0.10	0.125
0.25	0.299	0.25	0.313
0.50	0.535	0.50	0.625
0.75	0.705	0.75	0.938
1.00	0.825	1.00	1.250
1.50	0.978	1.50	1.875
2.00	1.070	2.00	2.500
∞	1.414	∞	∞

(c) Case III - Linear axial and swirl profiles,
 $H = w_{mo}/u_{mo}$

TABLE I (Continued)

S	I	S'	I
0.10	0.099	0.10	0.100
0.25	0.239	0.25	0.250
0.50	0.431	0.50	0.50
0.75	0.568	0.75	0.750
1.00	0.667	1.00	1.000
1.50	0.793	1.50	1.500
2.00	0.869	2.00	2.000
∞	1.155	∞	∞

(d) Case IV - Parabolic axial and linear swirl profiles, $I = w_{mo}/u_{mo}$

TABLE I (Continued)

S	J	S'	J
0.10	0.172	0.10	0.175
0.25	0.393	0.25	0.438
0.50	0.638	0.50	0.875
0.75	0.780	0.75	1.313
1.00	0.869	1.00	1.750
1.50	0.972	1.50	2.625
2.00	1.029	2.00	3.500
∞	1.225	∞	∞

(e) Case V - Parabolic axial and swirl profiles,
 $J = w_{mo}/u_{mo}$

TABLE II
SUMMARY OF OPERATING CONDITIONS

ϕ (degrees)	FS (rpm)	u_{in} (m/s)	$Re_d \times 10^{-5}$
0	1950	23.00	2.22
38	2265	13.30	1.30
45	2600	13.00	1.26
60	2800	9.20	0.90
70	2800	5.52	0.53

* Abbreviations used are:

ϕ Swirl vane angle

FS Fan speed

u_{in} Spatial-mean swirler exit axial velocity, deduced from independent upstream measurement, excluding presence of the hub and swirler

Re_d Swirler-exit Reynolds number based on u_{in} and swirler diameter

TABLE III
 NORMALIZED VELOCITY COMPONENTS, YAW ANGLE, PITCH
 ANGLE, AND STATIC PRESSURE DIFFERENCE ($p-p_\infty$)
 FROM RADIAL TRAVERSE, $\phi = 0$ DEG.
 (NO SWIRLER)

J	R/D	U/UIN	V/UIN	W/UIN	BETA	DELTA	P-PREF
10	0.230	1.025	0.058	-0.000	360.0	3.3	0.00
9	0.204	1.011	0.038	-0.000	360.0	2.1	11.12
8	0.179	1.001	0.020	-0.000	360.0	1.1	18.46
7	0.153	0.997	0.010	-0.000	360.0	0.6	21.07
6	0.128	0.996	0.008	-0.000	360.0	0.4	21.33
5	0.102	0.997	0.006	-0.000	360.0	0.3	21.93
4	0.077	0.997	0.011	-0.000	360.0	0.7	21.65
3	0.051	0.996	0.017	-0.000	360.0	1.0	0.00
2	0.026	0.995	0.021	-0.000	360.0	1.2	0.00
1	0.000	0.995	0.022	-0.000	360.0	1.3	0.00

TABLE IV

NORMALIZED VELOCITY COMPONENTS, YAW ANGLE, PITCH ANGLE, AND
 STATIC PRESSURE DIFFERENCE ($p-p_\infty$) FROM RADIAL TRAVERSE,
 $\phi = 0$ DEG. (SWIRLER INSTALLED)

J	R/D	U/UIN	V/UIN	W/UIN	BETA	DELTA	P-PREF
10	0.230	1.219	-0.019	0.000	0.0	-0.9	0.00
9	0.204	1.204	-0.046	-0.006	-0.3	-2.2	9.74
8	0.179	1.210	-0.063	0.000	0.0	-3.0	5.87
7	0.153	1.209	-0.073	-0.002	-0.1	-3.4	6.66
6	0.128	1.203	-0.091	-0.004	-0.2	-4.3	8.15
5	0.102	1.214	-0.092	0.002	0.1	-4.3	1.97
4	0.077	1.220	-0.102	0.011	0.5	-4.8	-6.51
3	0.051	0.000	0.000	0.000	0.0	0.0	0.00
2	0.026	0.000	0.000	0.000	0.0	0.0	0.00
1	0.000	0.000	0.000	0.000	0.0	0.0	0.00

TABLE V
 NORMALIZED VELOCITY COMPONENTS, YAW ANGLE, PITCH ANGLE, AND
 STATIC PRESSURE DIFFERENCE ($p-p_\infty$) FROM RADIAL TRAVERSE,
 $\phi = 38$ DEG.

J	R/D	U/U _{IN}	V/U _{IN}	W/U _{IN}	BETA	DELTA	P-PREF
10	0.230	1.018	0.176	0.751	36.4	7.9	0.00
9	0.204	1.435	0.364	1.145	38.6	11.2	1.78
8	0.179	1.417	0.385	1.139	38.8	11.9	9.09
7	0.153	1.454	0.486	1.112	37.4	14.9	-11.31
6	0.128	1.080	0.352	0.843	38.0	14.4	-17.49
5	0.102	0.817	0.250	0.483	30.6	14.8	-18.95
4	0.077	0.187	0.231	0.251	53.4	36.5	-16.45
3	0.051	0.000	0.000	0.000	0.0	0.0	0.00
2	0.026	0.000	0.000	0.000	0.0	0.0	0.00
1	0.000	0.000	0.000	0.000	0.0	0.0	0.00

TABLE VI
 NORMALIZED VELOCITY COMPONENTS, YAW ANGLE, PITCH ANGLE, AND
 STATIC PRESSURE DIFFERENCE ($p-p_\infty$) FROM RADIAL TRAVERSE,
 $\phi = 45$ DEG.

J	R/D	U/UIN	V/UIN	W/UIN	BETA	DELTA	P-PREF
10	0.230	1.706	0.584	1.494	41.2	14.4	0.00
9	0.204	1.662	0.522	1.539	42.8	13.0	5.35
8	0.179	1.540	0.541	1.396	42.2	14.6	-19.76
7	0.153	1.089	0.528	0.914	40.0	20.4	-43.66
6	0.128	0.672	0.549	0.632	43.2	30.8	-55.18
5	0.102	0.356	0.343	0.553	57.2	27.5	-56.10
4	0.077	0.351	0.332	0.196	29.2	39.5	-51.58
3	0.051	0.000	0.000	0.000	0.0	0.0	0.00
2	0.026	0.000	0.000	0.000	0.0	0.0	0.00
1	0.000	0.000	0.000	0.000	0.0	0.0	0.00

TABLE VII
 NORMALIZED VELOCITY COMPONENTS, YAW ANGLE, PITCH ANGLE, AND
 STATIC PRESSURE DIFFERENCE ($p-p_\infty$) FROM RADIAL TRAVERSE,
 $\phi = 60$ DEG.

J	R/D	U/UI ∞	V/UI ∞	W/UI ∞	BETA	DELTA	P-PREF
10	0.230	2.421	1.698	2.273	43.2	27.1	0.00
9	0.204	1.802	1.420	1.358	37.0	32.2	-14.52
8	0.179	1.312	1.070	0.982	36.8	33.1	-50.38
7	0.153	0.562	0.450	0.833	56.0	24.1	-34.46
6	0.128	-0.087	0.059	0.504	99.8	6.5	-37.27
5	0.102	-0.059	0.096	0.420	98.0	12.7	-40.04
4	0.077	0.546	0.068	0.527	44.0	5.1	-50.51
3	0.051	0.000	0.000	0.000	0.0	0.0	0.00
2	0.026	0.000	0.000	0.000	0.0	0.0	0.00
1	0.000	0.000	0.000	0.000	0.0	0.0	0.00

TABLE VIII
 NORMALIZED VELOCITY COMPONENTS, YAW ANGLE, PITCH ANGLE, AND
 STATIC PRESSURE DIFFERENCE ($p-p_\infty$) FROM RADIAL TRAVERSE,
 $\phi = 70$ DEG.

J	R/D	U/UIIN	V/UIIN	W/UIIN	BETA	DELTA	P-PREF
10	0.230	3.005	1.647	2.668	41.6	22.3	0.00
9	0.204	1.817	0.800	1.514	39.8	18.7	-18.26
8	0.179	0.176	0.034	1.001	80.0	1.9	-21.90
7	0.153	-0.512	-0.131	0.987	117.4	-6.7	-26.30
6	0.128	-0.475	-0.145	0.721	123.4	-9.5	-28.47
5	0.102	-0.158	-0.068	0.424	110.4	-8.5	-31.18
4	0.077	0.731	0.473	0.706	44.0	25.0	-36.11
3	0.051	0.000	0.000	0.000	0.0	0.0	0.00
2	0.026	0.000	0.000	0.000	0.0	0.0	0.00
1	0.000	0.000	0.000	0.000	0.0	0.0	0.00

TABLE IX

NORMALIZED VELOCITY COMPONENTS, YAW ANGLE, PITCH ANGLE, AND
 STATIC PRESSURE DIFFERENCE ($p-p_\infty$) FROM AZIMUTHAL
 TRAVERSE, $\phi = 0$ DEG. AT $r/D = 0.179$
 (SWIRLER INSTALLED)

K	THETA (DEG.)	U/UIIN	V/UIIN	W/UIIN	BETA	DELTA	P-PREF
1	-24.0	1.196	-0.066	-0.013	-0.6	-3.2	7.83
2	-18.0	1.196	-0.066	0.000	0.0	-3.1	8.60
3	-12.0	1.197	-0.065	0.013	0.6	-3.1	9.84
4	-6.0	1.199	-0.047	0.040	1.9	-2.2	7.20
5	0.0	0.278	0.201	0.002	0.5	35.9	46.01
6	6.0	1.201	-0.049	-0.042	-2.0	-2.4	8.12
7	12.0	1.201	-0.060	-0.010	-0.5	-2.9	8.85
8	18.0	1.174	-0.059	0.012	0.6	-2.9	8.20
9	24.0	0.992	-0.075	0.031	1.8	-4.3	12.15

TABLE X

NORMALIZED VELOCITY COMPONENTS, YAW ANGLE, PITCH ANGLE, AND
STATIC PRESSURE DIFFERENCE ($p-p_\infty$) FROM AZIMUTHAL
TRAVERSE, $\phi = 38$ DEG. AT $r/D = 0.179$

K	THETA (DEG.)	U/UIIN	V/UIIN	W/UIIN	BETA	DELTA	P-PREF
1	-24.0	1.342	0.637	1.187	41.5	19.6	-16.93
2	-18.0	1.236	0.453	1.067	40.8	15.5	2.72
3	-12.0	1.153	0.171	0.971	40.1	6.5	17.41
4	-6.0	1.488	0.184	1.192	38.7	5.5	0.95
5	0.0	1.486	0.307	1.186	38.6	9.2	0.02
6	6.0	1.458	0.419	1.189	39.2	12.6	1.75
7	12.0	1.408	0.536	1.228	41.1	16.0	-7.77
8	18.0	1.288	0.523	1.100	40.5	17.2	1.99
9	24.0	1.141	0.172	1.003	41.3	6.5	19.69

TABLE XI

NORMALIZED VELOCITY COMPONENTS, YAW ANGLE, PITCH ANGLE, AND
STATIC PRESSURE DIFFERENCE ($p-p_\infty$) FROM AZIMUTHAL
TRAVERSE, $\phi = 45$ DEG. AT $r/D = 0.179$

K	THETA (DEG.)	U/UIN	V/UIN	W/UIN	BETA	DELTA	P-PREF
1	-24.0	1.770	0.864	1.495	40.2	20.5	0.95
2	-18.0	1.683	1.175	1.443	40.6	27.9	4.71
3	-12.0	1.602	1.137	1.344	40.0	28.5	6.13
4	-6.0	1.473	0.530	1.402	43.6	14.6	1.79
5	0.0	1.658	0.416	1.579	43.6	10.3	-4.27
6	6.0	1.759	0.594	1.617	42.6	14.0	-8.37
7	12.0	1.721	0.828	1.616	43.2	19.3	-14.20
8	18.0	1.582	1.132	1.527	44.0	27.2	-22.61
9	24.0	1.201	0.764	1.059	41.4	25.5	-11.50

TABLE XII

NORMALIZED VELOCITY COMPONENTS, YAW ANGLE, PITCH ANGLE, AND
 STATIC PRESSURE DIFFERENCE ($p-p_\infty$) FROM AZIMUTHAL
 TRAVERSE, $\phi = 60$ DEG. AT $r/D = 0.179$

K	THETA (DEG.)	U/U _{IN}	V/U _{IN}	W/U _{IN}	BETA	DELTA	P-PREF
1	-24.0	1.144	0.296	1.210	46.6	10.1	-38.21
2	-18.0	1.112	0.406	1.257	48.5	13.6	-42.42
3	-12.0	1.067	0.529	1.185	48.0	18.3	-45.72
4	-6.0	1.107	0.596	1.062	43.8	21.2	-45.79
5	0.0	1.266	0.474	1.062	40.0	16.0	-44.74
6	6.0	1.351	0.324	1.216	42.0	10.1	-42.74
7	12.0	1.255	0.266	1.272	45.4	8.5	-42.11
8	18.0	1.011	0.226	1.123	48.0	8.5	-41.13
9	24.0	0.770	0.217	0.885	49.0	10.5	-16.09

TABLE XIII

NORMALIZED VELOCITY COMPONENTS, YAW ANGLE, PITCH ANGLE, AND
 STATIC PRESSURE DIFFERENCE ($p-p_\infty$) FROM AZIMUTHAL
 TRAVERSE, $\phi = 70$ DEG. AT $r/D = 0.179$

K	THETA (DEG.)	U/UIIN	V/UIIN	W/UIIN	BETA	DELTA	P-PREF
1	-24.0	0.034	-0.564	0.940	87.9	-30.9	-15.94
2	-18.0	0.011	-0.501	1.013	89.4	-26.3	-19.90
3	-12.0	-0.028	-0.445	1.004	91.6	-23.9	-20.27
4	-6.0	-0.017	-0.454	0.904	91.1	-26.7	-17.05
5	0.0	-0.022	-0.507	0.785	91.6	-32.9	-12.72
6	6.0	-0.024	-0.566	0.697	92.0	-39.0	-9.51
7	12.0	-0.049	-0.580	0.779	93.6	-36.6	-12.59
8	18.0	-0.042	-0.575	0.849	92.8	-34.1	-15.25
9	24.0	-0.011	-0.538	0.890	90.7	-31.1	-17.20

TABLE XIV

NORMALIZED VELOCITY COMPONENTS, YAW ANGLE, PITCH ANGLE, AND
STATIC PRESSURE DIFFERENCE ($p-p_\infty$) FROM AZIMUTHAL
TRAVERSE, $\phi = 70$ DEG. AT $r/D = 0.204$

K	THETA (DEG.)	U/UIN	V/UIN	W/UIN	BETA	DELTA	P-PREF
1	-24.0	2.184	0.187	1.866	40.5	3.7	-25.25
2	-18.0	2.087	0.133	1.840	41.4	2.7	-24.29
3	-12.0	1.859	0.174	1.645	41.5	4.0	-22.25
4	-6.0	1.512	0.244	1.343	41.6	6.9	-23.43
5	0.0	1.480	0.337	1.251	40.2	9.9	-23.85
6	6.0	1.883	0.368	1.542	39.3	8.6	-27.46
7	12.0	2.125	0.205	1.783	40.0	4.2	-24.44
8	18.0	2.127	0.126	1.849	41.0	2.6	-23.18
9	24.0	1.909	0.171	1.683	41.4	3.8	-22.15

TABLE XV

NORMALIZED VELOCITY COMPONENTS, YAW ANGLE, PITCH ANGLE, AND
 STATIC PRESSURE DIFFERENCE ($p-p_\infty$) FROM AZIMUTHAL
 TRAVERSE, $\phi = 70$ DEG. AT $r/D = 0.179$ MEASURED
 0.109 D DOWNSTREAM OF SWIRLER EXIT

K	THETA (DEG.)	U/UIIN	V/UIIN	W/UIIN	BETA	DELTA	P-PREF
1	-24.0	0.350	-0.691	1.041	71.4	-32.2	-10.99
2	-18.0	0.503	-0.613	1.246	68.0	-24.5	-16.03
3	-12.0	0.592	-0.523	1.401	67.1	-19.0	-20.74
4	-6.0	0.613	-0.479	1.473	67.4	-16.7	-21.19
5	0.0	0.595	-0.493	1.473	68.0	-17.2	-20.73
6	6.0	0.604	-0.441	1.495	68.0	-15.3	-21.83
7	12.0	0.621	-0.375	1.544	68.1	-12.7	-23.21
8	18.0	0.565	-0.350	1.526	69.7	-12.2	-22.75
9	24.0	0.470	-0.358	1.483	72.4	-13.0	-23.62

TABLE XVI

NORMALIZED VELOCITY COMPONENTS, YAW ANGLE, PITCH ANGLE, AND
 STATIC PRESSURE DIFFERENCE ($p-p_\infty$) FROM AZIMUTHAL
 TRAVERSE, $\phi = 70$ DEG. AT $r/D = 0.204$ MEASURED
 0.109 D DOWNSTREAM OF SWIRLER EXIT

K	THETA (DEG.)	U/UIIN	V/UIIN	W/UIIN	BETA	DELTA	P-PREF
1	-24.0	2.023	-0.129	2.608	52.2	-2.2	-25.43
2	-18.0	2.155	-0.042	2.798	52.4	-0.7	-27.87
3	-12.0	2.007	-0.055	2.588	52.2	-1.0	-27.34
4	-6.0	1.805	-0.089	2.270	51.5	-1.8	-18.39
5	0.0	1.913	-0.059	2.271	49.9	-1.1	-17.06
6	6.0	2.265	-0.011	2.643	49.4	-0.2	-25.08
7	12.0	2.307	0.046	2.789	50.4	0.7	-26.46
8	18.0	2.105	0.064	2.627	51.3	1.1	-28.21
9	24.0	1.755	-0.021	2.270	52.3	-0.4	-22.52

TABLE XVII

CALIBRATION SENSITIVITY COMPARISON, ACTUAL VS. 10% HIGHER
PITCH COEFFICIENT ONLY

K	θ (deg.)	Percent Difference		
		u/u_{in}	v/u_{in}	w/u_{in}
1	-24.0	1.91	-8.22	1.91
2	-18.0	0.80	-10.23	0.80
3	-12.0	0.27	-11.43	0.27
4	-6.0	0.92	-10.01	0.92
5	0.0	2.15	-7.89	2.15
6	6.0	1.87	-7.27	2.87
7	12.0	2.55	-7.51	2.55
8	18.0	2.29	-7.73	2.29
9	24.0	1.93	-8.17	1.93

TABLE XVIII
 CALIBRATION SENSITIVITY COMPARISON, ACTUAL VS. 10% HIGHER
 VELOCITY COEFFICIENT ONLY

K	θ (deg.)	Percent Difference		
		u/u_{in}	v/u_{in}	w/u_{in}
1	-24.0	4.86	4.86	4.86
2	-18.0	4.88	4.88	4.88
3	-12.0	4.88	4.88	4.88
4	-6.0	4.88	4.88	4.88
5	0.0	4.86	4.86	4.86
6	6.0	4.88	4.88	4.88
7	12.0	4.87	4.87	4.87
8	18.0	4.87	4.87	4.87
9	24.0	4.86	4.86	4.86

TABLE XIX

CALIBRATION SENSITIVITY COMPARISON, ACTUAL VS. 10% HIGHER,
BOTH PITCH AND VELOCITY COEFFICIENTS

K	θ (deg.)	Percent Difference		
		u/u_{in}	v/u_{in}	w/u_{in}
1	-24.0	6.87	-3.75	6.87
2	-18.0	5.72	-5.85	5.72
3	-12.0	5.15	-7.12	5.15
4	-6.0	5.84	-5.62	5.84
5	0.0	7.12	-3.41	7.12
6	6.0	7.88	-2.75	7.88
7	12.0	7.54	-3.01	7.54
8	18.0	7.27	-3.25	7.27
9	24.0	6.90	-3.70	6.90

TABLE XX
SWIRL NUMBERS S AND S' FROM RADIAL TRAVERSES

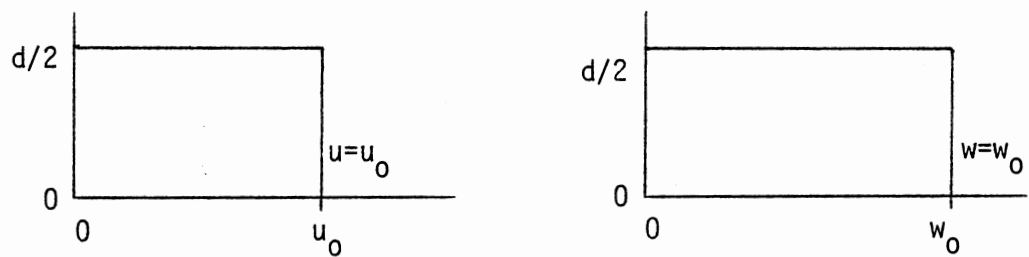
ϕ	S	S'	w_{mo}/u_{mo}
38	0.567	0.559	0.801
45	0.765	0.718	0.876
60	0.850	0.759	0.937
70	0.883	0.750	0.887

TABLE XXI
THEORETICAL SWIRL NUMBERS
BY TWO METHODS

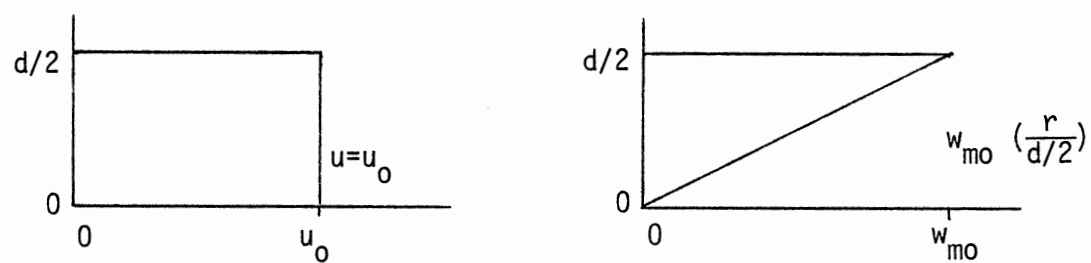
ϕ	Ideal Case I		Most Appropriate Case	Case	
	S	S'		S	S'
38	0.750	0.521	I	0.786	0.534
45	1.333	0.667	III	1.137	0.584
60	-2.309	1.155	V	1.291	0.625
70	-0.660	1.832	V	1.066	0.591

APPENDIX B

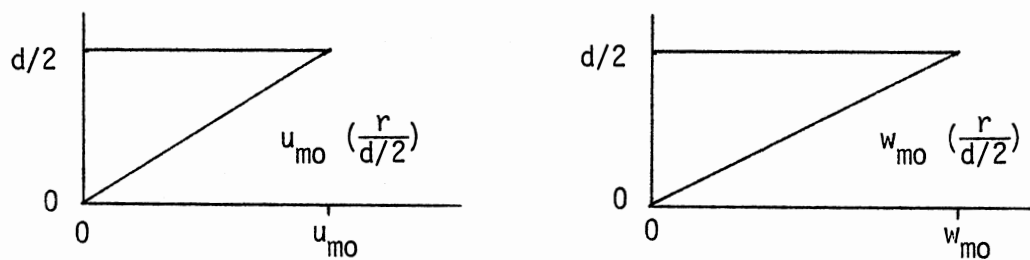
FIGURES



(a) Case I - Flat Axial and Swirl Profiles

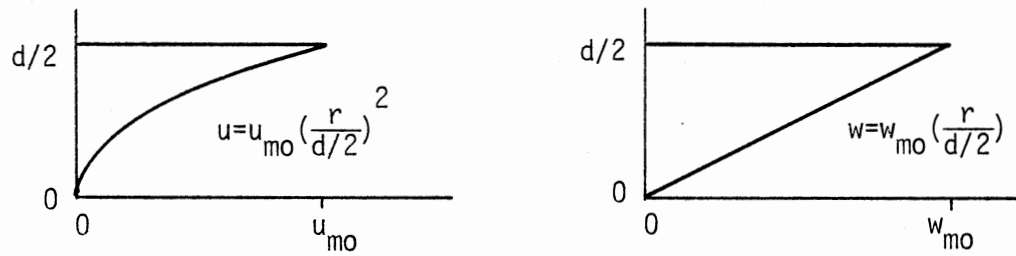


(b) Case II - Flat Axial and Linear Swirl Profiles

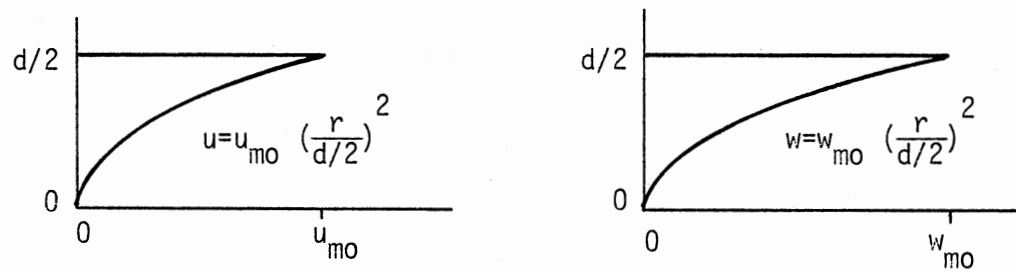


(c) Case III - Linear Axial and Swirl Profiles

Figure 1. Idealized Axial and Tangential Velocity Profile Cases



(d) Case IV - Parabolic Axial and Linear Swirl Profiles



(e) Case V - Parabolic Axial and Swirl Profiles

Figure 1 (continued)

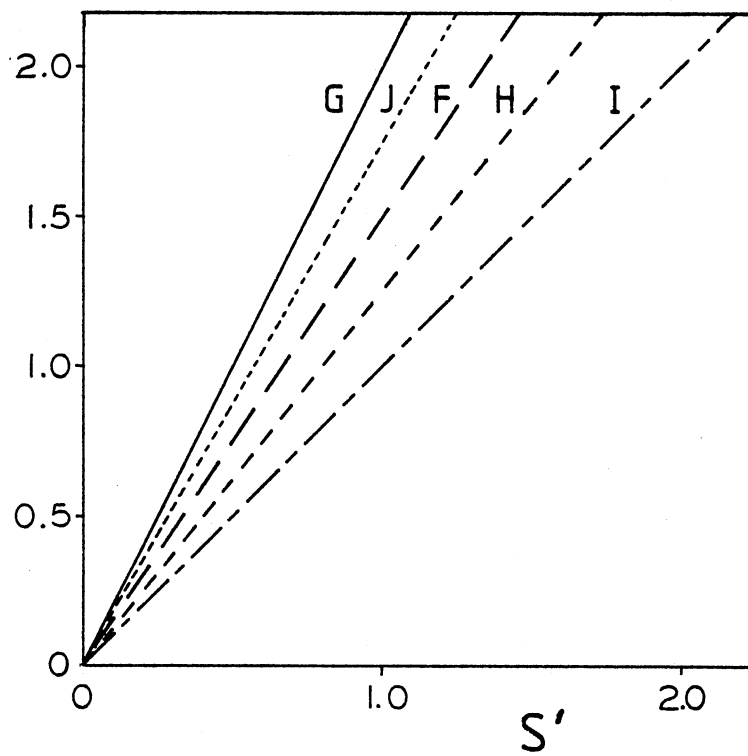
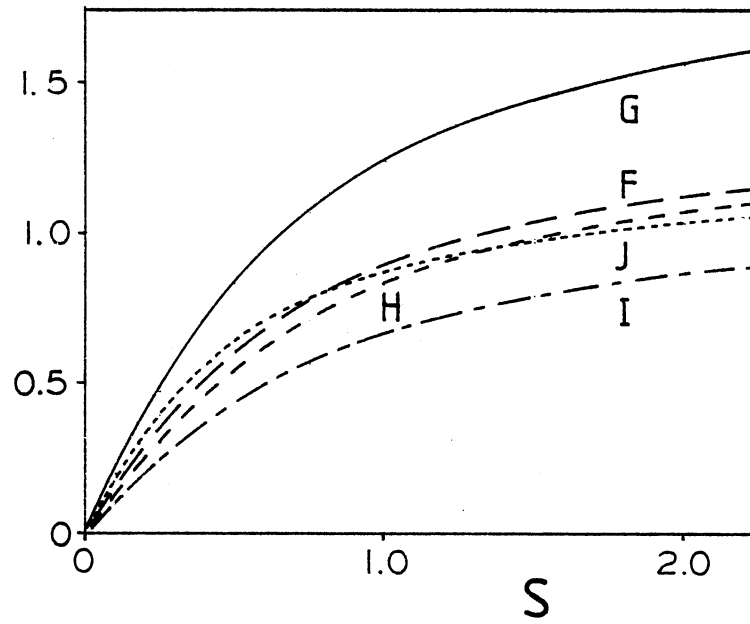


Figure 2. Variation of Velocity Ratios F Through J (Cases I Through V, respectively) with S and S'

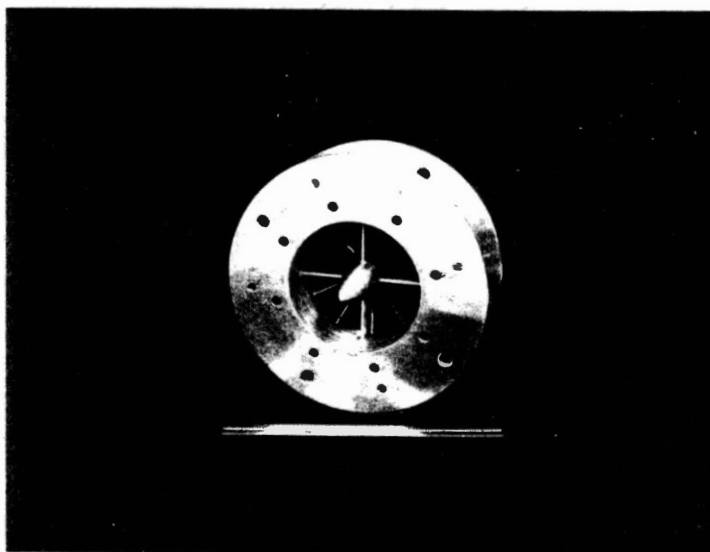


Figure 3. Photograph of Swirler - Upstream End

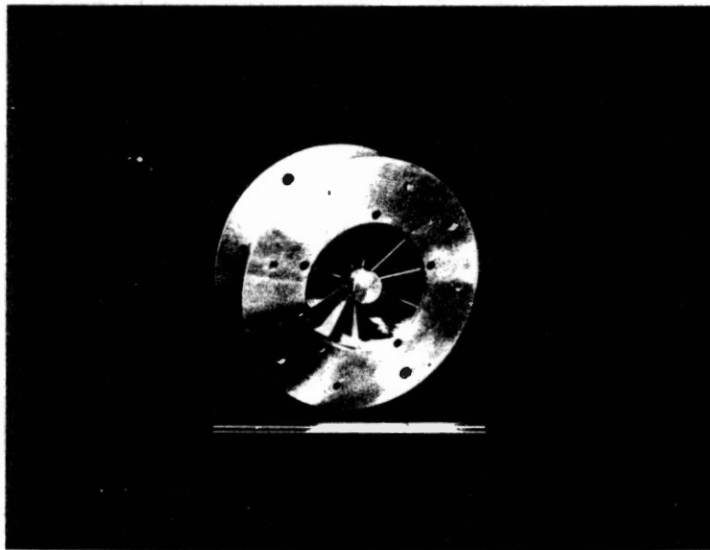


Figure 4. Photograph of Swirler - Downstream End

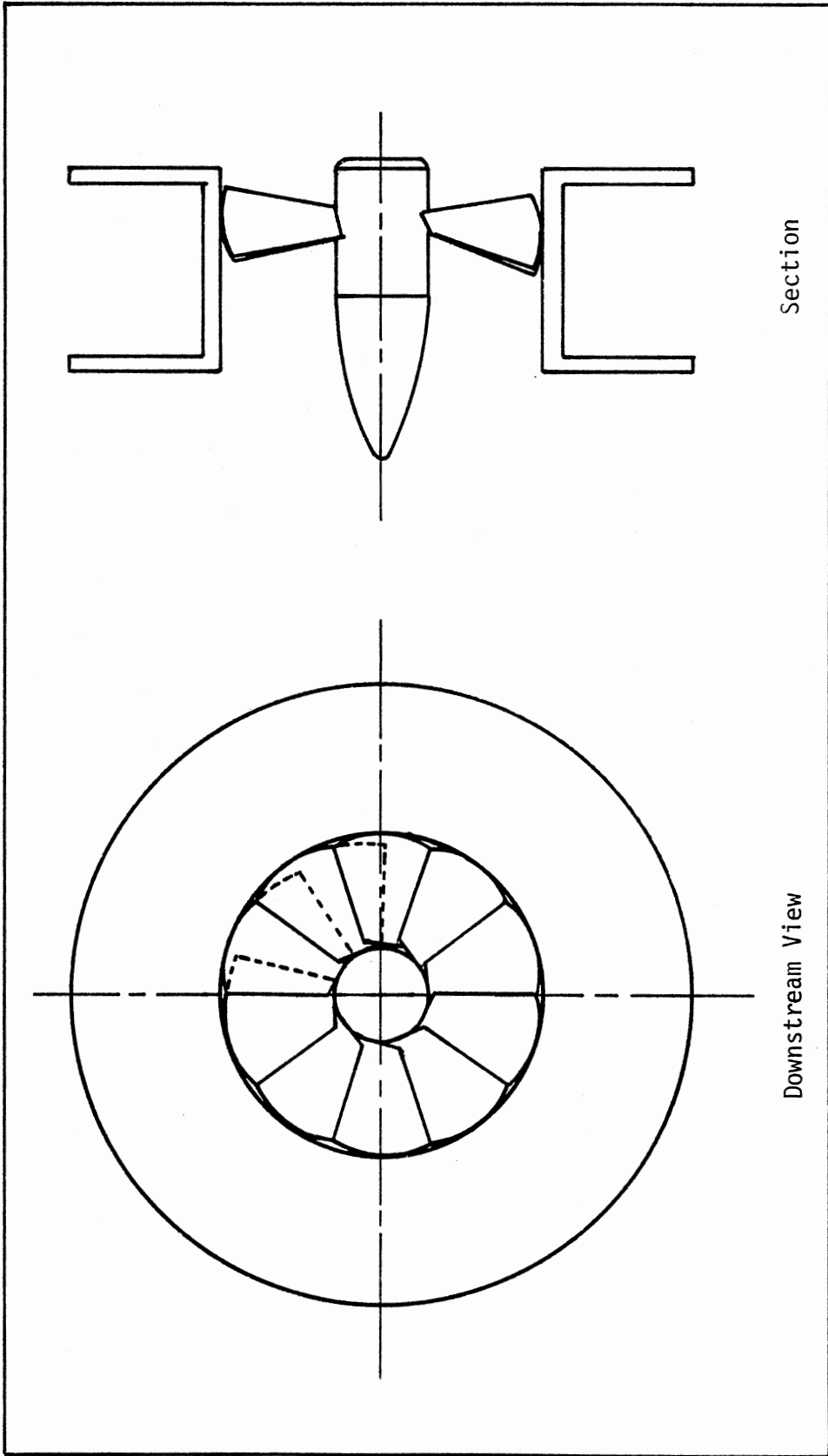


Figure 5. Diagram of Swirler - Section and Downstream View

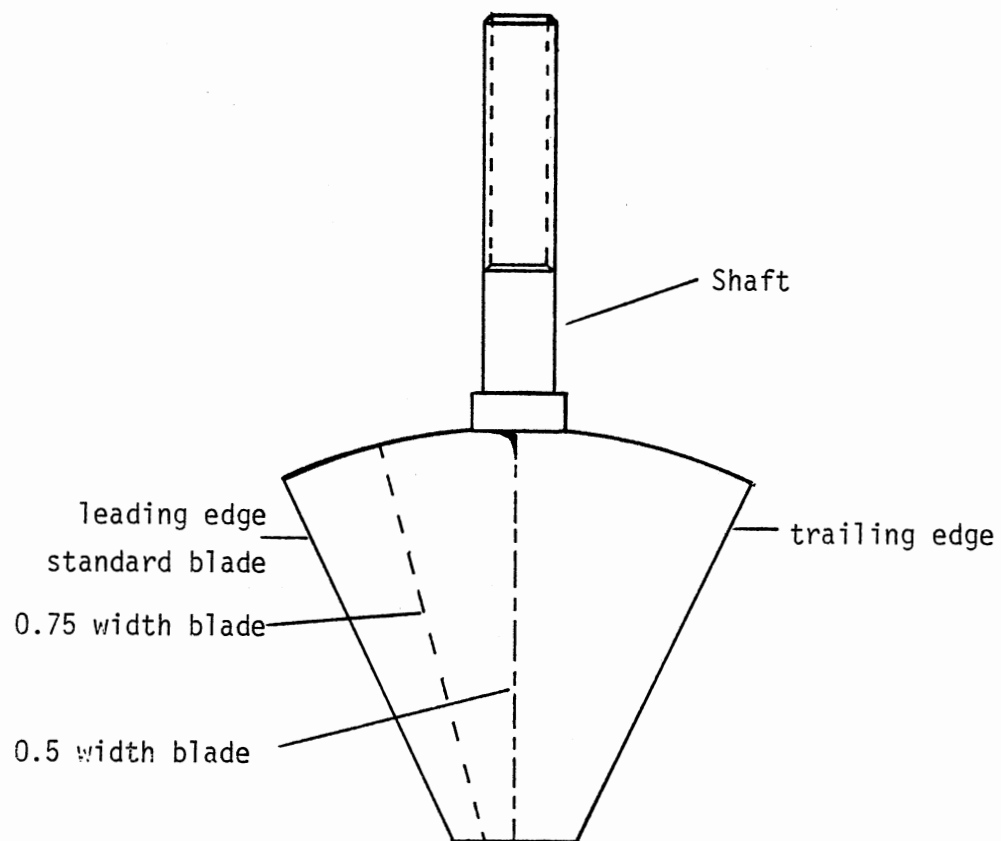


Figure 6. Swirl Vanes

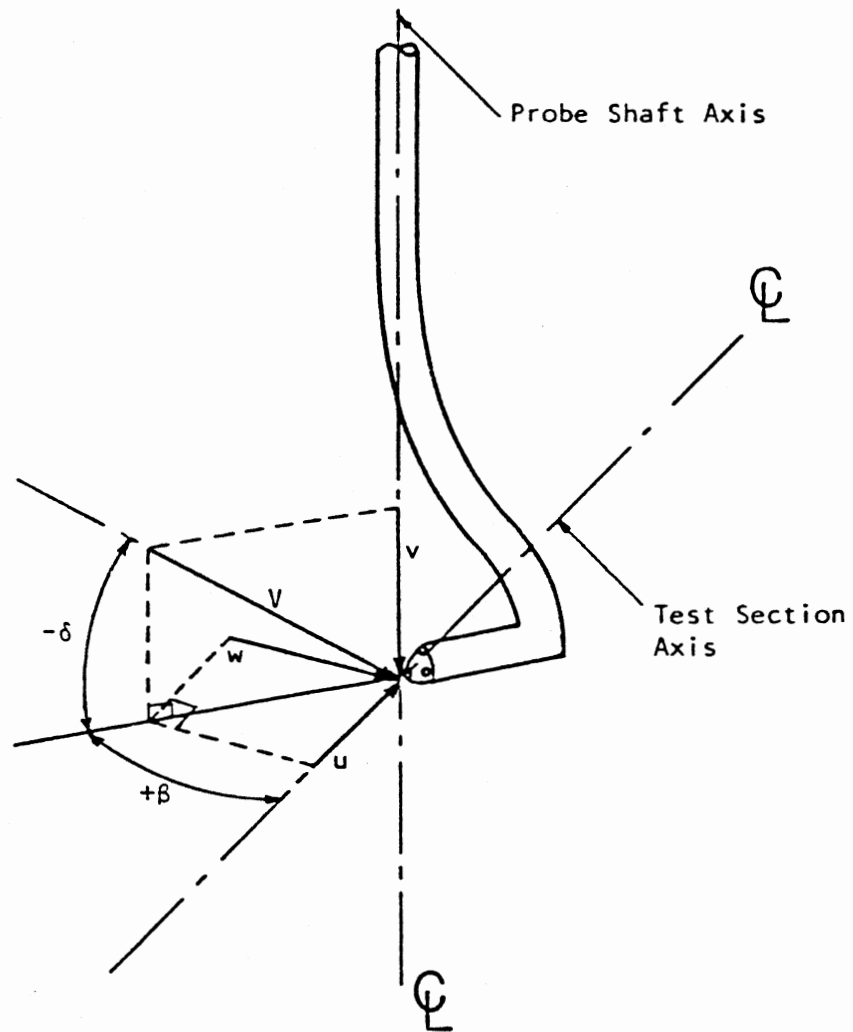


Figure 7. Five-Hole Pitot Probe With Angles and Velocities Measured

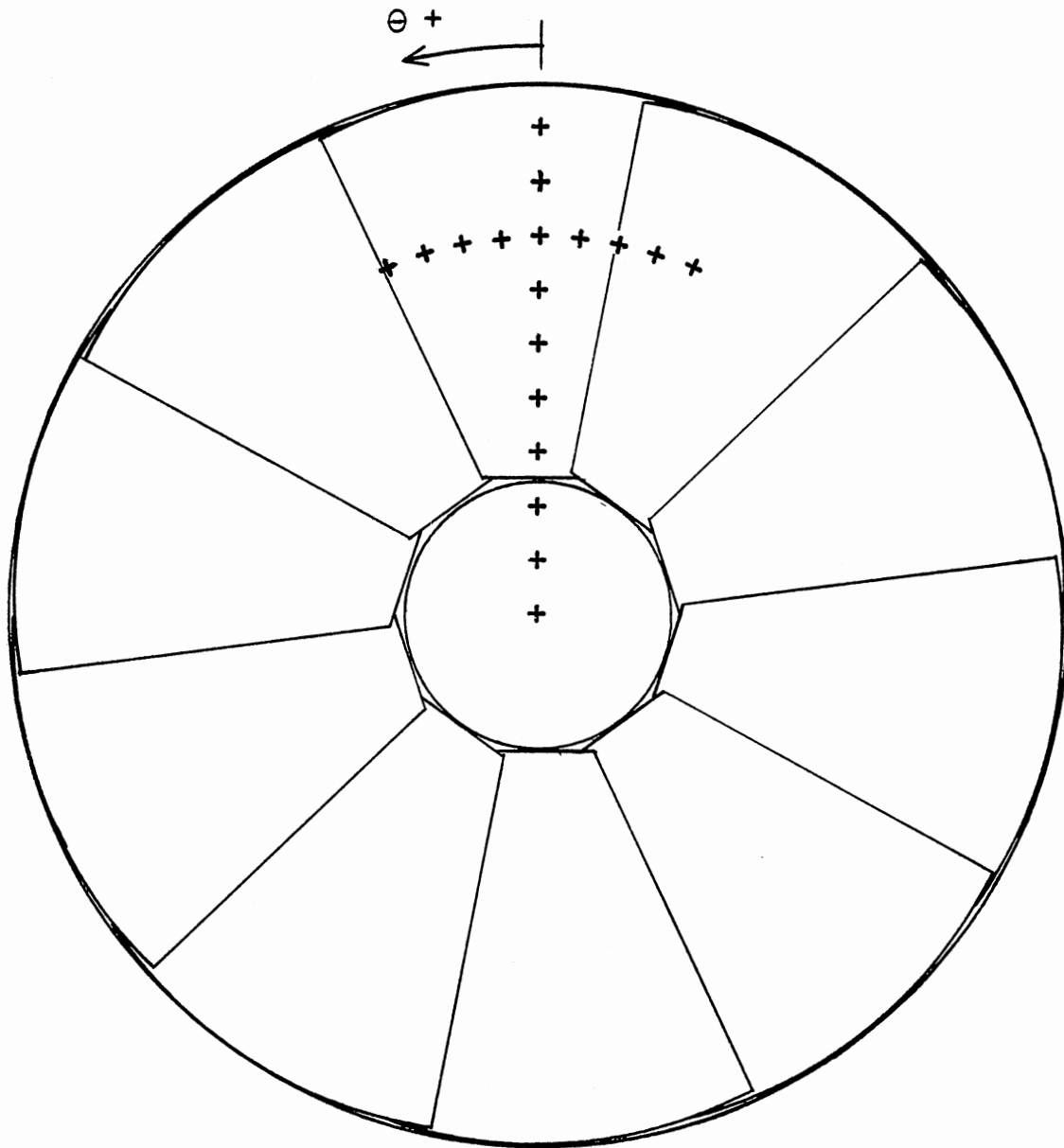


Figure 8. Measurement Locations - Radial and Azimuthal Traverses

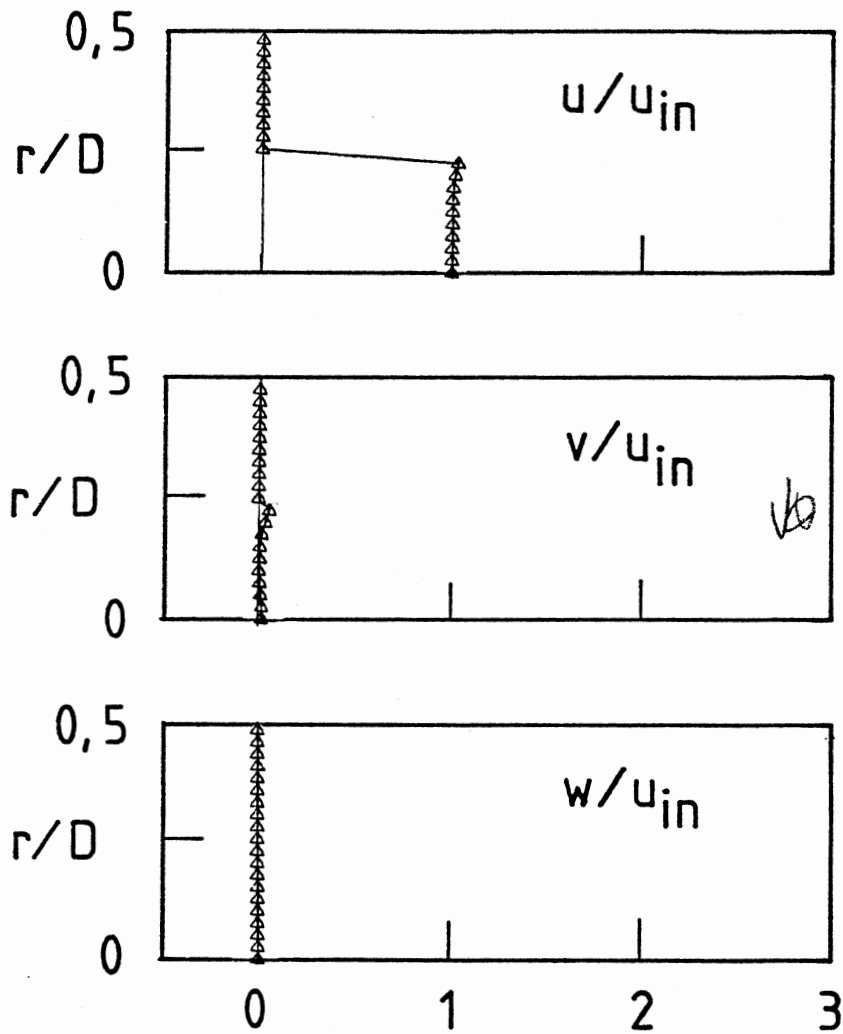


Figure 9. Normalized Velocity Profiles From Radial Traverse, $\phi = 0$ deg. (No Swirler)

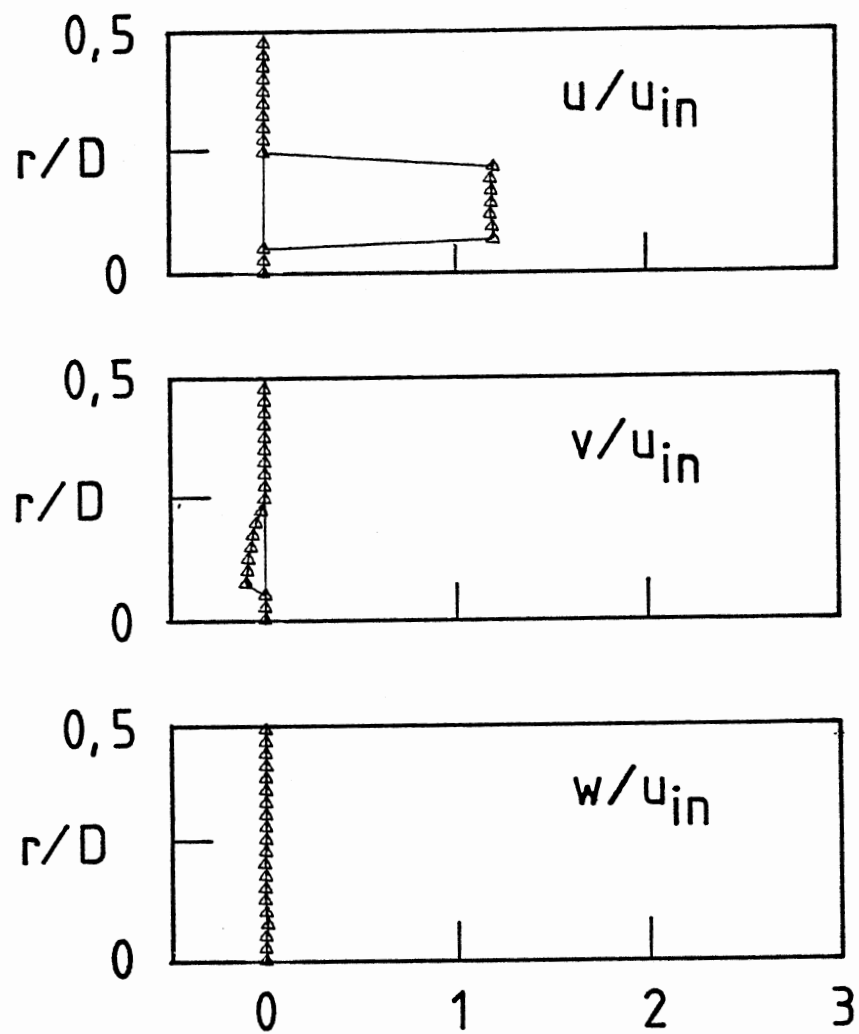


Figure 10. Normalized Velocity Profiles From Radial Traverse, $\phi = 0$ deg. (Swirler Installed)

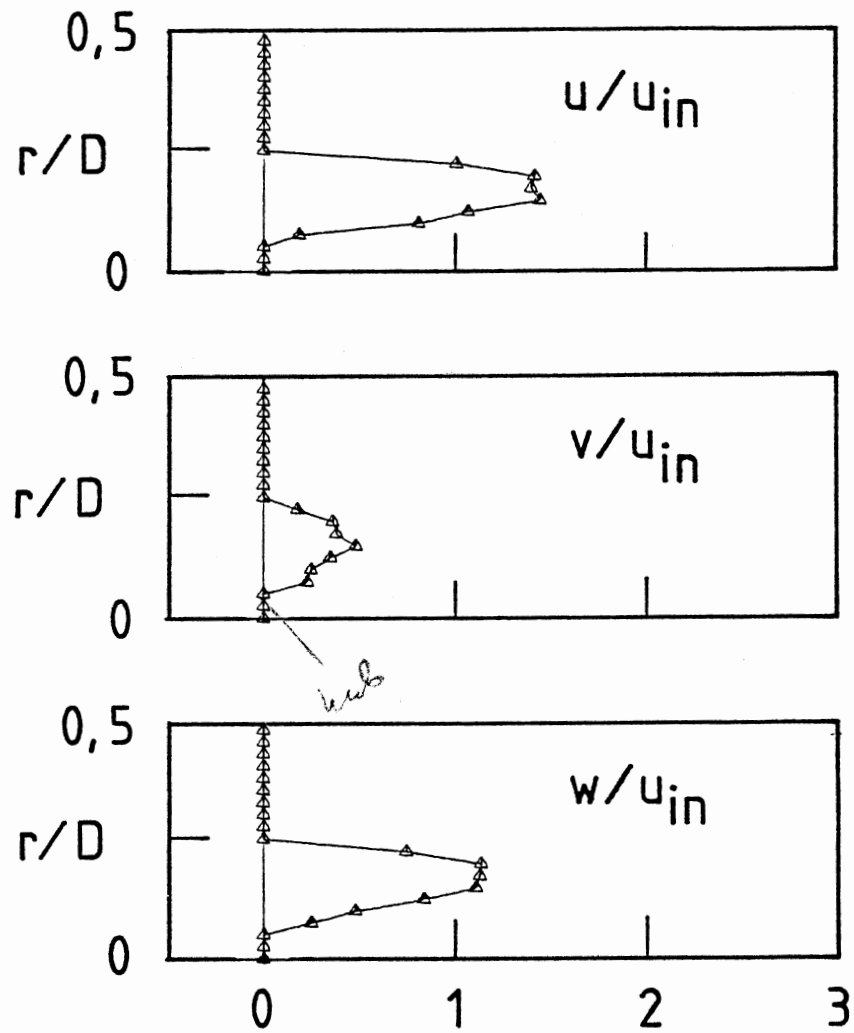


Figure 11. Normalized Velocity Profiles From Radial Traverse, $\phi = 38$ deg.

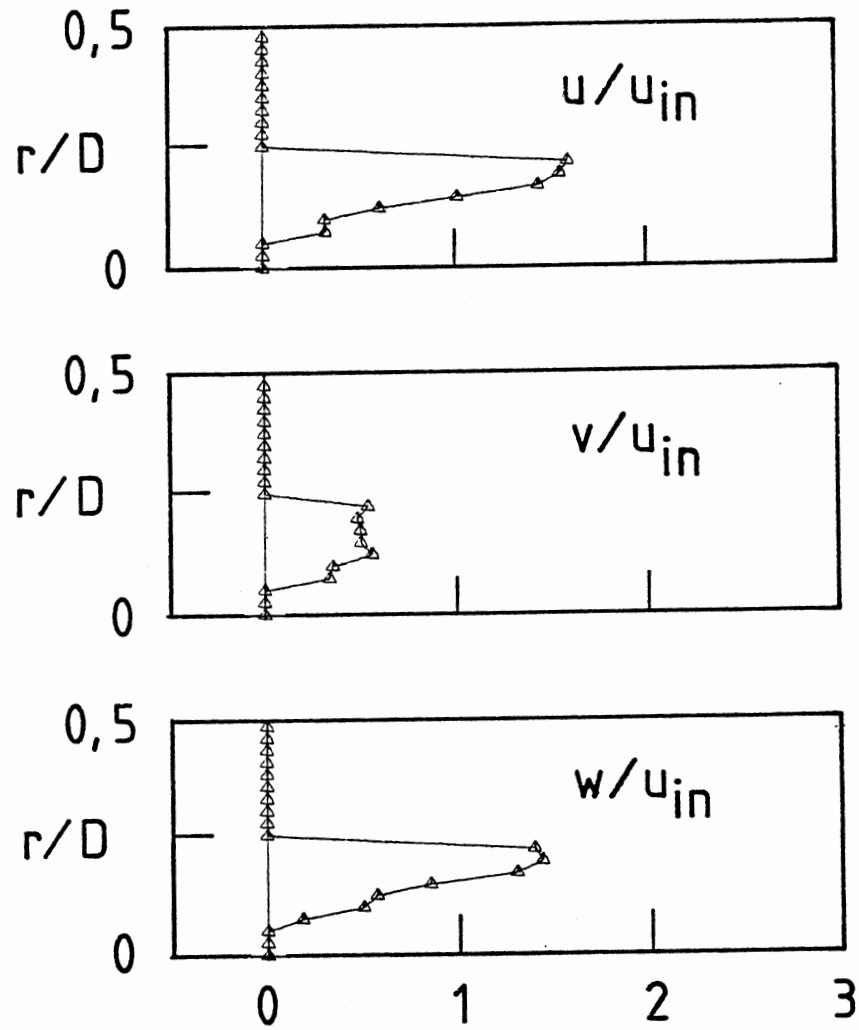


Figure 12. Normalized Velocity Profiles From Radial Traverse, $\phi = 45$ deg.

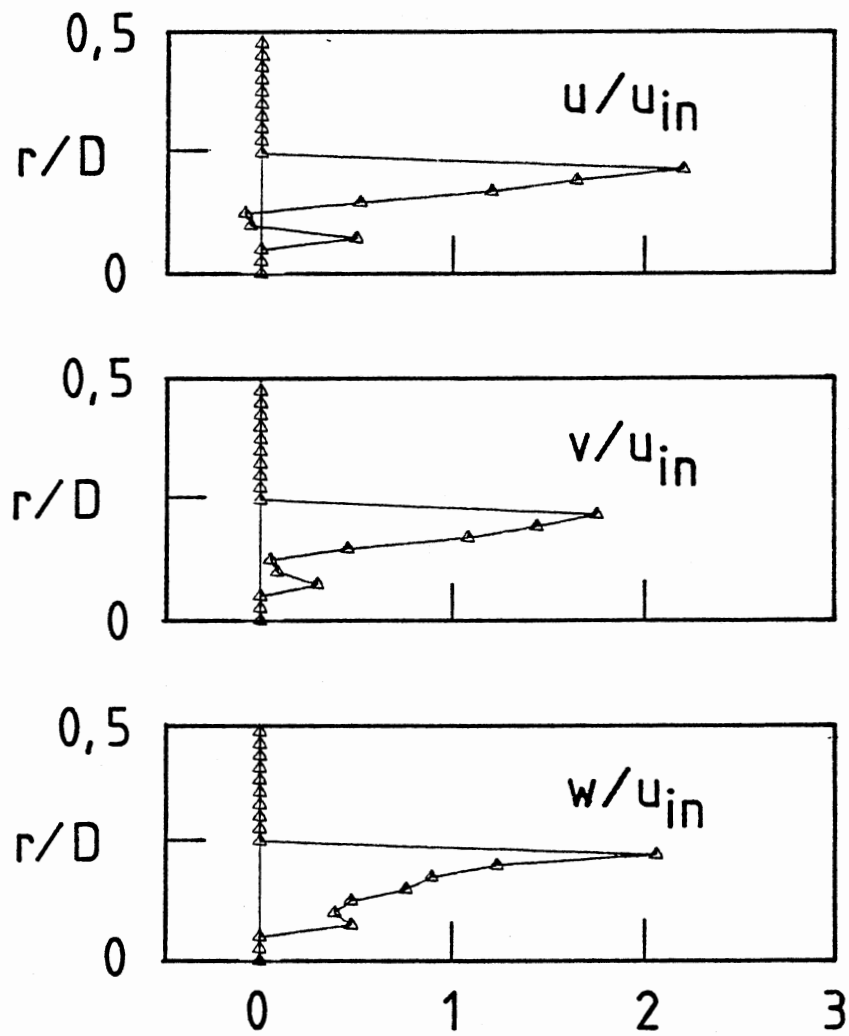


Figure 13. Normalized Velocity Profiles From Radial Traverse, $\phi = 60$ deg.

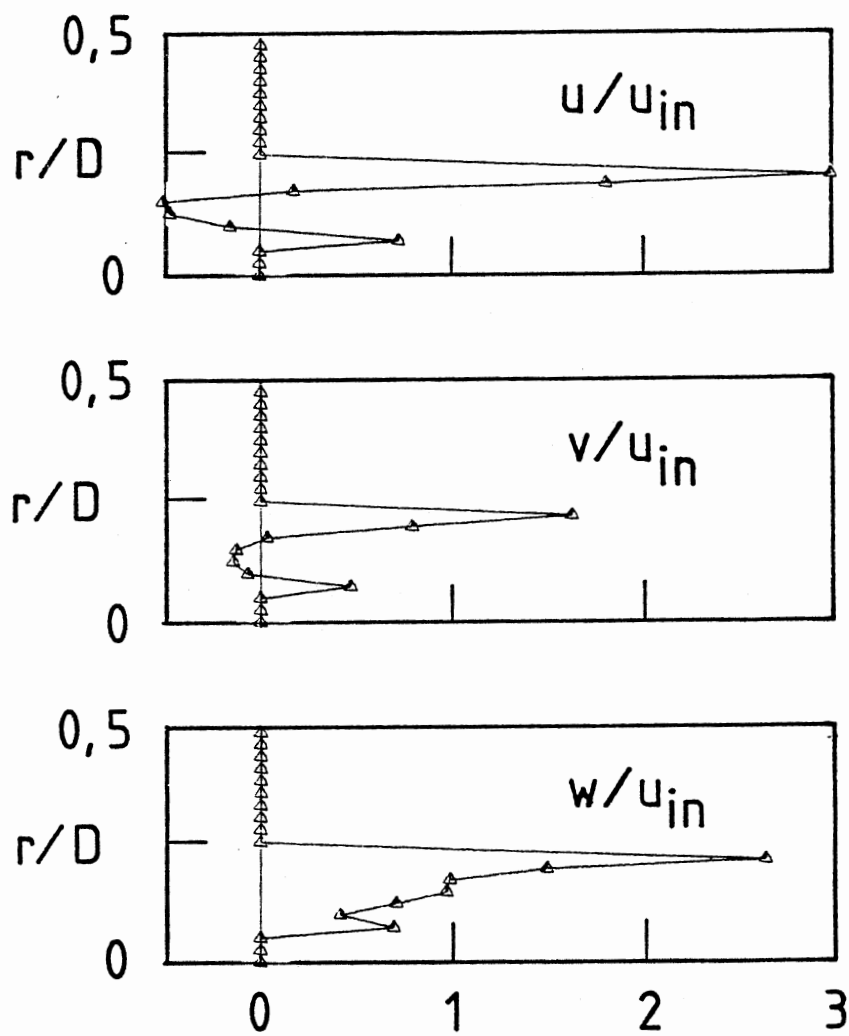


Figure 14. Normalized Velocity Profiles From Radial Traverse, $\phi = 70$ deg.

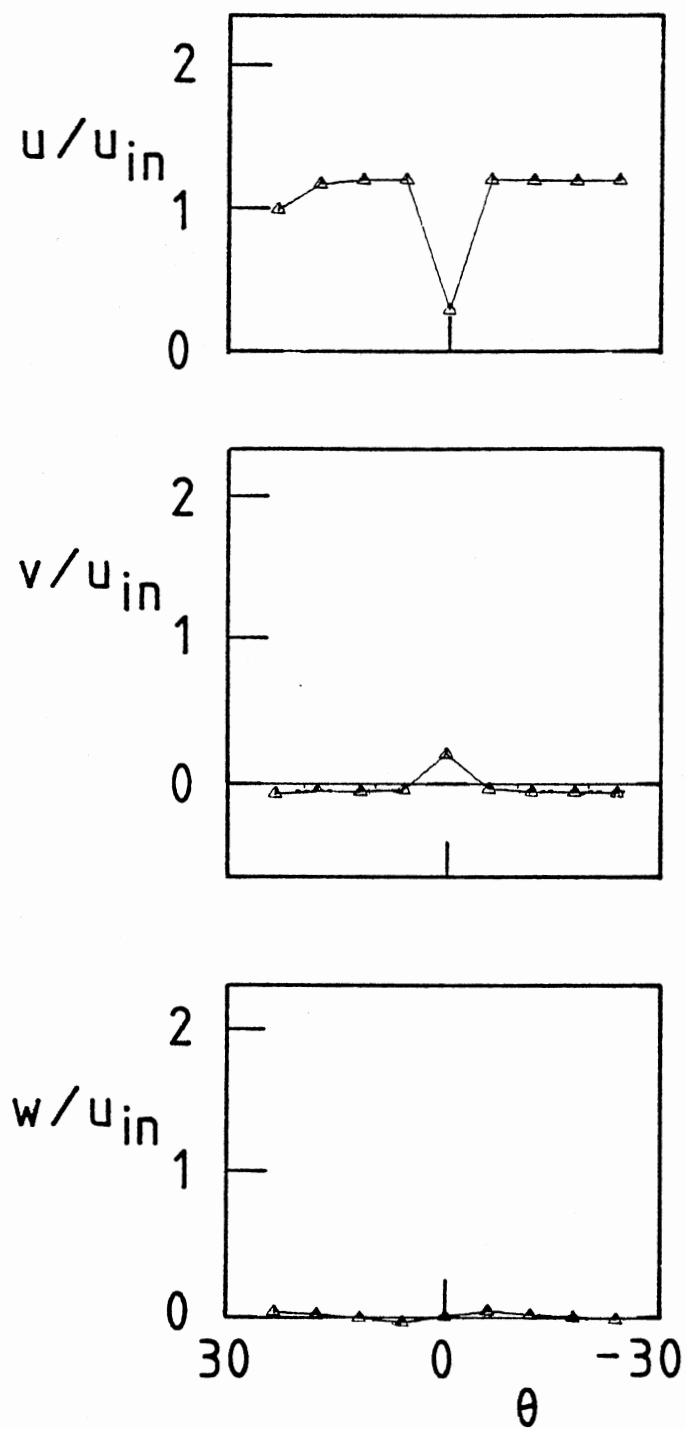


Figure 15. Normalized Velocity Profiles From Azimuthal Traverse, $\phi = 0$ deg. at $r/D = 0.179$ (Swirler Installed)

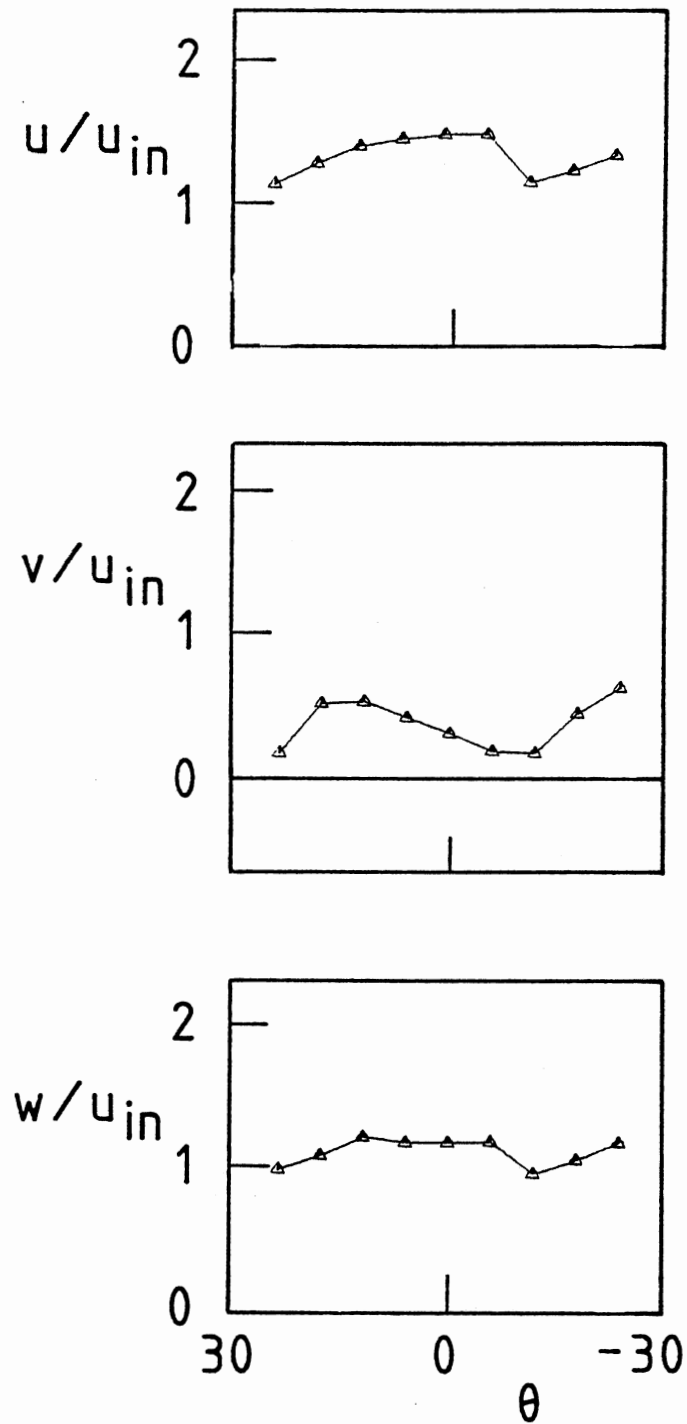


Figure 16. Normalized Velocity Profiles
From Azimuthal Traverse, ϕ
= 38 deg. at $r/D = 0.179$

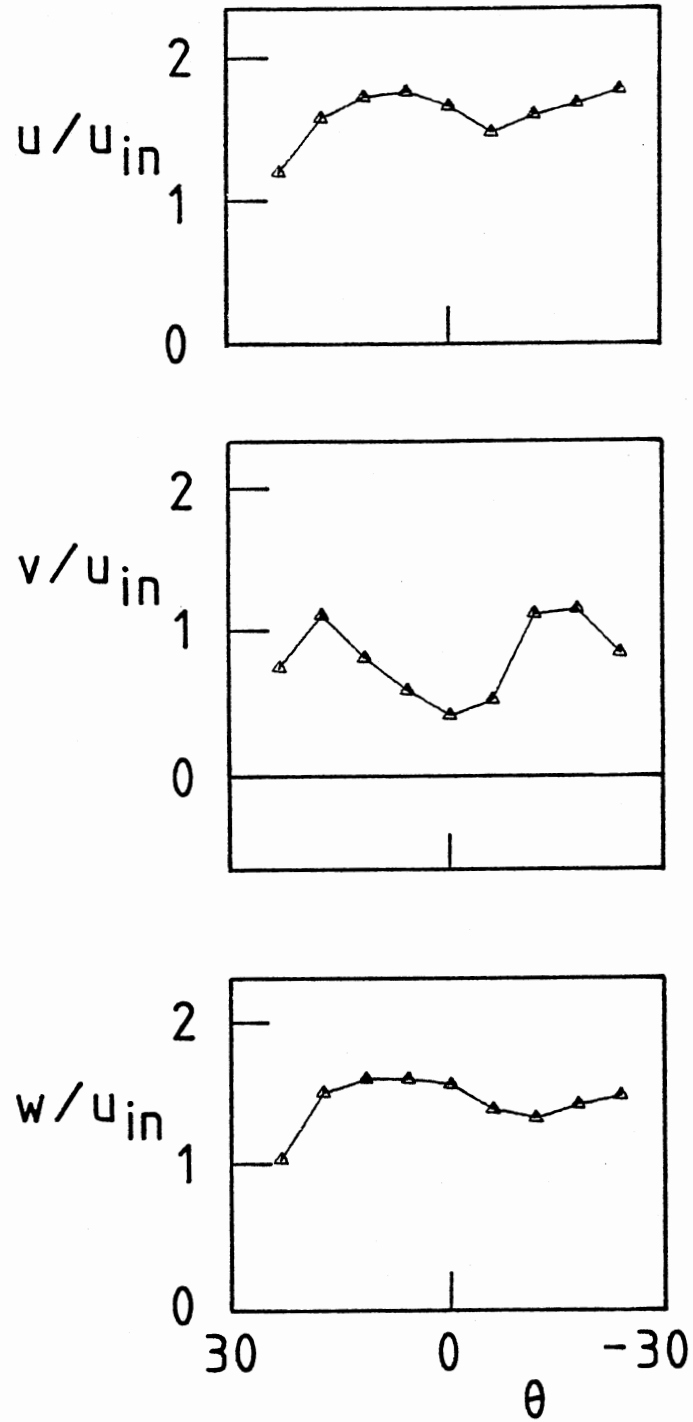


Figure 17. Normalized Velocity Profiles
From Azimuthal Traverse, ϕ
= 45 deg. at $r/D = 0.179$

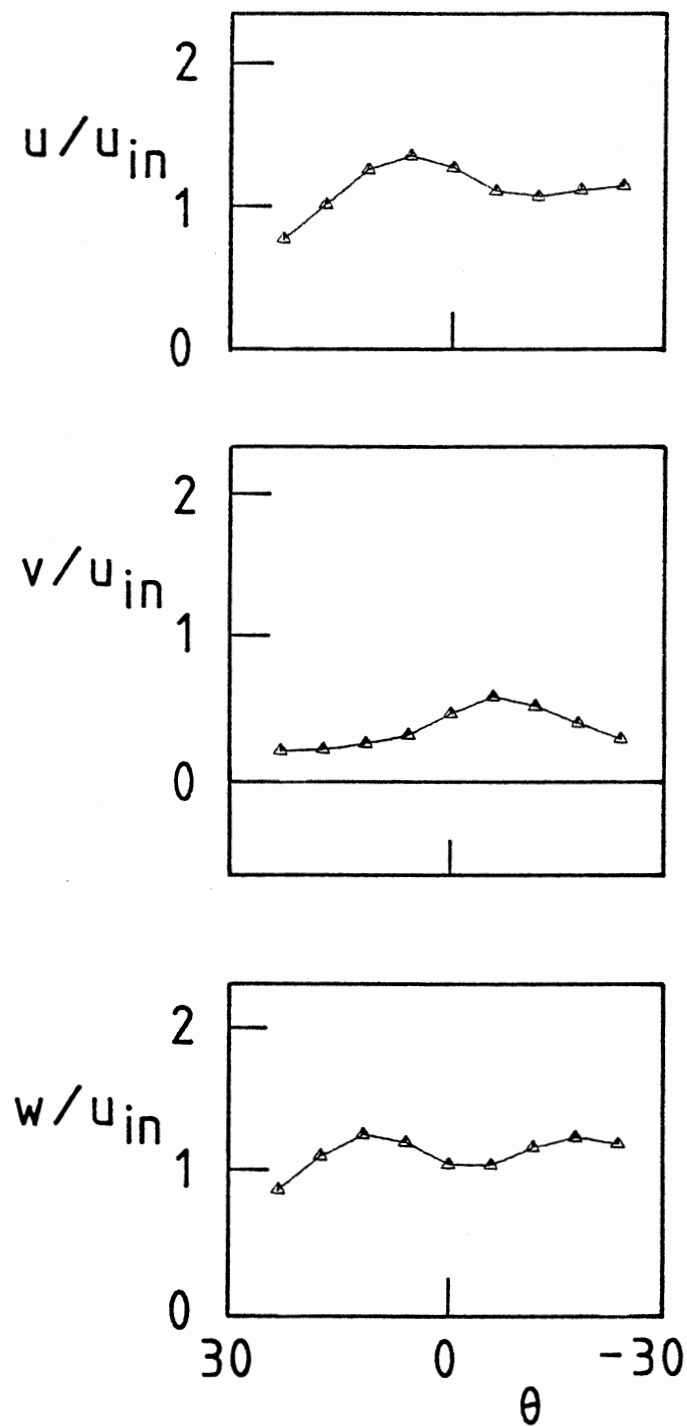


Figure 18. Normalized Velocity Profiles
From Azimuthal Traverse, ϕ
= 60 deg. at $r/D = 0.179$

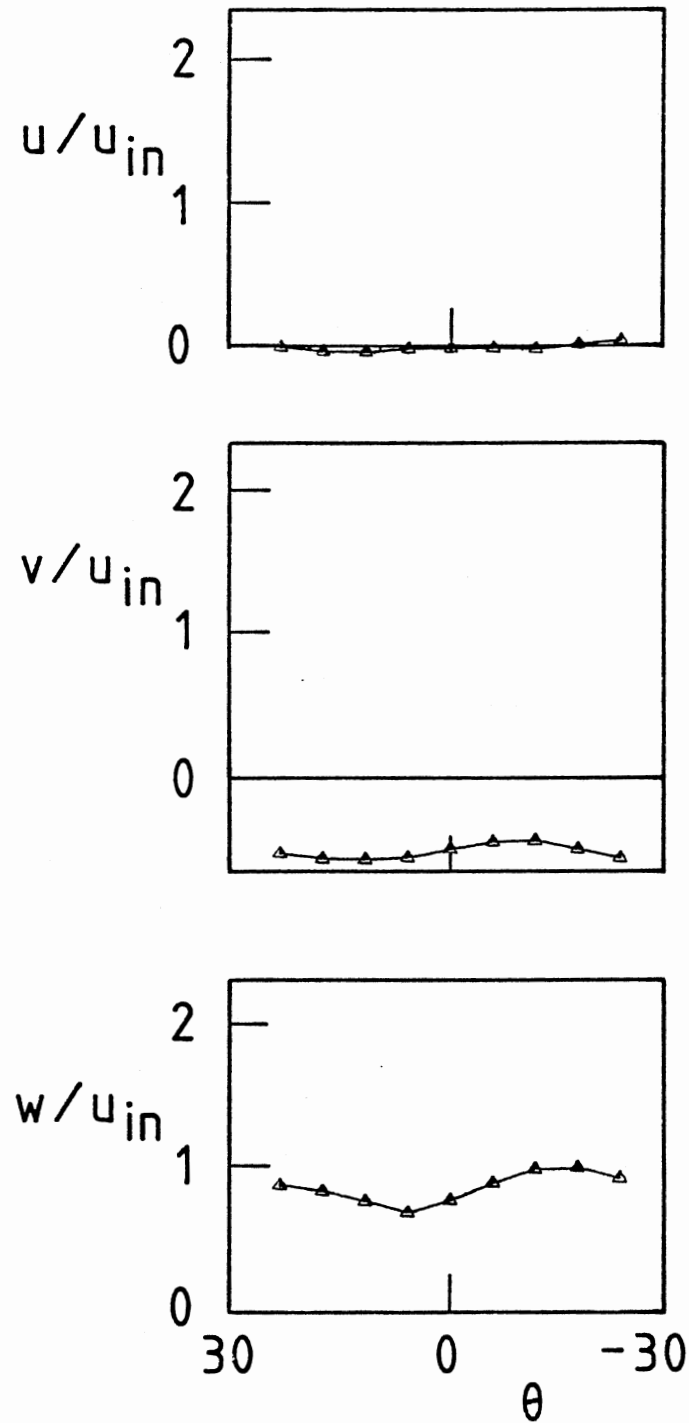


Figure 19. Normalized Velocity Profiles
From Azimuthal Traverse, ϕ
= 70 deg. at $r/D = 0.179$

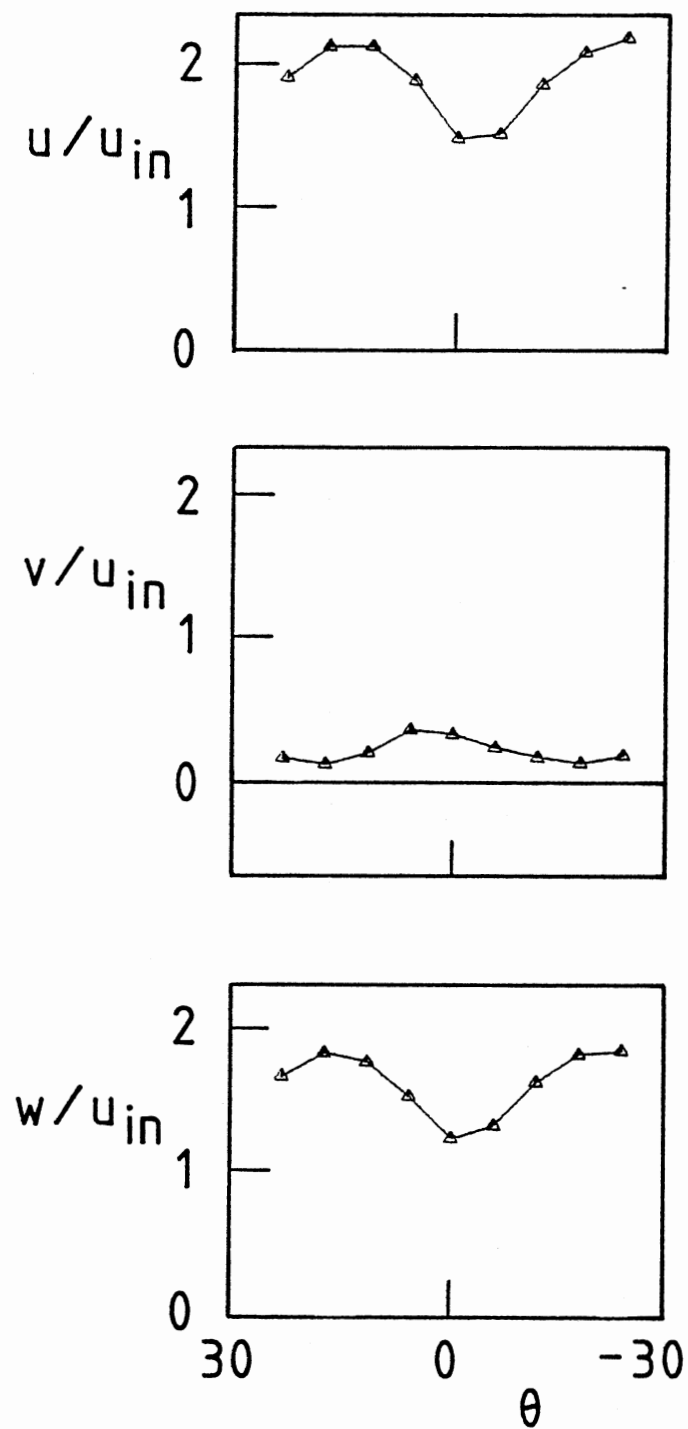


Figure 20. Normalized Velocity Profiles
From Azimuthal Traverse, ϕ
= 70 deg. at $r/D = 0.204$

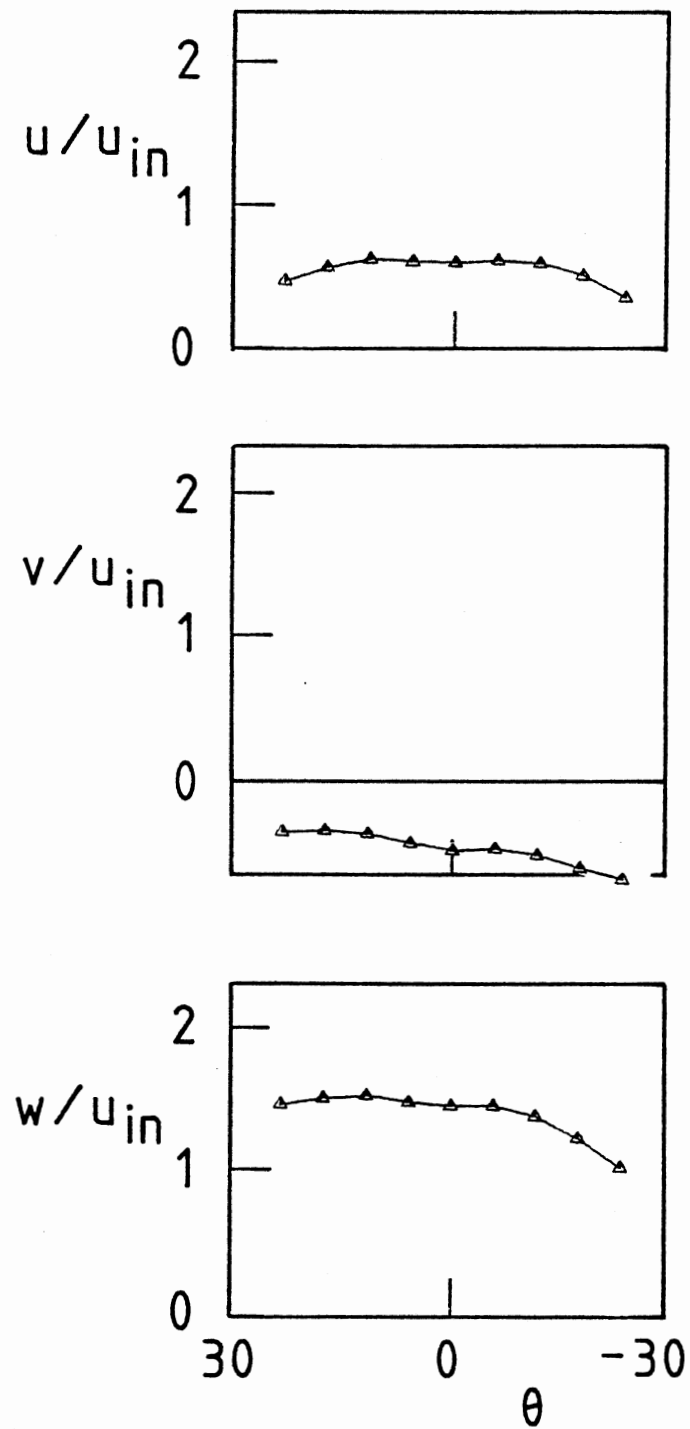


Figure 21. Normalized Velocity Profiles
From Azimuthal Traverse, ϕ
= 70 deg. at $r/D = 0.179$
Measured 0.109 D Down-
stream of Swirler Exit

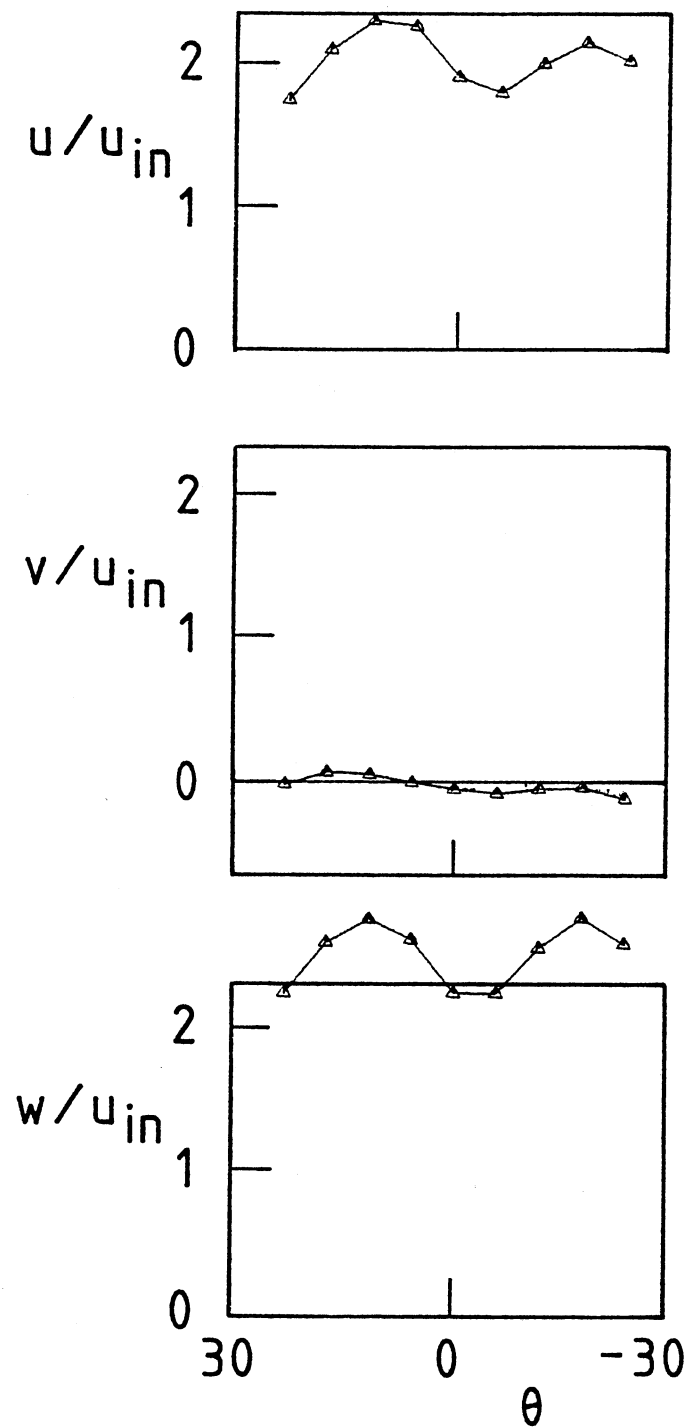


Figure 22. Normalized Velocity Profiles
From Azimuthal Traverse, ϕ
= 70 deg. at $r/D = 0.204$
Measured $0.109 D$ Down-
stream of Swirler Exit

APPENDIX C

DESCRIPTION OF REVISIONS TO COMPUTER PROGRAM
FOR FIVE-HOLE PITOT DATA REDUCTION

APPENDIX C

The data reduction program used for this project is a modification of a program written by Rhode (19) and described in some detail by Yoon (20). A brief overview of the entire program will be given, followed by a more detailed description of the major changes.

1. Program Overview

The reduction program consists of a main program, two function subprograms, and five subroutines. The main program first calls subroutine INIT to initialize all array variables to zero, then reads in calibration data, control parameters, and the data to be reduced. The actual data reduction is done by repeated calls to the function SPLINE, which uses a cubic spline interpolation method to find pitch angle, velocity, and static pressure at each point from the calibration data. The function H and subroutines ABUILD and GAUSS are called from SPLINE as part of this process.

Next a set of auxiliary calculations are performed. These include nondimensionalizing the output values, calculating momentum fluxes and swirl numbers for radial traverses, and computing averages of the output quantities over successive one-blade cycles for azimuthal traverses. Finally, the primary output values are written into an unformatted

output data set for disk storage, and all output variables are printed out in standard format using the subroutines WRITE and PRINT.

Changes were made to two sections of Rhode's original program: the main program and subroutine INIT. For brevity, only the changes to these sections will be considered in detail here. For information on the structure and function of the unmodified parts of the program, see Reference 20.

2. Additions and Modifications

The code's new capabilities include calculation of static pressure at each location and reduction of either radial or azimuthal traverse data. For radial traverses, the code calculates axial flux of axial momentum (with and without static pressure contribution) and swirl numbers S and S' . For azimuthal traverses, it calculates averages of the output values u , v , w , and $p - p_{\infty}$. In addition, substantial changes have been made in the way data is labeled, read in, and stored, in an effort to reduce storage requirements and make the code easier to use and understand.

Static Pressure Calculation

The static pressure is found using a method based on one described by Bryer and Pankhurst (21). The method uses the fact that the absolute pressure at any of the five holes in the probe tip can be expressed as

$$p_i = p_{st} + K_i q$$

where p_{st} is the local static pressure, K is an empirical coefficient which is a function of pitch angle δ , q is the local dynamic pressure

$\frac{1}{2}\rho V^2$, and the subscript i stands for any of the ports N, S, E, W, or C. Rearranging this and subtracting atmospheric pressure from both sides, we obtain for the central pressure port

$$p_{st} - p_{atm} = (p_C - p_{atm}) - K_C q \quad (C.1)$$

We now introduce the velocity coefficient,

$$VC = \frac{\frac{1}{2}\rho V^2}{(p_C - p_W)} = \frac{q}{(p_C - p_W)}$$

which is already used in the code to determine total velocity magnitude. In accordance with standard practice, it is assumed that the velocity coefficients under calibration and measurement conditions are identical at a given pitch angle δ_1 , regardless of differences in fluid velocity. That is, $VC_{\delta_1, cal} = VC_{\delta_1, meas}$ or

$$\frac{q_{cal}}{(p_C - p_W)_{\delta_1, cal}} = \frac{q_{meas}}{(p_C - p_W)_{\delta_1, meas}}$$

This rearranges to

$$q_{meas} = \frac{q_{cal}}{(p_C - p_W)_{\delta_1, cal}} \cdot (p_C - p_W)_{\delta_1, meas} \quad (C.2)$$

Now, from Equation (C.1), taken at δ_1 under calibration conditions:

$$K_{C, \delta_1, cal} = \left[\frac{p_C - p_{st}}{q} \right]_{\delta_1, cal} = \frac{(p_C - p_{atm})_{\delta_1, cal}}{q_{cal}},$$

since the static pressure equals atmospheric pressure in the free jet used for calibration. Substituting this and Equation (C.2) into

Equation (C.1), we get

$$(p_{st} - p_{atm})_{meas} = (p_C - p_{atm})_{\delta_1, meas} - \left[\frac{(p_C - p_{atm})_{\delta_1, cal}}{q_{cal}} \right] \cdot \left[\frac{q_{cal}}{(p_C - p_W)_{\delta_1, cal}} (p_C - p_W)_{\delta_1, meas} \right]$$

The calibration dynamic pressure cancels, and the remaining calibration pressures may be combined to form a dimensionless static pressure coefficient,

$$SPC = \frac{(p_C - p_{atm})}{(p_C - p_W)}$$

which is determined as a function of δ from calibration data. This leads to the final expression for the gage static pressure at a location where the pitch angle is δ_1 :

$$(p_{st} - p_{atm})_{\delta_1, meas} = (p_C - p_{atm})_{\delta_1, meas} - SPC_{\delta_1} (p_C - p_W)_{\delta_1, meas}$$

This last expression is used directly in the code. The value of SPC is found by the same third-order spline interpolation technique used to find the pitch and velocity coefficients at each measurement location. (See lines 2690-2720 and line 3070 in the listing in Appendix D.)

Radial and Azimuthal Capability

The reduction of both radial and azimuthal traverses was implemented by the addition of an integer flag in the input data to indicate which type of traverse is to be reduced. This flag, the variable KRADTR, is given a value of 1 for radial traverses and 0 for azimuthal ones. Since this value is read in only once for the entire run, all

traverses to be reduced in a single run must be of the same type - either all radial or all azimuthal.

Data for both traverse types is treated identically through Chapter I of the code, with the azimuth angles read in as values of radius, RINCHS. The major differences occur in Chapter II where the auxiliary calculations are performed. Depending on the value of KRADTR, radius values are nondimensionalized by the test section diameter or reset so that azimuth values remain in degrees. Next, the value of KRADTR is used to control branching to program segments which perform calculations unique to each traverse type, which are described in the next two sections. The last application of KRADTR is in Chapter III, Output. Here again, it controls branching to ensure that only those output values appropriate to the traverse type being reduced are printed out.

Radial Traverse Calculations

When reducing data from radial traverses, the code automatically performs a simple numerical integration procedure to find approximate values of mass flow rate and the momentum fluxes G_{θ} , G_x , and G_x' . These values are then used to calculate the swirl numbers S and S' as defined in Chapter II.

The integration procedure is effectively the same as that used by Rhode in his original reduction code, as well as in the STARPIC prediction code (22). However, the integration has been rewritten to calculate terms for the ring elements in a more straight-forward manner, and the central disk element has been added for completeness (lines 3830 through 3880 of Appendix D).

In the absence of true static pressure taps in the rim of the swirler, the reference pressure p_{∞} has been approximated by the measured static pressure at the measurement location nearest the wall of the swirler. This may introduce an error, but the results will still be useful for comparing trends.

Azimuthal Traverse Calculations

For the azimuthal data, an averaging procedure is used instead of the integration routine. Since the data is expected to be cyclic with a period of one blade width, averaging is performed over successive one-blade cycles. These successive averages may then be compared to check deviation from cyclic behavior or averaged again to get a single representative value for each of the major output quantities.

The code is set up to handle traverses having six points over the width of one blade; for example, six-degree increments for a ten-bladed swirler. For other spacings the value of NREP (line 4470 of the code) must be changed.

Since the reference pressure p_{∞} for each vane angle setting is taken from a radial traverse at the exit plane, the value of p_{∞} must be supplied by the user for azimuthal runs. This allows calculation of the pressure difference $p - p_{\infty}$ from azimuthal traverses for comparison with the values obtained from radial traverses. For those users not concerned with static pressure measurements, the supplied reference pressure PREF may be omitted or set equal to atmospheric pressure.

Miscellaneous Modifications

To make the code easier to use, all primary user inputs have been

separated from the body of the code and incorporated into the block of input data, which is stored in a separate dataset. This minimizes the need to make changes in the body of the code, and reduces the memory space required to keep a record of all input data for each run. New headings were added to the input dataset to identify both the calibration and measurement data, and additional variables are stored on disk for use by auxiliary programs which produce tables and profile plots. To improve readability of the code, all DO loops were indented and extensive comments were added. A listing of the reduction code with sample input and output appears in Appendix D.

APPENDIX D

LISTING OF FIVE-HOLE PITOT DATA REDUCTION
PROGRAM WITH SAMPLE INPUT DATA

```

00080 C
00090 C*****
00100 C
00110 C
00120 C      A COMPUTER PROGRAM FOR DATA REDUCTION OF FIVE-HOLE PITOT
00130 C      MEASUREMENTS IN TURBULENT, SWIRLING, RECIRCULATING FLOW
00140 C      IN COMBUSTOR GEOMETRIES.
00150 C
00160 C      VERSION OF MARCH, 1983 --
00170 C      MODIFICATIONS INCLUDE COMBINED RADIAL AND AZIMUTHAL CAPA-
00180 C      BILITY, REDUCTION OF STATIC PRESSURE DATA, AND CALCULATION
00190 C      OF MOMENTUM FLUXES AND SWIRL NUMBERS FOR RADIAL PROFILES.
00200 C
00210 C      BASED ON A PROGRAM BY D. L. RHODE (PHD THESIS, OSU, 1981)
00220 C
00230 C
00240 C      G. F. SANDER
00250 C      MECHANICAL AND AEROSPACE ENGINEERING
00260 C      OKLAHOMA STATE UNIVERSITY
00270 C      STILLWATER, OK      74078
00280 C
00290 C
00300 C*****
00310 C
00320 C---MAJOR FORTRAN VARIABLES IN MAIN PROGRAM (LISTED IN ORDER
00330 C      OF FIRST OCCURRENCE IN THE PROGRAM):
00340 C
00350 C IWRITE - LOGICAL FLAG FOR WRITING INTO OUTPUT DATASET (UNFORMATTED)
00360 C DIAGNS - FLAG FOR DIAGNOSTIC OUTPUT
00370 C IT      - MAX NO. OF TRAVERSES ALLOWED; DIMENSION VALUE IN SUBROUTINES
00380 C JT      - MAX NO. OF POINTS ALLOWED PER TRAVERSE; ALSO DIMENSION VALUE
00390 C HEDM ETC. - ALL VARIABLES STARTING WITH "HED" ARE ALPHANUMERIC ARRAYS
00400 C      FOR OUTPUT HEADINGS
00410 C NCAL    - NO. OF CALIBRATION DATA POINTS
00420 C CPITCH - CALIBRATION PITCH COEFF. -- (PN-PS)/(PC-PW)
00430 C CDELTA - CAL. PITCH ANGLE -- STANDARD RANGE -58 TO +58 DEG.
00440 C CVELCF - CAL. VELOCITY COEFF. -- (CAL. DYN. PRESS.)/(PC-PW)
00450 C CPSTCF - CAL. STATIC PRESSURE COEFF. -- (PC-PA)/(PC-PW)
00460 C HEDID1,HEDID2 - USER HEADINGS TO IDENTIFY THE RUN BEING REDUCED
00470 C ALPHA  - INLET SIDEWALL EXPANSION ANGLE
00480 C PHI    - SWIRL VANE ANGLE SETTING
00490 C DSINCH - INLET NOZZLE OR SWIRLER DIAMETER, DSMALL, IN INCHES
00500 C DLINCH - TEST SECTION DIAMETER, DLARGE, INCHES
00510 C KRADTR - INTEGER FLAG FOR TRAVERSE TYPE -- 1 FOR RADIAL, 0 FOR AZIM.
00520 C NSTATN - NO. OF TRAVERSES TO BE REDUCES
00530 C MAXJPT - MAX NO. OF POINTS IN ANY OF THE TRAVERSES BEING REDUCED
00540 C XINCHS - AXIAL POSITION OF EACH TRAVERSE, INCHES
00550 C NDATA  - NO. OF DATAPOINTS IN EACH TRAVERSE
00560 C RDNPRS - INLET DYNAMIC PRESSURE (UPSTREAM OF SWIRLER), TORR
00570 C PREF  - REF. PRESS. USED TO CALC. PDIFF FOR SWIRL NUMBER, TORR
00580 C FANSPD - FAN SPEED, RPM
00590 C TFLOW  - TEMPERATURE OF AIR IN TEST SECTION, DEG. CELSIUS
00600 C PATM  - ATMOSPHERIC PRESSURE, TORR
00610 C BZOFF  - BETA ZERO-OFFSET FOR YAW ANGLE READINGS
00620 C RINCHS - RADIAL POS. OF DATAPOINT, INCHES (THETA FOR AZIM. TRAVERSES)

```

00630 C RBETA - RAW VALUE OF YAW ANGLE BETA, DEG.
 00640 C RFNMP5 - MEAS. VALUE OF PNORTH - PSOUTH PRESS. DIFF, TORR
 00650 C RPCMPW - MEAS. VALUE OF PCENTER - PWEST, TORR
 00660 C RPCMPA - MEAS. VALUE OF PCENTER - PATMOSPHERE, TORR
 00670 C RSMALL - INLET NOZZLE OR SWIRLER RADIUS, METERS
 00680 C RLARGE - TEST SECTION RADIUS, METERS
 00690 C X - AXIAL POSITION OF TRAVERSE, METERS
 00700 C R - RADIAL POSITION OF DATAPOINT, METERS
 00710 C IIDID - FLAG TO USE ENTRY POINT SP IN SPLINE INTERPOLATION ROUTINE
 00720 C PICHCF - REDUCED PITCH COEFF. FOR EACH DATAPOINT
 00730 C DELTA - REDUCED PITCH ANGLE FOUND BY INTERPOLATION USING PICHCF
 00740 C VELCF - REDUCED VELOCITY COEFF. FROM INTERPOLATION USING DELTA
 00750 C PSTCF - REDUCED STATIC PRESS. COEFF. FROM INTERPOLATION USING DELTA
 00760 C RHO - DENSITY FOR EACH TRAVERSE, FROM IDEAL-GAS LAW
 00770 C BETA - REDUCED VALUE FOR PROBE YAW ANGLE, DEG.
 00780 C VTOTAL - TOTAL VELOCITY VECTOR MAGNITUDE, M/S
 00790 C U - AXIAL COMPONENT OF VELOCITY, M/S
 00800 C V - RADIAL COMP. OF VELOCITY, M/S
 00810 C W - TANGENTIAL (SWIRL) VELOCITY, M/S
 00820 C P - REDUCED VALUE OF STATIC PRESSURE, N/SQ. M (GAGE)
 00830 C XND - NONDIMENSIONAL AXIAL POSITION, X/DLARGE
 00840 C UIN - INLET REFERENCE VELOCITY (CALC. FROM RDNFRS), M/S
 00850 C MASFLO - INLET MASS FLOW RATE (ASSUMING UNIFORM AXIAL VELOCITY), KG/S
 00860 C VSTAR - NONDIM. TOTAL VELOCITY MAGNITUDE, VTOTAL/UIN
 00870 C USTAR - NONDIM. AXIAL VELOCITY, U/UIN
 00880 C VSTAR - NONDIM. RADIAL VELOCITY, V/UIN
 00890 C WSTAR - NONDIM. TANGENTIAL VEL., W/UIN
 00900 C PSTAR - NONDIM. STATIC PRESSURE, P/RDNFRS
 00910 C RND - NONDIM. RADIAL POS., R/DLARGE; ALSO THETA FOR AZIM. TRAVERSES
 00920 C DYPS - "DELTA-Y, POINT-SOUTH" (FOR RADIAL INTEGRATION; FROM STARPIC)
 00930 C DYNP - "DELTA-Y, NORTH-POINT" (SIM. TO DYPS)
 00940 C SNS - "SMALL NORTH-SOUTH" FROM STARPIC; USED AS DELTA-R FOR INTEGR.
 00950 C PDIFF - PRESS. DIFF. P - PREF USED TO CALCULATE SWIRL NUMBER, N/SQ. M
 00960 C AREA1 - AREA OF DISC ELEMENT AT CENTER OF INTEGRATION REGION
 00970 C FLOW - SUMMATION FOR MASS FLOW THROUGH RING ELEMENTS
 00980 C WMOM - SUMMATION FOR ANGULAR MOMENTUM FLUX
 00990 C UDMOM - SUMMATION FOR DYNAMIC AXIAL MOM. FLUX (NEGL. PRESS. TERM)
 01000 C UMOMP - SUMMATION FOR AXIAL MOMENTUM FLUX, INCL. PRESSURE DIFF. TERM
 01010 C AREAJ - AREA OF EACH RING ELEMENT, SQ. M
 01020 C MASS - INTEGRATED MASS FLOW RATE, KG/S
 01030 C UMEAN - INTEGRATED MEAN AXIAL VELOCITY, M/S
 01040 C ANG MOM - INTEGRATED AXIAL FLUX OF ANGULAR MOMENTUM, N-M
 01050 C AXMOM - INT. AXIAL FLUX OF DYNAMIC AXIAL MOM., N (NEGL. PRESS. TERM)
 01060 C AXMOMP - INT. AXIAL FLUX OF AXIAL MOMENTUM, N (INCL. PRESSURE TERM)
 01070 C SPRIME - SWIRL NUMBER CALC. USING DYNAMIC AXIAL MOMENTUM FLUX
 01080 C S - SWIRL NUMBER CALC. USING FULL AXIAL MOM. FLUX (INCL. PRESS.)
 01090 C USTAVG - AVERAGE OF USTAR VALUES FOR AZIM. TRAV., OVER ONE BLADE SPACE
 01100 C VSTAVG - AVG. OF VSTAR VALUES
 01110 C WSTAVG - AVG. OF WSTAR VALUES
 01120 C PDAVAVG - AVG. OF PDIFF VALUES
 01130 C VISCOS - LAMINAR ABS. VISCOSITY CALCULATED FOR EACH TRAVERSE, KG/M*
 01140 C REDIN - INLET REYNOLDS NUMBER, CALC. USING VISCOSITY FOR EACH TRAV.
 01150 C
 01160 G
 01170 CHAPTER 0 0 0 0 0 0 0 0 PRELIMINARIES 0 0 0 0 0 0 0 0
 01180 C
 01190 DIMENSION HEDM(9),HEDUM(9),HEDNMS(9),HEDCMW(9),HEDCMA(9),
 01200 #HEDU(9),HEDV(9),HEDW(9),HEDVT(9),HEDUST(9),
 01210 #HEDVST(9),HEDWST(9),HEDPST(9),HEDDEL(9),HEDBET(9),
 01220 #HEDMMF(9),HEDMIV(9),HEDMIP(9),HEDAM(9),
 01230 #HEDAX(9),HEDAXP(9),HEDSPR(9),HEDS(9),HEDP(9),HEDPDF(9),HEDRED(9),
 01240 #HEDID1(18),HEDID2(18),HEDUSA(9),HEDVSA(9),HEDWSA(9),HEDPDA(9),
 01250 #HEDFAN(9),HEDTFL(9),HEDPAT(9),HEDRHO(9),HEDVIS(9),HEDCAL(9)
 01260 C
 01270 COMMON
 01280 #/CALIB/CPITCH(26),CDELTA(26),CVELCF(26),CPSTCF(26)

```

01290      #/MEASUR/RBETA(8,24),RPNMFS(8,24),RPCMPW(8,24),RPCMPA(8,24),
01300      #   NDATA(8),MAXJPT,RINPRS(8),
01310      #   FANSPD(8),TFLOW(8),PATM(8),BZOFF(8)
01320      #/GEOM/X(8),R(24),XND(8),RND(24),DYFS(24),DYNP(24),
01330      #   SNS(24),NSTATN,XINCHS(8),RINCHS(24)
01340      #/CALC/VTOTAL(8,24),U(8,24),V(8,24),W(8,24),P(8,24),
01350      #   VTSTAR(8,24),USTAR(8,24),VSTAR(8,24),WSTAR(8,24),PSTAR(8,24),
01360      #   PICHCF(8,24),VELCF(8,24),DELTA(8,24),BETA(8,24),
01370      #   ANGMOM(8),UMEAN(8),MASS(8),MASFLO(8),UIN(8),
01380      #   PDIFF(8,24),PSTCF(8,24),AXMOM(8),AXMOMP(8),
01390      #   SPRIME(8),S(8),REDIN(8),PREF(8),RHO(8),VISCOS(8),
01400      #   USTAVG(8,24),VSTAVG(8,24),WSTAVG(8,24),PDFAVG(8,24)
01410      #/OUTPUT/STORE(8)
01420 C
01430      REAL MASS,MASFLO
01440      LOGICAL IWRITE,DIAGNS
01450 C
01460 C---SET IWRITE=.TRUE. FOR WRITING SOLN. ON DISK STORAGE;
01470 C   SET DIAGNS=.TRUE. TO ACTIVATE DIAGNOSTIC WRITE STATEMENTS
01480 C
01490      IWRITE=.TRUE.
01500      DIAGNS=.FALSE.
01510      IT=8
01520      JT=24
01530 C
01540 C---READ CHARACTER DATA FOR HEADINGS USED BY SUBROUTINES
01550 C   WRITE AND PRINT (ALSO CALIBRATION HEADING)
01560 C
01570      READ(5,205) HEDM,HEDUMN,HEDU,HEDV,HEDW,
01580      #   HEDVT,HEDUST,HEDVST,HEDWST,HEDPST,HEDEL,HEDBET,
01590      #   HEDNMS,HEDCMW,HEDCMA,HEDMMF,HEDMIV,HEDMIF,HEDAM,
01600      #   HEDAX,HEDAXP,HEDSPR,HEDS,HEDF,HEDPDF,HEDRED,
01610      #   HEDFAN,HEDTFL,HEDPAT,HEDRHO,HEDVIS,
01620      #   HEDUSA,HEDVSA,HEDWSA,HEDPDA,HEDCAL
01630      205 FORMAT(9A4)
01640 C
01650 C-----INITIALIZE VARIABLES TO ZERO
01660 C
01670      CALL INIT
01680 C
01690 C-----READ FIVE-HOLE PITOT CALIBRATION DATA
01700 C
01710      NCAL=25
01720      DO 10 I=1,NCAL
01730          READ(5,210) CPITCH(I),CDELTA(I),CVELCF(I),CPSTCF(I)
01740      10 CONTINUE
01750      210 FORMAT(4F10.5)
01760          IF(DIAGNS) WRITE(6,400) (CPITCH(I),I=1,25)
01770          IF(DIAGNS) WRITE(6,400) (CDELTA(I),I=1,25)
01780          IF(DIAGNS) WRITE(6,400) (CVELCF(I),I=1,25)
01790          IF(DIAGNS) WRITE(6,400) (CPSTCF(I),I=1,25)
01800      400 FORMAT(///,1X,13(F8.4,1X),//,5X,12(F8.4))
01810 C
01820 C---READ USER HEADINGS, GEOMETRIC AND CONTROL PARAMETERS APPLYING
01830 C   TO ENTIRE REDUCTION RUN
01840 C
01850      READ(5,215) HEDID1,HEDID2
01860      215 FORMAT(18A4)
01870      READ(5,216) ALPHA,PHI,DSINCH,DLINCH
01880      216 FORMAT(4F10.5)
01890      READ(5,217) KRADTR,NSTATN,MAXJPT
01900      217 FORMAT(3I10)
01910 C
01920 C---READ EXPERIMENT PARAMETERS SPECIFIC TO EACH TRAVERSE, THEN
01930 C   ACTUAL MEASUREMENT DATA IN TRAVERSE
01940 C

```

```

01950      DO 30 I=1,NSTATN
01960          READ(5,230) XINCHS(I),NDATA(I),RDNPRS(I),PREF(I)
01970          READ(5,216) FANSPD(I),TFLOW(I),PATM(I),BZOFF(I)
01980          JPTS=NDATA(I)
01990          DO 20 J=1,JPTS
02000              READ(5,220) RINCHS(J),RBETA(I,J),RPNMPS(I,J),RPCMPW(I,J),
02010          #          RPCMPA(I,J)
02020      20  CONTINUE
02030      30  CONTINUE
02040  C
02050  C-----CONVERT X'S AND R'S FROM INCHES TO METERS
02060  C
02070      RSMALL=DSINCH*0.0254/2.0
02080      RLARGE=DLINCH*0.0254/2.0
02090      DO 35 I=1,NSTATN
02100          X(I)=XINCHS(I)*0.0254
02110          JPTS=NDATA(I)
02120          DO 32 J=1,JPTS
02130              R(J)=RINCHS(J)*0.0254
02140      32  CONTINUE
02150      35  CONTINUE
02160      220 FORMAT(5F10.5)
02170      230 FORMAT(1F10.5,1I10,2F10.5)
02180      IF(DIAGNS) WRITE(6,470) (NDATA(I),I=1,NSTATN)
02190      IF(DIAGNS) WRITE(6,450) (X(I),I=1,NSTATN)
02200      IF(DIAGNS) WRITE(6,500) (R(J),J=1,JPTS)
02210      DO 37 I=1,NSTATN
02220          IF(DIAGNS) WRITE(6,500) (RBETA(I,J),J=1,JPTS)
02230          IF(DIAGNS) WRITE(6,500) (RPNMPS(I,J),J=1,JPTS)
02240          IF(DIAGNS) WRITE(6,500) (RPCMPW(I,J),J=1,JPTS)
02250          IF(DIAGNS) WRITE(6,500) (RPCMPA(I,J),J=1,JPTS)
02260      37  CONTINUE
02270      450 FORMAT(/,40X,1(F8.4,1X))
02280      470 FORMAT(///,40X,1(I8,1X))
02290      500 FORMAT(///,20X,10(F8.4))
02300  C
02310  CHAPTER 1 1 1 1 1 DATA REDUCTION 1 1 1 1 1
02320  C
02330  C-----CALC PICHCF AND INTERPOLATE FOR DELTA FROM
02340  C-----PITOT CALIBRATION CURVE
02350  C
02360      IDID=0
02370      DO 50 I=1,NSTATN
02380          JPTS=NDATA(I)
02390          DO 40 J=1,JPTS
02400              IF((RPCMPW(I,J).EQ.0.0).AND.(RPNMPS(I,J).EQ.0.0)) GO TO 38
02410              PICHCF(I,J)=RPNMPS(I,J)/(RPCMPW(I,J)+1.E-6)
02420              IF((PICHCF(I,J).GT.2.544).OR.(PICHCF(I,J).LT.-3.769)) GO TO 38
02430              IF(IDID.EQ.0) DELTA(I,J)=SPLINE(CPITCH,
02440          #          CDELTA,NCAL,PICHCF(I,J))
02450              IF(IDID.GT.0) DELTA(I,J)=SP(CPITCH,CDELTA,
02460          #          NCAL,PICHCF(I,J))
02470              IDID=1
02480              GO TO 40
02490      38  CONTINUE
02500          DELTA(I,J)=0.0
02510          WRITE(6,850) I,J
02520      850  FORMAT(20X,'PICHCF IS OUT OF RANGE OF CALIBRATION AT I=
02530          #          ',I3,' AND J=',I3)
02540      40  CONTINUE
02550      50  CONTINUE
02560  C
02570  C-----INTERPOLATE FOR VELCF AND PSTCF FROM PITOT CALIBRATION DATA
02580  C
02590      IDID=0
02600      DO 30 I=1,NSTATN

```



```

02610      JPTS=NDATA(I)
02620      DO 70 J=1,JPTS
02630          IF((RPCMPW(I,J).EQ.0.0).AND.(RPNMPS(I,J).EQ.0.0)) GO TO 65
02640          IF((ABS(DELTA(I,J))) .GT. 58.0) GO TO 65
02650          IF(IDID .EQ. 0) VELCF(I,J)=SPLINE(CDELTA,
02660      *      CVELCF,NCAL,DELTA(I,J))
02670          IF(IDID .GT. 0) VELCF(I,J)=SP(CDELTA,CVELCF,
02680      *      NCAL,DELTA(I,J))
02690          IF(IDID .EQ. 0) PSTCF(I,J)=SPLINE(CDELTA,
02700      *      CPSTCF,NCAL,DELTA(I,J))
02710          IF(IDID .GT. 0) PSTCF(I,J)=SP(CDELTA,CPSTCF,
02720      *      NCAL,DELTA(I,J))
02730          IDID=1
02740          GO TO 70
02750      65      CONTINUE
02760          VELCF(I,J)=0.0
02770          PSTCF(I,J)=0.0
02780          WRITE(6,890) I,J
02790      890      FORMAT(20X,'DELTA IS OUT OF RANGE OF CALIBRATION DATA
02800      *      AT I=',I3,' AND J=',I3)
02810      70      CONTINUE
02820      80      CONTINUE
02830      C
02840          DO 85 I=1,NSTATN
02850          IF(DIAGNS) WRITE(6,500) (PICHCF(I,J),J=1,JPTS)
02860          IF(DIAGNS) WRITE(6,500) (DELTA(I,J),J=1,JPTS)
02870          IF(DIAGNS) WRITE(6,500) (VELCF(I,J),J=1,JPTS)
02880          IF(DIAGNS) WRITE(6,500) (PSTCF(I,J),J=1,JPTS)
02890      85      CONTINUE
02900      C
02910      C-----CALC MAGNITUDE OF TOTAL MEAN VELOCITY VECTOR,
02920      C-----      U, V, & W COMPONENTS, AND STATIC PRESSURE
02930      C
02940          PI=3.14159
02950          DO 100 I=1,NSTATN
02960          RHO(I)=PATM(I)*(133.33)/(286.94*(TFLOW(I)+273.15))
02970          JPTS=NDATA(I)
02980          DO 90 J=1,JPTS
02990          BETA(I,J)=360.+BZOFF(I)-RBETA(I,J)
03000          IF((RPCMPW(I,J).EQ.0.0).AND.(RPNMPS(I,J).EQ.0.0))BETA(I,J)=0.0
03010          VTOTAL(I,J)=SQRT(ABS(2.0/RHO(I)*VELCF(I,J)*RPCMPW(I,J)*133.9))
03020          U(I,J)=VTOTAL(I,J) * COS(DELTA(I,J)*PI/180.0) *
03030      *      COS(BETA(I,J)*PI/180.0)
03040          V(I,J)=VTOTAL(I,J) * SIN(DELTA(I,J)*PI/180.0)
03050          W(I,J)=VTOTAL(I,J) * COS(DELTA(I,J)*PI/180.0) *
03060      *      SIN(BETA(I,J)*PI/180.0)
03070          P(I,J)=(RPCMPA(I,J)-PSTCF(I,J)*RPCMPW(I,J))*133.33
03080      90      CONTINUE
03090      100     CONTINUE
03100          IF(DIAGNS) WRITE(6,500)(VTOTAL(I,J),J=1,JPTS)
03110          IF(DIAGNS) WRITE(6,500)(U(I,J),J=1,JPTS)
03120          IF(DIAGNS) WRITE(6,500)(V(I,J),J=1,JPTS)
03130          IF(DIAGNS) WRITE(6,500)(W(I,J),J=1,JPTS)
03140          IF(DIAGNS) WRITE(6,500)(P(I,J),J=1,JPTS)
03150      C
03160      CHAPTER 2 2 2 2 2 2 AUXILIARY CALCULATIONS 2 2 2 2 2
03170      C
03180      C-----NONDIMENSIONALIZE LENGTHS AND VELOCITIES
03190      C
03200          DO 150 I=1,NSTATN
03210          XND(I)=X(I)/(2.0*RLARGE)
03220          JPTS=NDATA(I)
03230          UIN(I)=(SQRT(2.0/RHO(I)*RDNPRS(I)*133.33))*(6.312/5.938)**2
03240          MASFLO(I)=PI*RHO(I)*UIN(I)*RSMALL**2
03250          DO 140 J=1,JPTS
03260          VTSTAR(I,J)=VTOTAL(I,J)/UIN(I)

```

```

03270          USTAR(I,J)=U(I,J)/UIN(I)
03280          VSTAR(I,J)=V(I,J)/UIN(I)
03290          WSTAR(I,J)=W(I,J)/UIN(I)
03300          PSTAR(I,J)=P(I,J)/(RDNPRS(I)*133.33)
03310 140    CONTINUE
03320 150    CONTINUE
03330          IF(DIAGNS) WRITE(6,450) (UIN(I),I=1,NSTATN)
03340          IF(DIAGNS) WRITE(6,450) (MASFLO(I),I=1,NSTATN)
03350          DO 160 J=1,MAXJPT
03360              RND(J)=R(J)/(2.0*RLARGE)
03370              IF(KRADTR.EQ.0) RND(J)=RINCHS(J)
03380              IF(KRADTR.EQ.0) R(J)=RINCHS(J)
03390 160    CONTINUE
03400 C
03410          IF(KRADTR.EQ.0) GO TO 135
03420 C
03430 C---FOR RADIAL PROFILES: NUMERICAL INTEGRATION TO CALC. MASS
03440 C   FLOW AND MOMENTUM FLUXES FOR SWIRL NUMBER
03450 C
03460 C   FOR PROFILES AT AND UPSTREAM OF EXPANSION CORNER, RSMALL
03470 C   IS USED IN EXPRESSIONS FOR DYNP AND UMEAN; DOWNSTREAM OF
03480 C   EXPANSION, RLARGE IS USED.
03490 C
03500          DO 130 I=1,NSTATN
03510              JPTS=NDATA(I)
03520              JPTSM1=JPTS-1
03530              PREF(I)=P(I,JPTS)
03540              DYPS(1)=0.0
03550 C
03560              IF(XINCHS(I).GT.0.0) GO TO 107
03570              DYNP(JPTS)=2.0*(RSMALL-R(JPTS))
03580              GO TO 108
03590 107    DYNP(JPTS)=2.0*(RLARGE-R(JPTS))
03600 108    CONTINUE
03610 C
03620              DO 110 J=1,JPTSM1
03630                  DYNP(J)=R(J+1)-R(J)
03640                  DYPS(J+1)=DYNP(J)
03650 110    CONTINUE
03660              DO 115 J=1,JPTS
03670                  SNS(J)=0.5*(DYNP(J)+DYPS(J))
03680                  PDIFF(I,J)=P(I,J)-PREF(I)
03690 115    CONTINUE
03700 C
03710 C---INNER 3 (HUB) VALUES OF PDIFF ARE SET TO ZERO FOR SWIRLER
03720 C   EXIT-PLANE PROFILES; FOR DOWNSTREAM PROFILES, ACTUAL VALUES
03730 C   ARE USED
03740 C
03750          IF(XINCHS(I).GT.-1.28) GO TO 116
03760          PDIFF(I,1)=0.
03770          PDIFF(I,2)=0.
03780          PDIFF(I,3)=0.
03790 116    CONTINUE
03800 C
03810          IF(DIAGNS) WRITE(6,500) (DYNP(J),J=1,JPTS)
03820          IF(DIAGNS) WRITE(6,500) (SNS(J),J=1,JPTS)
03830          AREA1=PI*SNS(1)**2
03840          ARSUM=AREA1
03850          FLOW=RHO(I)*U(I,1)*AREA1
03860          WMOM=W(I,1)*R(2)/4.*FLOW
03870          UMON=U(I,1)*FLOW
03880          UMOMP=(RHO(I)*U(I,1)**2+PDIFF(I,1))*AREA1
03890          IF(DIAGNS) WRITE(6,2030) AREA1,ARSUM,FLOW,WMOM,UMON,UMOMP
03900          DO 120 J=2,JPTS
03910              AREAJ=2.*PI*R(J)*SNS(J)
03920              ARSUM=ARSUM+AREAJ

```

```

03930          FLOW=FLOW+RHO(I)*U(I,J)*AREAJ
03940          UMOM=UMOM+RHO(I)*U(I,J)**2*AREAJ
03950          UMOMP=UMOMP+(RHO(I)*U(I,J)**2+PDIFF(I,J))*AREAJ
03960          WMOM=WMOM+RHO(I)*U(I,J)*W(I,J)*R(J)*AREAJ
03970          IF(DIAGNS) WRITE(6,2040) AREAJ,ARSUM,FLOW,WMOM,UMOM,UMOMP
03980 120    CONTINUE
03990          MASS(I)=FLOW
04000 C
04010          IF(XINCHS(I).GT.0.0) GO TO 122
04020          UMEAN(I)=MASS(I)/(RHO(I)*PI*RSMALL**2)
04030          GO TO 123
04040 122    UMEAN(I)=MASS(I)/(RHO(I)*PI*RLARGE**2)
04050 123    CONTINUE
04060 C
04070          ANGMOM(I)=WMOM
04080          AXMOM(I)=UMOM
04090          AXMOMP(I)=UMOMP
04100          IF(DIAGNS) WRITE(6,2050) UMEAN(I),MASS(I),ANGMOM(I),AXMOM(I),
04110          #           AXMOMP(I)
04120 C
04130 2030  FORMAT(/4X,'AREAJ',5X,'ARSUM',5X,'FLOW',6X,'WMOM',6X,
04140          #           'UMOM',6X,'UMOMP'/'/'',6E10.3)
04150 2040  FORMAT(' ',6E10.3)
04160 2050  FORMAT(/14X,'UMEAN',5X,'MASS',6X,'ANGMOM',4X,'AXMOM',
04170          #           5X,'AXMOMP'/'/'',11X,5E10.3)
04180 C
04190          SPRIME(I)=ANGMOM(I)/(AXMOM(I)*RSMALL)
04200          S(I)=ANGMOM(I)/(AXMOMP(I)*RSMALL)
04210 130  CONTINUE
04220          IF(DIAGNS) WRITE(6,450) (UMEAN(I),I=1,NSTATN)
04230          IF(DIAGNS) WRITE(6,450) (MASS(I),I=1,NSTATN)
04240          IF(DIAGNS) WRITE(6,450) (ANGMOM(I),I=1,NSTATN)
04250          IF(DIAGNS) WRITE(6,450) (AXMOM(I),I=1,NSTATN)
04260          IF(DIAGNS) WRITE(6,450) (AXMOMP(I),I=1,NSTATN)
04270          IF(DIAGNS) WRITE(6,450) (SPRIME(I),I=1,NSTATN)
04280          IF(DIAGNS) WRITE(6,450) (S(I),I=1,NSTATN)
04290 135  CONTINUE
04300 C
04310          IF(KRADTR.EQ.1) GO TO 180
04320 C
04330 C---FOR AZIMUTHAL TRAVERSES:  CALC. PDIFF=(P-PREF) USING SUPPLIED
04340 C   VALUES OF PREF(I).
04350 C
04360          DO 178 I=1,NSTATN
04370             JPTS=NDATA(I)
04380             DO 177 J=1,JPTS
04390                PDIFF(I,J)=P(I,J)-PREF(I)*133.33
04400 177    CONTINUE
04410 178    CONTINUE
04420 C
04430 C---CALC. AVERAGE VALUES FOR AZIMUTHAL TRAVERSES -- NREP IS NO. OF
04440 C   POINTS IN REPEATING CYCLE ACROSS ONE BLADE; NAVE IS NO. OF
04450 C   AVERAGES POSSIBLE CONTAINING NREP CONSECUTIVE POINTS.
04460 C
04470          NREP=6
04480          DO 180 I=1,NSTATN
04490             NAVE=NDATA(I)-NREP+1
04500             DO 175 K=1,NAVE
04510                NAVEND=K+NREP-1
04520                USUM=0.
04530                VSUM=0.
04540                WSUM=0.
04550                FSUM=0.
04560                DO 174 J=K,NAVEND
04570                   USUM=USUM+USTAR(I,J)
04580                   VSUM=VSUM+VSTAR(I,J)

```

```

04590          WSUM=WSUM+WSTAR(I,J)
04600          PSUM=PSUM+PDIFF(I,J)
04610 174      CONTINUE
04620          USTAVG(I,K)=USUM/NREP
04630          VSTAVG(I,K)=VSUM/NREP
04640          WSTAVG(I,K)=WSUM/NREP
04650          PDFAVG(I,K)=PSUM/NREP
04660 175      CONTINUE
04670 180      CONTINUE
04680 C
04690 C---CALCULATE VISCOSITY AND INLET REYNOLDS NUMBER (BOTH TRAVERSE TYPES)
04700 C
04710 C---VISCOSITY FORMULA FROM LAN & ROSKAM, AIRPLANE AERODYNAMICS
04720 C & PERFORMANCE, P.42.
04730 C
04740          DO 162 I=1,NSTATN
04750          DENOM=TFLOW(I)+273.15+110.4
04760          VISCOS(I)=(1.458E-06)*(TFLOW(I)+273.15)**1.5/DENOM
04770          REDIN(I)=UIN(I)*2.*RSMALL*RHO(I)/VISCOS(I)
04780 162      CONTINUE
04790 C
04800 CHAPTER 3 3 3 3 3 OUTPUT 3 3 3 3 3 3 3
04810 C
04820          IF(.NOT. IWRITE) GO TO 165
04830          WRITE(11) XINCHS
04840          WRITE(11) RINCHS
04850          WRITE(11) USTAR
04860          WRITE(11) VSTAR
04870          WRITE(11) WSTAR
04880          WRITE(11) BETA
04890          WRITE(11) DELTA
04900          WRITE(11) PDIFF
04910          WRITE(11) UIN
04920          WRITE(11) PREF
04930 C
04940 165      CONTINUE
04950          WRITE(6,311)
04960          WRITE(6,312) HEDID1,HEDID2,HEDCAL
04970          WRITE(6,325) ALPHA
04980          WRITE(6,330) PHI
04990          WRITE(6,335) RSMALL
05000          WRITE(6,340) RLARGE
05010          CALL WRITE(1,1,NSTATN,1,IT,JT,XINCHS,RINCHS,FANSPD,HEDFAN)
05020          CALL WRITE(1,1,NSTATN,1,IT,JT,XINCHS,RINCHS,TFLOW,HEDTFL)
05030          CALL WRITE(1,1,NSTATN,1,IT,JT,XINCHS,RINCHS,PATM,HEDPAT)
05040          CALL WRITE(1,1,NSTATN,1,IT,JT,XINCHS,RINCHS,RHO,HEDRHO)
05050          CALL WRITE(1,1,NSTATN,1,IT,JT,XINCHS,RINCHS,VISCOS,HEDVIS)
05060          CALL WRITE(1,1,NSTATN,1,IT,JT,XINCHS,RINCHS,RDNPRS,HEDNIP)
05070          CALL WRITE(1,1,NSTATN,1,IT,JT,X,R,UIN,HEDMIV)
05080          CALL WRITE(1,1,NSTATN,1,IT,JT,X,R,MAFLO,HEDMMF)
05090          CALL WRITE(1,1,NSTATN,1,IT,JT,X,R,REDIN,HEDRED)
05100 C
05110          IF(KRADTR.EQ.0) GO TO 170
05120          CALL WRITE(1,1,NSTATN,1,IT,JT,X,R,MASS,HEDM)
05130          CALL WRITE(1,1,NSTATN,1,IT,JT,X,R,UMEAN,HEDUMN)
05140          CALL WRITE(1,1,NSTATN,1,IT,JT,X,R,ANGMOM,HEDAM)
05150          CALL WRITE(1,1,NSTATN,1,IT,JT,X,R,AXMOM,HEDAX)
05160          CALL WRITE(1,1,NSTATN,1,IT,JT,X,R,AXMOM,HEDAX)
05170          CALL WRITE(1,1,NSTATN,1,IT,JT,X,R,S,HEDS)
05180          CALL WRITE(1,1,NSTATN,1,IT,JT,X,R,SPRIME,HEDSPR)
05190 C
05200 170      CONTINUE
05210          CALL PRINT(1,1,NSTATN,MAXJPT,IT,JT,X,R,U,HEDU)
05220          CALL PRINT(1,1,NSTATN,MAXJPT,IT,JT,X,R,V,HEDV)
05230          CALL PRINT(1,1,NSTATN,MAXJPT,IT,JT,X,R,W,HEDW)
05240          CALL PRINT(1,1,NSTATN,MAXJPT,IT,JT,X,R,P,HEDP)

```

```

05250 CALL PRINT(1,1,NSTATN,MAXJPT,IT,JT,X,R,DELTA,HEDDEL)
05260 CALL PRINT(1,1,NSTATN,MAXJPT,IT,JT,X,R,BETA,HEDBET)
05270 CALL PRINT(1,1,NSTATN,MAXJPT,IT,JT,X,R,VTOTAL,HEDVT)
05280 CALL PRINT(1,1,NSTATN,MAXJPT,IT,JT,XND,RND,USTAR,HEDUST)
05290 CALL PRINT(1,1,NSTATN,MAXJPT,IT,JT,XND,RND,VSTAR,HEDVST)
05300 CALL PRINT(1,1,NSTATN,MAXJPT,IT,JT,XND,RND,WSTAR,HEDWST)
05310 CALL PRINT(1,1,NSTATN,MAXJPT,IT,JT,XND,RND,PSTAR,HEDPST)
05320 CALL PRINT(1,1,NSTATN,MAXJPT,IT,JT,XND,RND,PDIFF,HEDPDF)
05330 CC CALL PRINT(1,1,NSTATN,MAXJPT,IT,JT,XND,RND,VTSTAR,HEDVTS)
05340 C
05350 IF(KRADTR.EQ.1) GO TO 172
05360 CALL PRINT(1,1,NSTATN,MAXJPT,IT,JT,XINCHS,RINCHS,USTAVG,HEDUSA)
05370 CALL PRINT(1,1,NSTATN,MAXJPT,IT,JT,XINCHS,RINCHS,VSTAVG,HEDVSA)
05380 CALL PRINT(1,1,NSTATN,MAXJPT,IT,JT,XINCHS,RINCHS,WSTAVG,HEDWSA)
05390 CALL PRINT(1,1,NSTATN,MAXJPT,IT,JT,XINCHS,RINCHS,PDFAVG,HEDPDA)
05400 C
05410 172 CONTINUE
05420 CALL PRINT(1,1,NSTATN,MAXJPT,IT,JT,XINCHS,RINCHS,RPNMPS,HEDNMS)
05430 CALL PRINT(1,1,NSTATN,MAXJPT,IT,JT,XINCHS,RINCHS,RPCMPW,HEDCMW)
05440 CALL PRINT(1,1,NSTATN,MAXJPT,IT,JT,XINCHS,RINCHS,RPCMPA,HEDCMA)
05450 STOP
05460 C
05470 C-----FORMAT STATEMENTS
05480 C
05490 311 FORMAT(1H1,T37,'AXISYMMETRIC,ISOTHERMAL,GT COMBUSTOR FLOWFIELD ',
05500 # 'MEASUREMENTS',//,T53,'USING A FIVE-HOLE PITOT PROBE')
05510 312 FORMAT(/T10,18A4/T10,18A4//T10,9A4)
05520 325 FORMAT(/T10,'EXPANSION ANGLE(DEG.) =',T50,1PE13.3)
05530 330 FORMAT(/T10,'SWIRL VANE ANGLE(DEG.) =',T50,1PE13.3)
05540 335 FORMAT (/T10,'INLET RADIUS(M) =',T50,1PE13.3)
05550 340 FORMAT(/T10,'COMBUSTOR RADIUS(M) =',T50,1PE13.3)
05560 END
05570 C
05580 SUBROUTINE INIT
05590 C*****
05600 C
05610 COMMON
05620 #/MEASUR/RBETA(8,24),RPNMPS(8,24),RPCMPW(8,24),RPCMPA(8,24),
05630 # NDATA(8),MAXJPT,RDNFRS(8),
05640 # FANSPD(8),TFLOW(8),PATM(8),BZOFF(8)
05650 #/GEOM/X(8),R(24),XND(8),RND(24),DYNP(24),
05660 # SNS(24),NSTATN,XINCHS(8),RINCHS(24)
05670 #/CALC/VTOTAL(8,24),U(8,24),V(8,24),W(8,24),P(8,24),
05680 # VTSTAR(8,24),USTAR(8,24),VSTAR(8,24),WSTAR(8,24),PSTAR(8,24),
05690 # PICHCF(8,24),VELCF(8,24),DELTA(8,24),BETA(8,24),
05700 # ANGMOM(8),UMEAN(8),MASS(8),MASFLO(8),UIN(8),
05710 # PDIFF(8,24),PSTCF(8,24),AXMOM(8),AXMOMP(8),
05720 # SPRIME(8),S(8),REDIN(8),PREF(8),RHO(8),VISCOS(8),
05730 # USTAVG(8,24),VSTAVG(8,24),WSTAVG(8,24),PDFAVG(8,24)
05740 C
05750 REAL MASS,MASFLO
05760 C
05770 DO 20 I=1,NSTATN
05780 MASFLO(I)=0.0
05790 MASS(I)=0.0
05800 ANGMOM(I)=0.0
05810 AXMOM(I)=0.0
05820 AXMOMP(I)=0.0
05830 SPRIME(I)=0.0
05840 S(I)=0.0
05850 UMEAN(I)=0.0
05860 UIN(I)=0.0
05870 DO 10 J=1,MAXJPT
05880 VTOTAL(I,J)=0.0
05890 U(I,J)=0.0
05900 V(I,J)=0.0

```

```

05910      W(I,J)=0.0
05920      P(I,J)=0.0
05930      VTSTAR(I,J)=0.0
05940      USTAR(I,J)=0.0
05950      VSTAR(I,J)=0.0
05960      WSTAR(I,J)=0.0
05970      PSTAR(I,J)=0.0
05980      PDIFF(I,J)=0.0
05990      RBETA(I,J)=0.0
06000      BETA(I,J)=0.0
06010      RPNMFS(I,J)=0.0
06020      RPCMPW(I,J)=0.0
06030      RPCMPA(I,J)=0.0
06040      PICHCF(I,J)=0.0
06050      VELCF(I,J)=0.0
06060      PSTCF(I,J)=0.0
06070      DELTA(I,J)=0.0
06080      USTAVG(I,J)=0.0
06090      VSTAVG(I,J)=0.0
06100      WSTAVG(I,J)=0.0
06110      PDFAVG(I,J)=0.0
06120      10 CONTINUE
06130      20 CONTINUE
06140      RETURN
06150      END
06160 C
06170      FUNCTION SPLINE(X, FX, N, X1)
06180 C*****
06190 C      CUBIC SPLINE CURVE FITTING IN 2 DIMENSIONAL DATA PLANE
06200 C      INPUT VALUES :
06210 C      X, FX      DATA ARRAYS, ONE DIMENSIONAL, X IN INCREASING ORDER
06220 C      N          NUMBER OF DATA POINTS IN X, MAX 26
06230 C      X1        POINT OF INTEREST, WHERE F(X1) IS TO BE FOUND
06240 C
06250 C      RETURN VALUE :
06260 C      SPLINE OR SP = F(X1)
06270 C      THIS ROUTINE ACTIVATES ROUTINE ABUILD, H, AND GAUSS.
06280 C      FOR INTERPOLATION OF A LARGE NUMBER OF DATA POINTS, FUNCTION
06290 C      SPLINE MAY BE CALLED ONLY ONCE , AND SUBSEQUENT CALLS MAY USE
06300 C      ENTRY POINT SP.
06310 C*****
06320      DIMENSION X(1), FX(1), A(26,27)
06330 C
06340 C-----CONSTRUCT SPLINE MATRIX
06350 C
06360      N1=N+1
06370      DO 10 I=1, N
06380          DO 10 J=1, N1
06390      10      A(I,J)=0.
06400      M1=N-1
06410      DO 20 I=2, M1
06420      20      CALL ABUILD(X, FX, A, N, I)
06430      A(1,1)=H(X,2)
06440      A(1,2)=-H(X,1)-H(X,2)
06450      A(1,3)=H(X,1)
06460      M2=N-2
06470      A(N,M2)=H(X,M1)
06480      A(N,M1)=-H(X,M2)-H(X,M1)
06490      A(N,N)=H(X,M2)
06500 C
06510 C-----FIND SECOND DERIVATIVES
06520 C
06530      CALL GAUSS(A, N, N1)
06540      ENTRY SP(X, FX, N, X1)
06550 C
06560 C-----FIND F(X1)

```

```

06570 C
06580 DO 40 I=1, M1
06590 I1=I+1
06600 IF(X1 .EQ. X(I)) GO TO 50
06610 IF(X1 .LT. X(I) .AND. X1 .GT. X(I1)) GO TO 41
06620 IF(X1 .GT. X(I) .AND. X1 .LT. X(I1) ) GO TO 41
06630 40 CONTINUE
06640 IF(X1 .EQ. X(N)) GO TO 60
06650 WRITE(6, 42) X1
06660 42 FORMAT(' X1=', G14.7, ' OUT OF INTERPOLATION RANGE, RETURNED VALUE
06670 * =0')
06680 SF=0.
06690 SPLINE=0.
06700 STOP
06710 C
06720 41 CONTINUE
06730 I1=I+1
06740 HI=H(X,I)
06750 HX=X(I1)-X1
06760 HX2=X1-X(I)
06770 FX1=HX**3/HI-HI*HX
06780 FX1=FX1*A(I,N1)
06790 STO=HX2**3/HI - HI*HX2
06800 FX1=(FX1+STO*A(I1,N1) )/6.
06810 SPLINE=(FX(I)*HX+FX(I1)*HX2)/HI+FX1
06820 SF=SPLINE
06830 RETURN
06840 C
06850 50 CONTINUE
06860 SPLINE=FX(I)
06870 SF=SPLINE
06880 RETURN
06890 C
06900 60 CONTINUE
06910 SPLINE=FX(N)
06920 SF=SPLINE
06930 RETURN
06940 END
06950 C
06960 FUNCTION H(X,I)
06970 C*****
06980 C CALCULATE DELTA X WHICH IS USUALLY CALLED H.
06990 C*****
07000 DIMENSION X(1)
07010 I1=I+1
07020 H=X(I1)-X(I)
07030 RETURN
07040 END
07050 C
07060 SUBROUTINE ABUILD(X, F, A, N, I)
07070 C*****
07080 C CONSTRUCT SPLINE MATRIX FOR FINDING 2ND DERIVATIVES.
07090 C*****
07100 DIMENSION X(1), F(1), A(26,27)
07110 IM1=I-1
07120 I1=I+1
07130 N1=N+1
07140 STO=H(X,I)
07150 HIM1=H(X,IM1)
07160 A(I,IM1)=HIM1
07170 A(I,I)=2.*(HIM1+STO)
07180 A(I,I1)=STO
07190 A(I,N1)=( (F(I1)-F(I))/STO - (F(I)-F(IM1))/HIM1 ) *6.
07200 RETURN
07210 END
07220 C

```

```

07230      SUBROUTINE GAUSS(A, K, M)
07240 C*****
07250 C      GAUSS-JORDAN ELIMINATION
07260 C*****
07270      DIMENSION A(26,27)
07280      M1=M-1
07290      K1=K-1
07300      DO 3 L=1, K1
07310          L1=L+1
07320          DO 3 I=L1, K
07330              CONST=A(I,L)/A(L,L)
07340              DO 3 J=L, M
07350                  3      A(I,J)=A(I,J)-CONST*A(L,J)
07360          DO 6 I=1, K1
07370              I1=I+1
07380              DO 6 L=I1, M1
07390                  CONST=A(I,L)/A(L,L)
07400                  DO 6 J=I, M
07410                      6      A(I,J)=A(I,J)-CONST*A(L,J)
07420          DO 10 I=1, K
07430              A(I,M)=A(I,M)/A(I,I)
07440          10      A(I,I)=1.
07450      RETURN
07460      END
07470 C
07480      SUBROUTINE PRINT(ISTART,JSTART,NI,NJ,IT,JT,X,Y,PHI,HEAD)
07490 C*****
07500 C
07510      DIMENSION PHI(IT,JT),X(IT),Y(JT),HEAD(9)
07520      COMMON /OUTPUT/ STORE(8)
07530      ISKIP=1
07540      JSKIP=1
07550      WRITE(6,110)HEAD
07560      ISTA=ISTART-10
07570      100 CONTINUE
07580      ISTA=ISTA+10
07590      IEND=ISTA+9
07600      IF(NI.LT.IEND)IEND=NI
07610      WRITE(6,111)(I,I=ISTA,IEND,ISKIP)
07620      WRITE(6,114)(X(I),I=ISTA,IEND,ISKIP)
07630      WRITE(6,112)
07640      DO 101 JJ=JSTART,NJ,JSKIP
07650          J=JSTART+NJ-JJ
07660          DO 120 I=ISTA,IEND
07670              A=PHI(I,J)
07680              IF(ABS(A).LT.1.E-20) A=0.0
07690          120      STORE(I)=A
07700          101      WRITE(6,113)J,Y(J),(STORE(I),I=ISTA,IEND,ISKIP)
07710          IF(IEND.LT.NI)GO TO 100
07720          RETURN
07730          110 FORMAT(1H0,17(2H*-),7X,9A4,7X,17(2H*))
07740          111 FORMAT(1H0,15H          I =          ,I2,9I11)
07750          112 FORMAT(8H0 J      Y)
07760          113 FORMAT(I3,0PF8.4,1X,10(1X,E10.3))
07770          114 FORMAT(13H          X = ,F8.4,9F11.4)
07780          END
07790 C
07800      SUBROUTINE WRITE(ISTART,JSTART,NI,NJ,IT,JT,X,Y,PHI,HEAD)
07810 C*****
07820 C
07830      COMMON /OUTPUT/ STORE(8)
07840      DIMENSION PHI(IT),X(IT),Y(JT),HEAD(9)
07850      ISKIP=1
07860      JSKIP=1
07870      WRITE(6,110)HEAD
07880      ISTA=ISTART-12

```



```

07890 100 CONTINUE
07900   ISTA=ISTA+12
07910   IEND=ISTA+11
07920   IF(NI.LT.IEND)IEND=NI
07930   WRITE(6,111)(I,I=ISTA,IEND,ISKIP)
07940   WRITE(6,114)(X(I),I=ISTA,IEND,ISKIP)
07950   DO 101 JJ=JSTART,NJ,JSKIP
07960     J=JSTART+NJ-JJ
07970     DO 120 I=ISTA,IEND
07980       A=PHI(I)
07990       IF(ABS(A).LT.1.E-20) A=0.0
08000     120   STORE(I)=A
08010   101   WRITE(6,113) (STORE(I),I=ISTA,IEND,ISKIP)
08020     IF(IEND.LT.NI)GO TO 100
08030   RETURN
08040 110 FORMAT(1H0,17(2H*-),7X,9A4,7X,17(2H-*))
08050 111 FORMAT(1H0,15H          I =          ,I2,9I11)
08060 113 FORMAT(/12X,1F10E11.3)
08070 114 FORMAT(13H          X = ,F8.4,9F11.4)
08080   END

```

The following listing is of a dataset containing the input data for the reduction code. The two datasets are submitted together as a single batch job; they are merged by the computer before execution.

```

00010 //GO.FT11F001 DD DSN='U12686A.NA70R21N.DATA',DISP=OLD
00020 //GO.SYSIN DD *
00030   COMPUTED MASS FLOW RATE (KG/S)
00040   COMPUTED MEAN AXIAL VELOCITY (M/S)
00050     U VELOCITY (M/S)
00060     V VELOCITY (M/S)
00070     W VELOCITY (M/S)
00080   TOTAL VELOCITY MAGNITUDE (M/S)
00090   DIMENSIONLESS U VELOCITY
00100   DIMENSIONLESS V VELOCITY
00110   DIMENSIONLESS W VELOCITY
00120   DIMENSIONLESS STATIC PRESS. P/RDNPRS
00130   PROBE PITCH ANGLE (DEG.)
00140   PROBE YAW ANGLE (DEG.)
00150   P(NORTH) - P(SOUTH) (VOLTS)
00160   P(CENTER) - P(WEST) (VOLTS)
00170   P(CENTER) - P(ATM.) (VOLTS)
00180   MEAS. INLET MASS FLOW RATE (KG/S)
00190   MEAS. INLET AXIAL VELOCITY (M/S)
00200   MEAS. INLET DYNAMIC PRESS. (TORR)
00210   AXIAL FLUX OF ANGULAR MOMENTUM (N-M)
00220   AXIAL FLUX OF AXIAL MOM. (NEGL. PST)
00230   AXIAL FLUX OF AXIAL MOM. (INCL. PST)
00240   SWIRL NO. S-PRIME (NEGL. PST)
00250   SWIRL NO. S (INCL. PST)
00260   STATIC PRESSURE, GAGE (N/SQ. M)
00270   STAT. PRESS. DIFF., P-PREF (N/SQ.M)
00280   INLET REYNOLDS NUMBER
00290     FAN SPEED (RPM)
00300   REP. FLOW TEMP. (DEG CELSIUS)
00310   ATMOSPHERIC PRESSURE (TORR)
00320     DENSITY (KG/CU. M)

```

```

00330 ABS. (LAM.) VISCOSITY (KG/M-S)
00340 AVERAGES OF NONDIM. U-VELOCITY
00350 AVERAGES OF NONDIM. V-VELOCITY
00360 AVERAGES OF NONDIM. W-VELOCITY
00370 AVERAGES OF STATIC PRESS. DIFFERENCE
00380 CALIBRATION NO. 19 -- 10/10/82 (GFS)
00390 2.544 -58.0 1.661 -0.878
00400 2.233 -55.0 1.452 -0.602
00410 1.914 -50.0 1.289 -0.250
00420 1.608 -45.0 1.150 0.023
00430 1.365 -40.0 1.091 0.248
00440 1.155 -35.0 1.053 0.430
00450 0.966 -30.0 1.024 0.575
00460 0.801 -25.0 0.990 0.709
00470 0.663 -20.0 0.934 0.788
00480 0.537 -15.0 0.912 0.835
00490 0.412 -10.0 0.906 0.873
00500 0.270 -5.0 0.917 0.908
00510 0.110 0.0 0.912 0.915
00520 -0.050 5.0 0.940 0.906
00530 -0.209 10.0 0.946 0.880
00540 -0.346 15.0 0.977 0.856
00550 -0.476 20.0 1.017 0.823
00560 -0.664 25.0 1.091 0.759
00570 -0.896 30.0 1.196 0.664
00580 -1.157 35.0 1.236 0.496
00590 -1.487 40.0 1.300 0.278
00600 -1.869 45.0 1.397 0.000
00610 -2.319 50.0 1.541 -0.340
00620 -3.063 55.0 1.892 -0.823
00630 -3.769 58.0 2.300 -1.246
00640 AZ. TRAV. AT R=2.1 FOR PHI=70, EXIT PLANE (NO BLOCK)
00650 MEAS. 11/21/82 BY G. SANDER; DATAFILE NAME 'NA70R21N'
00660 90.0 70.0 5.938 11.75
00670 0 1 9
00680 -1.281 9 0.105 -0.273
00690 2900. 38.0 741.4 0.0
00700 -24.0 272.1 0.156 0.156 -0.307
00710 -18.0 270.6 0.143 0.170 -0.307
00720 -12.0 268.4 0.126 0.164 -0.305
00730 -6.0 268.9 0.116 0.136 -0.310
00740 0.0 268.4 0.120 0.112 -0.313
00750 6.0 268.0 0.131 0.099 -0.316
00760 12.0 266.4 0.144 0.118 -0.323
00770 18.0 267.2 0.150 0.134 -0.326
00780 24.0 269.3 0.141 0.140 -0.326
00790 //

```

Output generated by the reduction code using the example data given above appears on the following pages.

AXISYMMETRIC, ISOTHERMAL, GT COMBUSTOR FLOWFIELD MEASUREMENTS

USING A FIVE-HOLE PITOT PROBE

AZ. TRAV. AT R=2.1 FOR PHI=70. EXIT PLANE (NO BLOCK)
 MEAS. 11/21/82 BY G. SANDER; DATAFILE NAME 'NA70R21N'

CALIBRATION NO. 19 -- 10/10/82 (GFS)

EXPANSION ANGLE(DEG.) = 9.000E+01
 SWIRL VANE ANGLE(DEG.) = 7.000E+01
 INLET RADIUS(M) = 7.541E-02
 COMBUSTOR RADIUS(M) = 1.492E-01

```

-----*-----*-----*-----*-----*
I = 1
X = -1.2810
2.800E+03
-----*-----*-----*-----*-----*
REP. FLOW TEMP. (DEG CELSIUS)
-----*-----*-----*-----*-----*
I = 1
X = -1.2810
3.800E+01
-----*-----*-----*-----*-----*
ATMOSPHERIC PRESSURE (TORR)
-----*-----*-----*-----*-----*
I = 1
X = -1.2810
7.414E+02
-----*-----*-----*-----*-----*
DENSITY (KG/CU. M)
-----*-----*-----*-----*-----*
I = 1
X = -1.2810
1.107E+00
-----*-----*-----*-----*-----*
ABS. (LAM.) VISCOSITY (KG/M-S)
-----*-----*-----*-----*-----*
I = 1
X = -1.2810
1.898E-05
-----*-----*-----*-----*-----*
MEAS. INLET DYNAMIC PRESS. (TORR)
-----*-----*-----*-----*-----*
I = 1
X = -1.2810
1.050E-01
-----*-----*-----*-----*-----*
MEAS. INLET AXIAL VELOCITY (M/S)
-----*-----*-----*-----*-----*
I = 1
X = -0.0325
5.682E+00
-----*-----*-----*-----*-----*
MEAS. INLET MASS FLOW RATE (KG/S)
-----*-----*-----*-----*-----*
I = 1
X = -0.0325
1.124E-01
-----*-----*-----*-----*-----*
INLET REYNOLDS NUMBER
-----*-----*-----*-----*-----*
I = 1
X = -0.0325
4.999E+04
-----*-----*-----*-----*-----*
U VELOCITY (M/S)
-----*-----*-----*-----*-----*
I = 1
X = -0.0325
-----*-----*-----*-----*-----*
J Y
9 24.0000 -0.618E-01
8 18.0000 -0.236E+00
7 12.0000 -0.279E+00
6 6.0000 -0.138E+00
5 0.0000 -0.125E+00
4 -6.0000 -0.987E-01
3 -12.0000 -0.159E+00
2 -18.0000 0.603E-01
1 -24.0000 0.196E+00

```

```

-----
                                V VELOCITY (M/S)                                -----
                                I = 1
                                X = -0.0325

J      Y
9 24.0000 -0.306E+01
8 18.0000 -0.327E+01
7 12.0000 -0.330E+01
6  6.0000 -0.321E+01
5  0.0000 -0.288E+01
4 -6.0000 -0.258E+01
3-12.0000 -0.253E+01
2-18.0000 -0.285E+01
1-24.0000 -0.320E+01

-----
                                W VELOCITY (M/S)                                -----
                                I = 1
                                X = -0.0325

J      Y
9 24.0000  0.506E+01
8 18.0000  0.482E+01
7 12.0000  0.443E+01
6  6.0000  0.396E+01
5  0.0000  0.446E+01
4 -6.0000  0.514E+01
3-12.0000  0.571E+01
2-18.0000  0.576E+01
1-24.0000  0.534E+01

-----
                                STATIC PRESSURE, GAGE (N/SQ. M)                    -----
                                I = 1
                                X = -0.0325

J      Y
9 24.0000 -0.536E+02
8 18.0000 -0.516E+02
7 12.0000 -0.490E+02
6  6.0000 -0.459E+02
5  0.0000 -0.491E+02
4 -6.0000 -0.534E+02
3-12.0000 -0.567E+02
2-18.0000 -0.563E+02
1-24.0000 -0.523E+02

-----
                                PROBE PITCH ANGLE (DEG.)                          -----
                                I = 1
                                X = -0.0325

J      Y
9 24.0000 -0.311E+02
8 18.0000 -0.341E+02
7 12.0000 -0.366E+02
6  6.0000 -0.390E+02
5  0.0000 -0.329E+02
4 -6.0000 -0.267E+02
3-12.0000 -0.239E+02
2-18.0000 -0.263E+02
1-24.0000 -0.309E+02

-----
                                PROBE YAW ANGLE (DEG.)                            -----
                                I = 1
                                X = -0.0325

J      Y
9 24.0000  0.907E+02
8 18.0000  0.928E+02
7 12.0000  0.936E+02
6  6.0000  0.920E+02
5  0.0000  0.916E+02
4 -6.0000  0.911E+02
3-12.0000  0.916E+02
2-18.0000  0.894E+02
1-24.0000  0.879E+02

-----
                                TOTAL VELOCITY MAGNITUDE (M/S)                    -----
                                I = 1
                                X = -0.0325

J      Y
9 24.0000  0.591E+01
8 18.0000  0.583E+01
7 12.0000  0.553E+01
6  6.0000  0.510E+01
5  0.0000  0.531E+01
4 -6.0000  0.575E+01
3-12.0000  0.624E+01
2-18.0000  0.642E+01
1-24.0000  0.623E+01

```

```

-----
                I =      1
                X =    -0.1090

J      Y
9 24.0000  -0.109E-01
8 18.0000  -0.415E-01
7 12.0000  -0.490E-01
6  6.0000  -0.243E-01
5  0.0000  -0.219E-01
4 -6.0000  -0.174E-01
3-12.0000  -0.280E-01
2-18.0000  0.106E-01
1-24.0000  0.345E-01
-----
                I =      1
                X =    -0.1090

J      Y
9 24.0000  -0.538E+00
8 18.0000  -0.575E+00
7 12.0000  -0.580E+00
6  6.0000  -0.566E+00
5  0.0000  -0.507E+00
4 -6.0000  -0.454E+00
3-12.0000  -0.445E+00
2-18.0000  -0.501E+00
1-24.0000  -0.564E+00
-----
                I =      1
                X =    -0.1090

J      Y
9 24.0000  0.890E+00
8 18.0000  0.849E+00
7 12.0000  0.779E+00
6  6.0000  0.697E+00
5  0.0000  0.785E+00
4 -6.0000  0.904E+00
3-12.0000  0.100E+01
2-18.0000  0.101E+01
1-24.0000  0.940E+00
-----
                I =      1
                X =    -0.1090

J      Y
9 24.0000  -0.383E+01
8 18.0000  -0.369E+01
7 12.0000  -0.350E+01
6  6.0000  -0.328E+01
5  0.0000  -0.351E+01
4 -6.0000  -0.382E+01
3-12.0000  -0.405E+01
2-18.0000  -0.402E+01
1-24.0000  -0.374E+01
-----
                I =      1
                X =    -0.1090

J      Y
9 24.0000  -0.172E+02
8 18.0000  -0.152E+02
7 12.0000  -0.126E+02
6  6.0000  -0.951E+01
5  0.0000  -0.127E+02
4 -6.0000  -0.171E+02
3-12.0000  -0.203E+02
2-18.0000  -0.199E+02
1-24.0000  -0.159E+02
-----
                I =      1
                X =    -1.2810

J      Y
9 24.0000  0.000E+00
8 18.0000  0.000E+00
7 12.0000  0.000E+00
6  6.0000  0.000E+00
5  0.0000  0.000E+00
4 -6.0000  -0.275E-01
3-12.0000  -0.304E-01
2-18.0000  -0.217E-01
1-24.0000  -0.777E-02
-----

```

DIMENSIONLESS U VELOCITY

DIMENSIONLESS V VELOCITY

DIMENSIONLESS W VELOCITY

DIMENSIONLESS STATIC PRESS. P/RDNPRS

STAT. PRESS. DIFF., P-PREF (N/SQ.M)

AVERAGES OF NONDIM. U-VELOCITY

-----*

AVERAGES OF NONDIM. V-VELOCITY

-----*

I = 1
X = -1.2810

J	Y	
9	24.0000	0.000E+00
8	18.0000	0.000E+00
7	12.0000	0.000E+00
6	6.0000	0.000E+00
5	0.0000	0.000E+00
4	-6.0000	-0.537E+00
3	-12.0000	-0.521E+00
2	-18.0000	-0.509E+00
1	-24.0000	-0.506E+00

-----*

AVERAGES OF NONDIM. W-VELOCITY

-----*

I = 1
X = -1.2810

J	Y	
9	24.0000	0.000E+00
8	18.0000	0.000E+00
7	12.0000	0.000E+00
6	6.0000	0.000E+00
5	0.0000	0.000E+00
4	-6.0000	0.817E+00
3	-12.0000	0.836E+00
2	-18.0000	0.864E+00
1	-24.0000	0.891E+00

-----*

AVERAGES OF STATIC PRESS. DIFFERENCE

-----*

I = 1
X = -1.2810

J	Y	
9	24.0000	0.000E+00
8	18.0000	0.000E+00
7	12.0000	0.000E+00
6	6.0000	0.000E+00
5	0.0000	0.000E+00
4	-6.0000	-0.141E+02
3	-12.0000	-0.146E+02
2	-18.0000	-0.153E+02
1	-24.0000	-0.159E+02

-----*

P(NORTH) - P(SOUTH) (VOLTS)

-----*

I = 1
X = -1.2810

J	Y	
9	24.0000	0.141E+00
8	18.0000	0.150E+00
7	12.0000	0.144E+00
6	6.0000	0.131E+00
5	0.0000	0.120E+00
4	-6.0000	0.116E+00
3	-12.0000	0.126E+00
2	-18.0000	0.143E+00
1	-24.0000	0.156E+00

-----*

P(CENTER) - P(WEST) (VOLTS)

-----*

I = 1
X = -1.2810

J	Y	
9	24.0000	0.140E+00
8	18.0000	0.134E+00
7	12.0000	0.118E+00
6	6.0000	0.990E-01
5	0.0000	0.112E+00
4	-6.0000	0.136E+00
3	-12.0000	0.164E+00
2	-18.0000	0.170E+00
1	-24.0000	0.156E+00

-----*

P(CENTER) - P(ATM.) (VOLTS)

-----*

I = 1
X = -1.2810

J	Y	
9	24.0000	-0.326E+00
8	18.0000	-0.326E+00
7	12.0000	-0.323E+00
6	6.0000	-0.316E+00
5	0.0000	-0.313E+00
4	-6.0000	-0.310E+00
3	-12.0000	-0.305E+00
2	-18.0000	-0.307E+00
1	-24.0000	-0.307E+00

VITA

Glenn Ferris Sander

Candidate for Degree of

Master of Science

Thesis: AXIAL VANE-TYPE SWIRLER PERFORMANCE CHARACTERISTICS

Major Field: Mechanical Engineering

Biographical:

Personal Data: Born in Stillwater, Oklahoma, March 2, 1959,
the son of Dr. and Mrs. David A. Sander.

Education: Graduated from C. E. Donart High School, Stillwater,
Oklahoma, in May, 1977; received Bachelor of Science in
Mechanical Engineering degree (Aerospace Option) from
Oklahoma State University in May, 1982; completed
requirements for the Master of Science degree at Oklahoma
State University in July, 1983.

Professional Experience: Research and teaching assistant,
School of Mechanical and Aerospace Engineering, Oklahoma
State University, Stillwater, Oklahoma, 1981 - 1983.

Honorary Organization: Pi Tau Sigma

Professional Organizations: AIAA, ASME, NSPE